Final Scientific/Technical Report (DOE F 241.3) 9-29-17

Project Title: Development and Implementation of an Automatic Continuous Online Monitoring and Control Platform for Polymerization Reactions to Sharply Boost Energy and Resource Efficiency in Polymer Manufacturing

Award Number: DE-EE0005776 DOE/EERE/ Office of Advanced Manufacturing Program (AMO)

Project Period: 12/24/2014 – 6/23/2017

Recipient Organization: Administrators of the Tulane Educational Fund (Tulane University)
6823 St. Charles Avenue
New Orleans, LA 70118-5698

Principal Investigator: Dr. Wayne F. Reed, 504-862-3185, wreed@tulane.edu

Business Contact: Norey B. Laug, 504-865-5272, norey@tulane.edu

Partners: Fluence Analytics (formerly Advanced Polymer Monitoring Technologies, Inc.)
Louisiana State University (Prof. José Romagnoli group)

Acknowledgment, Disclaimer and Proprietary Data Notice – DOCUMENT AVAILABILITY

Acknowledgment: "The information, data, or work presented herein was funded in part by the Office of Energy Efficiency and Renewable Energy (EERE), U.S. Department of Energy, under Award Number DE- EE0005776."

Table of Contents

List of Acronyms

ACOMP= automatic continuous online monitoring of polymerization reactions
ACOMP/CI= ACOMP with control interface
Ac= sodium acrylate
Am= acrylamide
ATRP=atom transfer radical polymerization
CCD=charge coupled device
CESMII=Clean energy smart manufacturing innovation institute
CGS= centigram-gram-second system of units
MALS=multi-angle light scattering
MIR= mid infra-red
MWD= molecular weight distribution
NIR= near infra-red
NMP=nitroxide mediated polymerization
NNMI= National network of manufacturing institutes
RAFT=reversible addition fragmentation chain transfer
ROMP=Ring opening metathesis polymerization
SS= styrene sulfonate
TBtu= Tera BTU (10^{12} BTU)
TF= Tulane/Fluence joint work, especially as in the TF basic principles controller
UV= ultraviolet

Physical Quantities

cP= centi-poise, a CGS measure of total solution viscosity
$F_{inst,A}$= instantaneous mass fraction of monomer A incorporated into a copolymer chain
$F_{inst,B}$= instantaneous mass fraction of monomer B incorporated into a copolymer chain
M_w= cumulative weight average molecular weight of a solution of polymer (g/mole)
$M_{w,inst}$= instantaneous weight average molecular weight of a solution of polymer (g/mole)
R_g= square root of z-average mean square radius of a scattering molecule or particle (cm or nm)

List of Figures

Figure 5. Photographs of the two ACOMP/CI units built by Fluence Analytics.

Figure 6. The first active manual control of M_w during Am polymerization

Figure 7. Automatic control of conversion (black) along a sinusoidal target trajectory (blue). Also shown is the uncontrolled batch trajectory (red).

Figure 8. M_w and $M_{w,inst}$ for the reaction shown in figure 7.

Figure 9. Linearly increasing target M_w trajectory (red), and the reaction that followed it (black). Also shown is the uncontrolled, batch trajectory for M_w.

Figure 10. $M_{w,inst,e}$ computed from $M_{w,e}$ via equation 2 is shown, together with $M_{w,e}$. Also shown is the target trajectory for $M_{w,inst,t}$ given by equation 46

Figure 11. C_p and C_m in the reactor (g/cm^3) during the reaction of figure 5. Also shown is the flow rate as modulated by the automatic controller. The control interval is 120s.

Figure 12. Data for η_r and $\eta_{r,inst}$ corresponding to the reaction of figure 9.

Figure 13. Power law plots of $R_{g,inst}$ and $\eta_{r,inst}$ vs $M_{w,inst}$

Figure 14. Automatic M_w controller results when the reactor temperature is changing.

Figure 15. Fractional monomer conversion versus time for varying [CTA]/[monomer], and for three different temperatures: 45^oC, 55^oC, and 65^oC.

Figure 16. Effects on final M_w of changing $[CTA]_0/[M]_0$, T, and $100*[I_2]_0/[M]_0$.

Figure 17: Batch reaction of polyacrylamide with increasing CTA concentration and determination of CTC.

Figure 18. The effect of CTA on intrinsic viscosity [η].

Figure 19. M_w and $M_{w,inst}$ during the production of a bimodal polymer production

Figure 20. The CTA and monomer flow rates into the reactor during the reaction of figure 19.

Figure 21. Behavior of η_r and $\eta_{r,inst}$ for the bimodal reaction of figure 6.

Figure 22. Determination of A and β in equation 48 for $\eta_{r,inst}$ vs $M_{w,inst}$, from the average values of the high and low mass modes.

Figure 23. A trimodal population produced by two additions of CTA.

Figure 24. MWD by both the $M_{w,inst}$ data from ACOMP with the log-normal assumption for instantaneous MWD, and by GPC using PEO calibration standards.

Figure 25. Superposition of normalized bimodal and trimodal MWD from the $M_{w,inst}$ computations.

Figure 26. Copolymer control for constant composition and monomer concentration

Figure 27. Pump rates $Q_{SS}(t)$ and $Q_{Am}(t)$ for Case 1, the reaction of figure 26.

Figure 28. Both composition and M_w are held constant. The horizontal gray lines show the target trajectories for composition, $F_{SS,t}(t)$, and for $M_{w,t}(t)$.

Figure 29. M_w and composition F_{SS} are both targeted to rise linearly. The composition and target trajectories $F_{SS,t}(t)$ and $M_{w,t}(t)$ are shown in gray scale.

Figure 30. Production of a trimodal composition distribution, while holding M_w constant.

Figure 31. Dependence of p on F_{SS}; $p(F_{SS})$, as first defined in equation 50b.

Figure 32. shows the computed values of p, α_{SS}, and α_{Am} for production of the trimodal distribution of figure 30

Figure 33. Average and full model based composition distributions for the trimodal composition distribution

Figure 34. The black trace shows monomer conversion for Am in inverse emulsion

Figure 35. The rising T sequence to produce the target conversion trajectory in figure 34 (blue), and the initiator flow sequence controlled by the operator to follow the target trajectory in figure 34 (red)

Figure 36. Raw dilute solution viscosity traces for the three experiments.

Figure 37. Graphical representation of the NMR pulse sequence used for reactions.

Figure 38. NMR data for the batch (uncontrolled) terpolymerization of Am, Ac, and SS.

Figure 39. The instantanous mass fractions of Am, SS and Ac from combined NMR and UV data from ACOMP for the batch terpolymerization of figure 38..

Figure 40. The M_w and reduced viscosity behavior associated with the batch terpolymerization reaction of figure 38.

Figure 41. First results for composition control of a terpolymerization reaction using combined NMR and UV data from ACOMP.

Figure 42. Contrast between M_w and $M_{w,inst}$, both of which are model-free characteristics determined by ACOMP during polymerization reactions.

Figure 43. The MWD using GPC with PEO standards (grey) and MWD computed from $M_{w,inst}$ histogram (inset) using w_i=w=2 and the use of the corresponding log normal distribution.

Figure 44. Conversion vs time (s) for different levels of O_2 in the reactor during Am free radical polymerization

Figure 45. Effect of O_2 on M_w during free radical polymerization of Am

Figure 46. Model centric framework for integrated simulation, estimation, optimization and feedback control of polymerization systems

Figure 47. Schematic representation of the optimization problem in polymerization processes

Figure 48. Schematic of experimental setup

Figure 49. Flow Diagram of DEKF, PID feedback control and process behavior coupled

Figure 50. State estimation, monitoring and feedback control framework

Figure 51. Confidence ellipsoids for *Ad-f0* and *Ap-At*

Figure 52. Confidence ellipsoids for final estimated parameters

Figure 53. Simulation results applying the optimal trajectories for the decreasing M_w trend

Figure 54. Simulation results using the optimal trajectories for the constant M_w trajectory

Figure 55. Simulation results using the optimal trajectories for the increasing M_w trajectory

Figure 56. Final MWD of optimal trajectories

Figure 57. a) Convergence profile when tuning offline the DEKF free parameters using *ParLMSRBF*-R b) Eigenvalues of the estimation error dynamics for the three OL experiments for different M_w, where ■ increasing, ◆ constant and ● decreasing trajectory.

Figure 58. Results for increasing M_w trajectory OL. a) M_w and M_n time evolution, b) Monomer concentration time evolution, c) Reactor volume time evolution, d) Chain length distribution estimated by DEKF and experimental results, e) Chain length distribution estimated by DEKF evolution along the reaction.

Figure 59. Results for constant M_w trajectory OL. a) M_w and M_n time evolution, b) Monomer

List of Tables

Executive Summary

The goal of this project was to create an energy saving paradigm shift in how polymers are manufactured in the 21st century. It used Automatic Continuous Online Monitoring of Polymerization reactions (ACOMP) integrated for the first time with automatic active control to create the innovative 'ACOMP/Control Interface', or 'ACOMP/CI'. ACOMP/CI will begin the transformation from old, inefficient processes into highly evolved, energy and resource efficient ones. The ACOMP platform is broadly applicable to many types of reactions and processes throughout the vast polymer industry. The industry provides materials for sectors such as automotive, aerospace, oil recovery, agriculture, paints, resins, adhesives, pharmaceuticals and therapeutic proteins, optics, electronics, lightweight building materials, and many more.

The U.S. chemical industry is one of the last major sectors in which the U.S. has top global stature. It consumes 24.4% of all U.S. manufacturing energy, produces over $800B of product annually, supports 25% of the U.S. GDP (via its support of auto, heavy equipment, aerospace, and other sectors) and employs over 6 million people.* It is also a major source of GHG emissions. Polymers make up approximately 30% of this sector. It is estimated that annually 60 TBtu of energy could be saved and 3 million tons less of GHG emissions produced by optimizing production in the polyolefin manufacturing sector alone.

The scope of this project included the first time design and prototyping of an ACOMP/CI, the creation of active reaction controllers coupled to the ACOMP data stream, demonstration of control capabilities on ideal, low concentration polymerization reactions, and a first set of demonstrations towards reactions of a more industrial nature. All these elements of the scope were met, including advances and findings not originally anticipated. Extensions to more complex reactions, beyond the reactor capabilities of the current project ACOMP/CI, such as polyolefins and other high pressure/high temperature reactions, are being proposed in Fall 2017 to CESMII, a DoE based NNMI. This is discussed below.

The initial proposal was for a three year funded project, but this was reduced to a two year project and budget due to funding constraints. Hence, some of the original plans for the project, such as adaptation of the ACOMP/CI to more relevant industrial processes, such as emulsion and dispersion technologies, could not be carried out. A third year of funding was requested at the end of the project, but DoE did not have resources available to grant this.

The sub-contractor Fluence Analytics (previously Advanced Polymer Monitoring Technologies, Inc) designed, prototyped, and commissioned a working ACOMP/CI within the first six months of the project (by June 2015). This gave a leap to the project which avoided the refurbishing of a used ACOMP system for preliminary control interfacing, and led to active manual control of polymerization reactions by the end of the first year.

The control dimension of the project was staged as i) active manual control, ii) active computer-assisted manual control, and iii) fully automatic active control. The reaction characteristics to be controlled were i) conversion kinetics, ii) molecular weight , iii) copolymer composition, and iv) simultaneous molecular weight and composition.

A two pronged control strategy was used. The Tulane/Fluence group took a basic principles approach that did not rely on kinetic models, and took direct advantage of the abundant, realtime polymer and reaction characteristics provided by ACOMP to control polymerization reactions. The LSU group took a more complex, non-linear model-oriented approach which involved complete

* American Chemistry Council research and DoE-EIA energy consumption and emissions survey.

kinetic descriptions of the reaction system together with estimators and Kalman filters. Each of these approaches proved successful in their own way.

Active manual control and active computer-assisted manual control were achieved for controlling reaction kinetics early in the project, after which the project focused exclusively on fully automatic active control. The manual controllers can be of significant value, nonetheless, since, as active control of polymerization is introduced into polymer manufacturing, there will likely be an initial period of adoption in which active manual control will be favored so that operators are directly capable of influencing reactions, as they currently are. It is surmised that, as manufacturers become more accustomed to active control, the fully automatic controllers will soon be implemented.

By April 2016 (the project's second year) fully automatic control of conversion and weight average molecular weight, M_w, trajectories was achieved using the Tulane/Fluence (TF) basic principles controller. Similar results were obtained by the LSU non-linear model controller by August 2016. The demonstration system was aqueous free radical polymerization of acrylamide, Am. The control variables used in these demonstrations were temperature, and semi-batch feed to the reactor of Am monomer and initiator. An early demonstration of active manual conversion control in an industrial process using high solids in inverse emulsion polymerization of Am was achieved.

During the Summer of 2016 the TF controller was used in conjunction with a chain transfer agent, yet another control variable, to automatically produce multi-modal molecular weight distributions, MWD, in a single reactor. Industrially, multi-modal MWD are usually produced by mixing products made in separate reactors, requiring significant extra time, energy, and reactor resources. Recognizing the industrial potential a patent on automatic production of multi-modal polymers was filed, and DoE acknowledged.

In the Fall of 2016 the TF team developed a basic principles controller for copolymer composition and demonstrated it on aqueous free radical copolymerization of the comonomers Am and styrene sulfonate, SS. Shortly thereafter, TF fused the MWD and composition controllers to achieve simultaneous control of both molecular weight and copolymer composition trajectories. Numerous simultaneous trajectories were demonstrated, including a trimodal composition distribution with constant M_w. Meanwhile, the LSU group developed a Kalman filter to improve the results of their automatic molecular weight and conversion controller and successful tests were carried out.

During the project the TF team developed a means of computing full MWD during polymer synthesis without need for any chromatographic separation, based on model distributions. This means that the polymer product is 'born characterized' and this can eliminate post-manufacture analytical laboratory quality control. TF filed a joint patent application on this new approach to chromatography-free determination of MWD with acknowledgment to DoE.

The Tulane group obtained a 60MHz NMR during the project and has recently completed the first work on separating three comonomers, Am, SS, and Na-acrylate, with a first demonstration of terpolymer composition control with the T/F basic principles controller.

Widespread dissemination of ACOMP/CI in the polymer manufacturing sector will bolster DoE goals of energy efficiency and reduced GHG emissions: The ability to monitor and actively control polymerization reactions will lead to more efficient use of energy and non-renewable resources, plant and labor time, increase the safety of manufacturing personnel, and will enhance product quality and lead to feasibility of manufacturing of polymers currently too complex for industrial scale production, while leading to less GHG emissions per kilo of product, and allowing for increased U.S. competitiveness in this enormous manufacturing sector. When ACOMP/CI is expanded to the

polyolefin industry it is estimated that 60 TeraBTU/year of energy can be saved. Much of this saving is anticipated to come from optimized control of grade changeovers in steady state reactors and maintenance of steady states.

Conclusions: Thanks to ACOMP's ability to provide continuous realtime data streams of measured polymer and reaction characteristics it is possible, for the first time, to directly and automatically control free radical polymerization reactions. Two different automatic control approaches were developed. An industrial client of Fluence Analytics has requisitioned the first ACOMP/CI which uses the TF basic principles controller. This sets the stage for FA to add control features to the ACOMP systems it has begun to install on the industrial scale beginning in 2014.

Recommendations: This successful project has been limited to ideal polymerizations not of an industrial sort, albeit early demonstration of conversion control of industrial-type inverse emulsion polymerization was made. The most energy intensive portion of polymer manufacturing is polyolefins. Adoption of ACOMP/CI to this enormous industrial sector faces the enormous challenges of high temperature, high pressure continuous sampling and high temperature sensor operation to obtain the continuous data needed for direct reaction control. The project team has a strategy for achieving this ambitious goal and will present it in Fall 2017 as a proposal to CESMII/DoE. It is recommended that this upcoming proposal be funded in order to make full use of the achievements of this just ended DoE project as the next step towards making polyolefin ACOMP/CI an energy saving reality. It is projected that ACOMP/CI can have its first polyolefin testbed demonstrations within two years of beginning the proposed project.

Introduction

The long range, ultimate goal of this project is to increase energy savings by 60 TBtu in the polymer manufacturing industry, while considerably reducing GHG emissions per kilo of product, via widespread dissemination of ACOMP/CI. Other benefits include more efficient use of non-renewable resources, plant and personnel time, higher quality products, and enhanced worker safety.

The enabling technology is ACOMP (automatic continuous online monitoring of polymerization reactions). Most monitoring technologies attempt to insert sensors into reactors to obtain online data on reactions. For small molecule reactions this is often effective, using different spectroscopic methods, such as near IR (NIR) and mid-IR (MIR), and Raman scattering. For polymerization reactions, however, the reaction medium is frequently too harsh and heterogeneous for immersing sensors. The polymerization reaction is often very viscous (up to 10^6 cP), heterogeneous (e.g. emulsions or dispersions), may contain microgels and other unwanted particulates, and is frequently at high pressure and temperature.

Because of the difficulty of using sensors directly in polymerization reactors the most widely used method for polymerization monitoring in industry is periodic manual sampling of discrete aliquots, typically performed by a technician who directly samples the reactor and then brings the sample to a nearby analytical laboratory, where measurements are then made on this single time point from the reaction. The disadvantages of this industry-standard procedure is that there is a long delay between sampling and measurement, typically one or more hours, making control decisions based on this procedure of little value, and the technicians are exposed to hazardous reactor conditions (e.g. volatile organic compounds), while inordinate amounts of harmful volatile material (e.g. hexane) may be released in the process.

ACOMP approaches the problem as follows: It automatically withdraws a continuous,

small stream of reactor liquid, dilutes and conditions this stream, and thus produces a continuous, analytical quality sample flow that can then be continuously measured by any set of detectors needed to gain realtime data on the polymerization process. This then sets the stage for active control of the polymerization process based directly on polymer and reaction characteristics, such as molecular weight, conversion kinetics, monomer and polymer concentrations, intrinsic viscosity, and copolymer composition.

This DoE project was precisely to couple active reaction control to ACOMP thus creating, for the first time, the ACOMP/Control Interface, or ACOMP/CI. Current control strategies lack the type of direct realtime data provided by ACOMP, and use signals such as temperature, pressure, and flow rates to build indirect, inferential models. While there is some industrial utility to such models, they are typically time and labor intensive to develop, are very specific to given reaction types, and cannot normally handle deviations from model behavior due to common real-world problems (e.g. change of heat transfer coefficients as polymeric debris coats heat exchangers and other elements).

Two approaches to automatic control were taken. The Tulane/Fluence group developed basic principles control that does not involve kinetic models, while the LSU group developed non-linear model-based control.

The target of the first ACOMP/CI was readily accessible reactions. For this free radical reactions of butyl acrylate in butyl acetate at moderate temperatures 45^{o}C to 70^{o}C were targeted, followed by free radical aqueous polymerization of acrylamide (Am) in homogeneous phase. Later, as an early demonstration of basic control in inverse emulsion polymerization of Ac was made, this reaction being representative of industrial reactions.

The results from the ACOMP/CI from this project can be prototyped to perform well for high value specialty polymers, such as acrylates and water soluble polymers such as acrylamide and vinyl pyrrolidone. In fact, Fluence Analytics is currently developing the basic principles controller from the Fluence/Tulane portion of the collaboration into a prototype for a private sector polymer producer. This is an immediate demonstration of industrial interest in the specialty polymer sector. Fluence plans to aggressively pursue opportunities and marketing in this area.

However, the bulk of industrial manufacturing tonnage is in the polyolefin area, including polyethylene, polypropylene, and copolymers of these. There are serious inefficiencies in the polyolefin industry for solution, slurry, and gas phase reactors. The majority of the production involves continuous reactors, and the large inefficiencies are found in two areas; 1) the changeover between polymer product grades, which typically results in the wastage of many tons of polymer per hour, and 2) deviations from steady state during production which lead to off grade materials. As an example, a large manufacturer may be producing 25 tons per hour of polymer in a single reactor, and grade changeover can last from several hours to over one day. Losses during change over can exceed $1M, with corresponding waste of energy and non-renewable feedstocks.

IT is estimated that 60 TBtu per year in the U.S. can be saved by increasing the efficiency of the polyolefin industry alone. Such estimates are based on studies by Franklin Associates, Nexant, and Bloomberg, and correspond well to DoE Chemical bandwidth studies.

While this project has provided a commercialization path for ACOMP/CI in specialty chemicals, the largest energy and GHG reduction will result from bringing ACOMP/CI to the polyolefin industry. The challenges associated with automatic continuous sampling at high

pressure and temperature, production of an analytical grade sample stream, and making continuous high temperature measurements are formidable but surmountable, and the payoff for success will be great.

Because of the intense secrecy of chemical manufacturers' concerning their specific processes, it is essential to seek 'agnostic' support for the polyolefin development. DoE is the agency best poised to support such work in such a fashion that the results will be widely deployed in manufacturing for maximum energy efficiency and GHG reduction. While it is likely that support for such work from a single, large manufacturer might be found, such a business would require exclusivity of the results for a period of time, thus significantly delaying the deployment of the technology.

Development of the high temperature sampling, measurement, and data analysis portion of the polyolefin project will last about two years, during which Tulane will work on the fundamental aspects, whose results are handed off to Fluence for engineering prototype instrumentation. During this development there will be cross-correlations between the continuous polymer and reaction characteristics from ACOMP and the industry standard characterization using GPC, CRYSTAF, TREFF, and other methods. Meanwhile, the LSU and other groups can develop control software and emulators, using a data driven approach, such that when the ACOMP/polyolefin prototype is ready the data stream can be fed directly into the controllers. At the end of the second year the Fluence prototype can be implemented on a testbed, either at a university reactor, or at a company which agrees to extract particular benefit but not to demand exclusivity. The idea is that once a generic polyolefin reaction controller is developed, Fluence can work with specific companies to adapt the technology to their processes.

Background

Quantitative control of polymerization reactions can open the possibility both for more efficient and higher quality production of polymers, and for achieving complex polymeric structures and compositions that might otherwise be unobtainable. The global polymer industry is vast and involves thousands of different products. It is generally recognized that there is a large margin for improved efficiency in the use of energy, non-renewable feedstocks, plant and labor time, and an opportunity for improved worker safety and reduction in emission per kilo of polymeric product. The ability to actively and quantitatively control molecular weight and composition distributions, branching, crosslinking, and other polymer characteristics during synthesis may lead to the ability to produce advanced polymers by specifying the desired properties. Applications requiring highly specific molecular weight distributions (MWD), such as in electronic and optical devices, may benefit from this type of approach.[1,2] It may be especially enabling for stimuli responsive polymers and other that make use of controlled radical polymerization.

The weight average molecular weight M_w and MWD of a polymer are usually the most important characteristics used to assess its properties, and were the focus of this group's first work in active control of polymerization reactions. Obtaining polymer MWD by such methods as Gel Permeation Chromatography (GPC),[3] Field Flow Fractionation (FFF),[4] Matrix Assisted Laser Desorption Ionization – Time of Flight mass spectroscopy (MALDI-TOF),[5] and others, constitutes a sub-field in its own right.

Several methods for attempting to control final MWD have been devised but until now, most are inferential in nature, and none are based on direct, continuous measurements of molecular weight, simply because such continuous measurements have not commonly been available. With the

advent of ACOMP, however, M_w and other properties are continuously and directly measured. Hence, the object of this work is to take these continuous data directly and build a controller for M_w that does not require either a detailed kinetic model or an inferential approach. A model independent histogram representation of the full MWD is also available. To go further a model must be invoked to relate the instantaneous M_w, or $M_{w,inst}$, to specific MWD, such as the binomial distribution, or its daughter geometric and normal distributions. These aspects are addressed in the Results.

Work in polymer reaction engineering has been multidisciplinary, combining monitoring, modeling, control, and optimization approaches.[6] The complexities of time critical data gathering and analyses have tended to separate online monitoring and control approaches in the literature.[7] There are also major distinctions based on reaction scale (microscale, laboratory scale, pilot, and large industrial reactors) and type (batch, semi-batch, continuous), and the nature of the process; homogeneous or heterogeneous phase, bulk, high temperature, high viscosity, etc. [6,7] Currently there is no widely applicable control scheme that incorporates both on-line process multi-variable characterization with active process control.[8]

Small scale research oriented studies maximize accuracy of the information about the system using advanced on-line monitoring techniques.[6,8,9,10] The kinetic information gained from online characterization has been left for future model predictive control (MPC) and process optimization in most cases. Spectroscopic techniques such as on-line GPC,[11] UV, and NMR[12] can be used for direct measurement of process variables, while Raman,[13] ATR FTIR,[14] NIRS,[15] and Low Resolution Raman [16] can be used in combination with other techniques to obtain calibration curves related to conversion, molecular weight, copolymer composition and other process characteristics.[6,11] The limitations of all the above mentioned methods is detailed in the literature.[6] Incorporation of control and online optimization with on-line active process characterization were presented by Skilton et al.,[14] using NMR, and Sans et al.,[17] using ATR FT-IR. Both utilized continuous flow reactors and small molecule esterification reactions, not polymerization reactions, for proof of on-line closed loop optimization. Nogueira and Pinto used near IR spectroscopy and viscosity deduced from reactor stirring torque and used these two measurements together to gauge and automatically control both conversion and molecular weight in a polyurethane reaction using calibration curve fits for the IR and conversion correlation.[15]

Optimization and Control of industrial reactors has been proposed with open loop model predictive control utilizing commonly monitored process variables such as temperature and pressure, and state estimation techniques, extensively described in the literature, to estimate online process data to update the model in real time. A major issue for industrial control applications is the computational time required by state estimation and related techniques. These long times can delay control action leading to dangerous run away reaction situations. Furthermore, observability and convergence are not guaranteed due to the non-linearity of polymerization processes.[18,19] The model utilized must balance the need for high accuracy and precision with the quick response time required for active control[7,18] while maintaining desired quality.[20,21] The most commonly used method for state estimation is calorimetry and much literature has been devoted to the refinement of this technique to estimate the conversion.[11,22,23] Lack of convergences or even observability over the entire reaction[24] and time severally limits this technique for dynamic control throughout an entire reaction. Vega et al[25] proposed an alternative to calorimetry and typical state estimation techniques using aliquot measurements of viscosity and density correlated to molecular weight and conversion, combined with a simplified process model. The use of conversion and molecular weight as the

optimized variables shows how refined online process characterization eases the burden requirement for process control and optimization. [26]

Automatic Continuous Online Monitoring of Polymerization reactions (ACOMP) was introduced in 1998 and used to monitor the free radical polymerization of vinyl pyrrolidone.[27] Since then, it has been used in a wide variety of reactions including controlled radical polymerization, step growth, emulsions and inverse emulsions, and batch, semi-batch, and continuous reactors.[28]

The basic principle of ACOMP is to automatically and continuously withdraw a small sample stream from the polymerization reactor, and conditioning it so that a highly dilute sample stream results, which is of an analytical grade and which flows continuously through a series of detectors chosen to continuously monitor desired characteristics of the reaction; e.g. using multi-angle static light scattering (MALS), refractive index (RI), ultraviolet absorption (UV), and a viscometer, allows weight average molecular weight M_w, intrinsic viscosity [η], and monomer conversion and copolymer co-conversion and composition to be monitored.

Figure 1 shows the principle of ACOMP along with a schematic. It is noted that ACOMP is not a chromatographic method, but a chromatographic system, such as GPC, can be used with it since the continuous dilute, conditioned sample stream is at the same concentration as used for GPC injections.

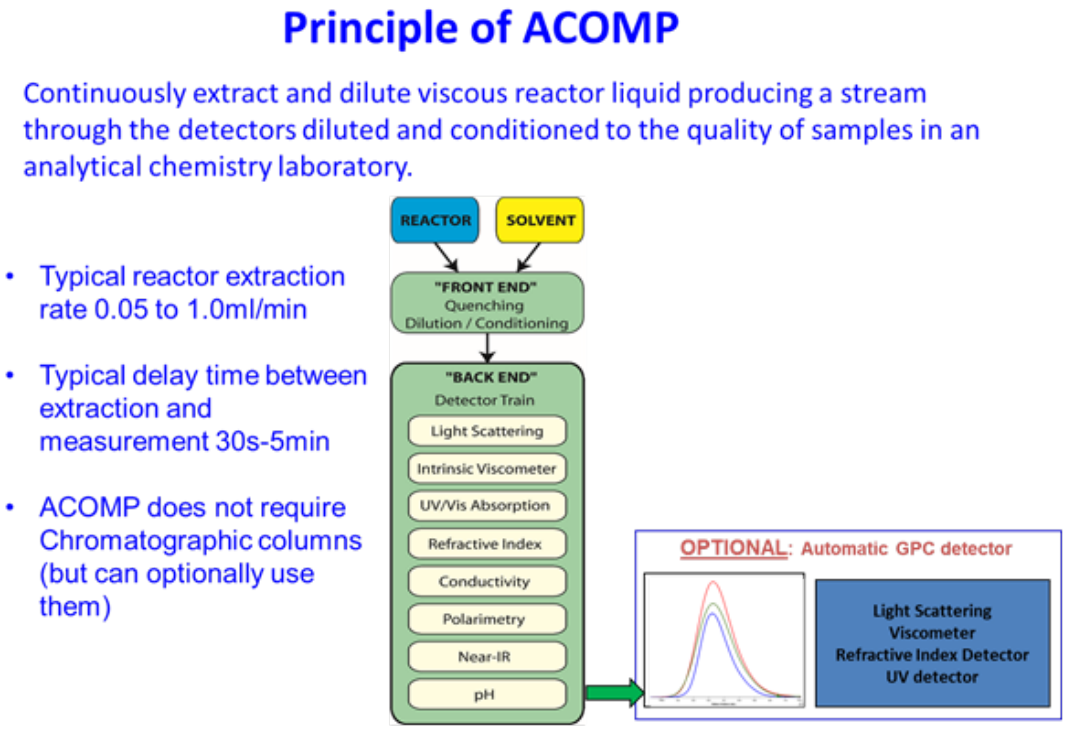

Figure 1. ACOMP principle of operation and schematic

Figure 2 shows typical data from ACOMP, in this case from a batch free radical terpolymerization reaction. It shows how a subset of signals from the UV, light scattering, viscosity, and refractive index detectors change as the comonomers are first added stepwise, and then after the reaction is initiated.

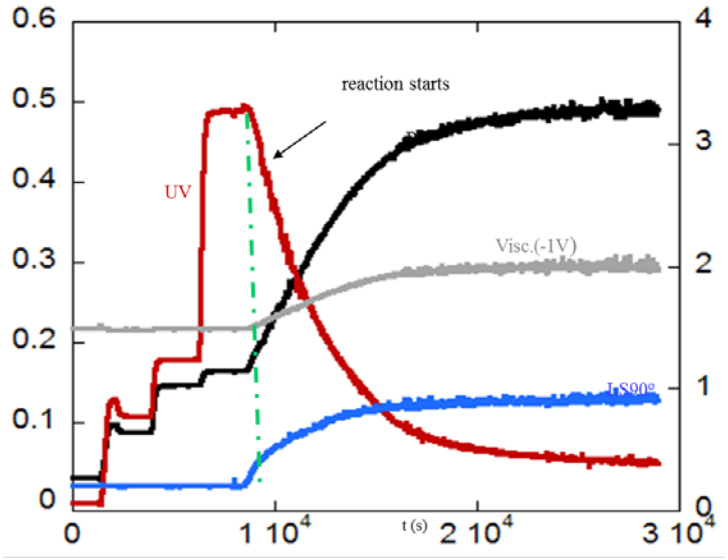

Figure 2. A subset of raw ACOMP detector signals for a free radical terpolymerizati0n reaction

ACOMP was previously used as a means of predicting polymerization trajectories for molecular weight[29] and, separately, for copolymer composition.[30] In those reports, however, there was no active control during the polymerization. Instead, based on kinetics and M_w from prior ACOMP data, feed rates of monomer and comonomers needed to follow a desired path were computed offline, implemented on the ACOMP reactions, and followed without change.

From the beginning the guiding strategy for polymerization reaction control in this project is the following: Target trajectories can be established, versus time or versus polymer concentration, for critical polymer and reaction characteristics, which will lead to very specific endproducts. If a reaction follows the target trajectory then the same product will result each time. Examples include conversion, MWD, intrinsic viscosity, and copolymer composition vs time or vs polymer concentration. In the long run it will be possible to determine which polymer distributions yield which specific properties, and optimal target trajectories leading to these distributions can be computed, and then followed in realtime with ACOMP/CI.

Figure 3 illustrates the above principle. It shows a target trajectory for fractional monomer conversion of Am vs time (black), where the temperature was incremented from T=40^{o}C to 65^{o}C during the reaction (dashed black). In the next step an operator provided active manual control, holding the temperature constant at T= 45^{o}C and manually controlling the pump rate of initiator into the reactor in order to follow the target trajectory. As seen, the active manual control succeeded in keeping the trajectory within 5% of the target trajectory at all times. These two reactions were termed an 'isomorphic reaction pair', since they have the same shape, but the shape is attained in two different ways; i) varying T and holding initiator concentration fixed, and ii) varying initiator concentration and holding T fixed. It is noted that this was the first instance of successful control in the project and preceded the 12-22-2015 go/no-go milestone of active manual control of M_w.

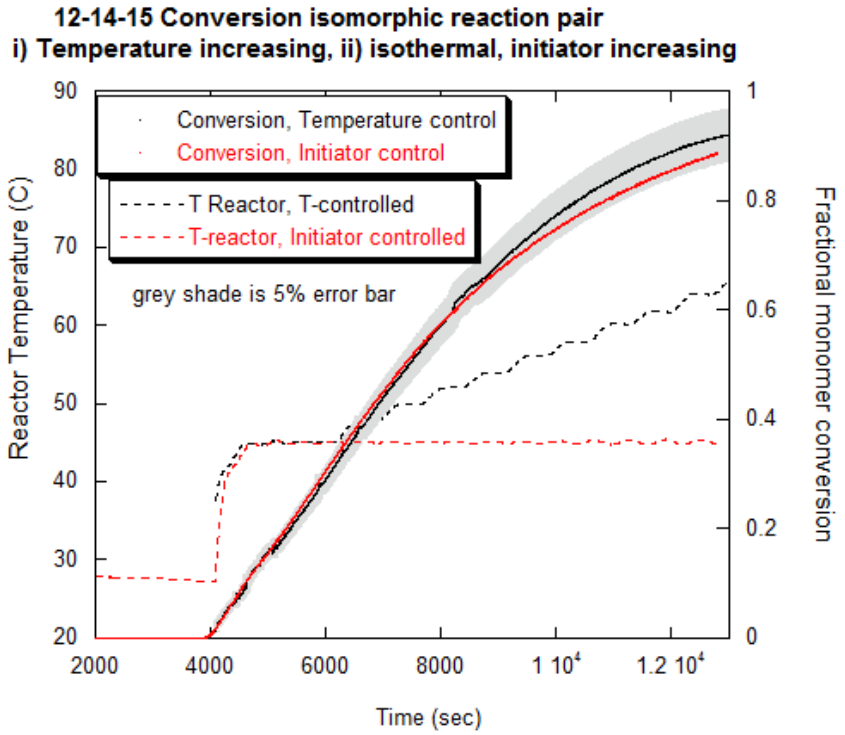

Figure 3. The first success at active manual control of conversion to follow a free radical polymerization target trajectory. This is an isomorphic reaction pair.

The control variables that can be used include temperature, initiator, chain transfer agent, oxygen, nitrogen, comonomers, branching agents, etc.

Figure 4 shows a schematic of how the entire ACOMP/CI works: The extraction pump continuously removes liquid from the reactor recirculation loop, and this stream is diluted and conditioned and fed through the detector train. Via software the detector signal are analyzed to give the process characteristics, such as M_w, conversion, etc., and these are then fed to the process controller. This latter can then actuate various process control variables, such as nitrogen, monomer, initiator, T, etc.

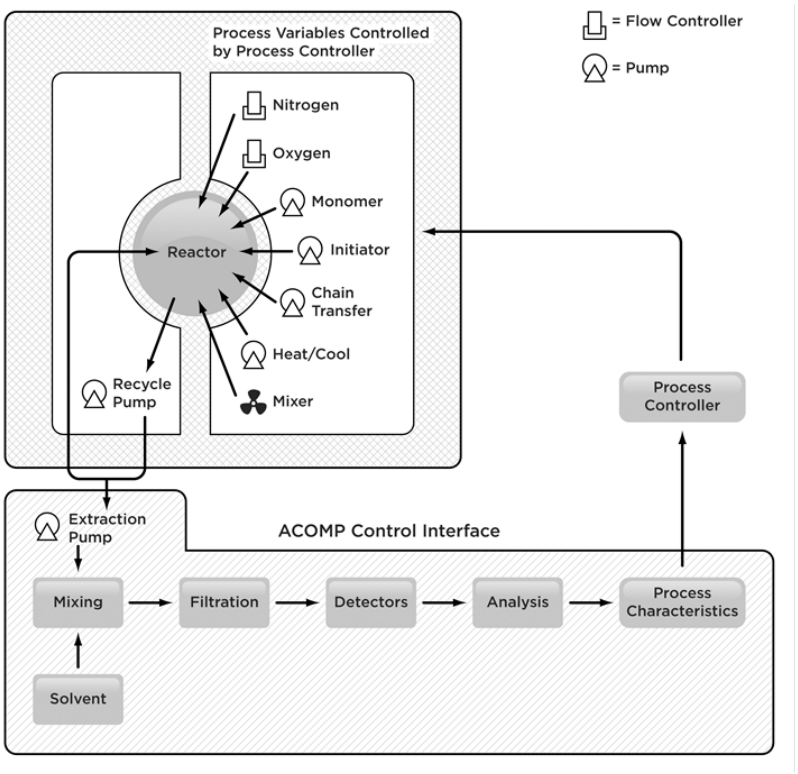

Figure 4. Schematic of the complete ACOMP/CI

In developing the fully automatic controller in this work three steps in active control were made: i) Active manual control, ii) Computationally assisted active manual control, and iii) Active automatic control. Practically speaking any of these approaches can be used for MWD control, since no previous direct means of active control is available, although the automatic one may generally be preferred.

The control strategies use break into two approaches: 1) full non-linear modeling based on full kinetic equations, together with parameter estimation and Kalman filters, and 2) basic principles control where maximum use of the available continuous high level polymer and reaction characteristics is made and basic reaction principles are used rather than full kinetic models.

The agenda for increasing sophistication and control capabilities using aqueous Am free radical polymerization was led by the following path:

1) Control conversion in batch homopolymerization with temperature and initiator concentration
2) Control M_w in batch homopolymerization with temperature and initiator concentration
3) Control conversion in semi-batch homopolymerization using monomer feed to the reactor
4) Control M_w in semi-batch homopolymerization using monomer feed to the reactor
5) Automatically produce multimodal MWD with combined feeds of monomer and chain transfer agent
6) Control copolymer composition in semi-batch operation, using control of reactor feeds from two separate comonomer reservoirs
7) Simultaneously control both M_w and copolymer composition by combining the M_w and composition controllers with dual reservoir feeds. Use this to follow a variety of different M_w and composition target trajectories simultaneously.

In addition

8) Make the first forays into industrially relevant reactions, i) via copolymerization work in 6)-7) above, and by taking a full industrial process, inverse emulsion polymerization of Am, and control conversion.
9) Introduce, for the first time, process NMR (60 MHz) to separate three monomers in terpolymer reactions. This opens the door to three and more comonomers as are frequently used industrially; e.g. adhesive polymer production frequently uses five or more comonomers
10) A model based method for chromatography-free determination of MWD was found during the project.

The project was led from Tulane University, W.F. Reed, PI. The PI has been active in the physical characterization of polymer equilibrium properties and non-equilibrium processes for the past 32 years. This activity has included design and patenting of new instrumentation, new theories and numerical analyses, extensive work with polymer manufacturers and biotechnology companies, training undergraduate, graduate, and postdoctoral students, and co-founding the spin off company Fluence Analytics (previously called Advanced Polymer Monitoring Technologies). He holds numerous patents and has published many articles and book chapters.

The Fluence Analytics lead was Michael F. Drenski, the Chief Technical Officer of Fluence Analytics and a former graduate student of the PI. He has the most extensive experience in the world in prototyping and building ACOMP systems and is co-author on many of the PI's publications. Fluence is an engineering company providing solutions to polymer manufacturers to increase the efficiency of their operations and enable production of more advanced polymeric materials.

Jose A. Romagnoli is the Gordon A. & Mary Cain Chair and M.E. Gautreaux/Ethyl Chair Professor and Fellow of the Australian Academy of Technological Sciences and Engineering at Louisiana State University (LSU). His work experience includes many senior consultancy works for many international private companies. He has supervised a large number of graduate students over his career (50 PhD and7 MS students). He is currently advising at LSU, 5 PhD and two MS students. Jose A. Romagnoli has authored or co-authored over 300 referred journal articles most of which are in the areas of advanced optimal process operations and intelligent systems. He is also the author of two books (one of them a textbook in process control).

Results and Discussion

Bulleted Summary of major milestones

- Fluence Analytics designed and built two first ever ACOMP/CI instruments by 6/2015
- Active manual control of conversion trajectories was achieved by 10/2015
- Demonstration of O_2 as a potential control variable for both kinetics and M_w was made by 11/2015
- Active manual control of M_w trajectories was achieved by 12/2015
- A basic principles, nearly model-free active automatic controller was developed by the Tulane/Fluence group by 3/2016
- The T/F basic principles automatic controller followed target conversion trajectories automatically by 3/2016

- The LSU group developed a first-principles mathematical model by using reaction rate laws available in polymerization literature.
- The LSU model was validated by comparing the simulations with experimental data
- The validated LSU model was used to perform parameter estimation and adjust the kinetic parameters for the proposed system.
- LSU conducted model-based optimization analysis, formulated a nonlinear state estimation strategy, and tested alternative linear and nonlinear control strategies.
- A means for model based chromatography free MWD was completed by the Tulane/Fluence group by 4/2016
- The basic principles automatic controller followed target M_w trajectories by 5/2016
- The basic principles M_w automatic controller was used to produce targeted multimodal molecular weight distributions by 7/2016
- The LSU model based non-linear automatic controller followed conversion target trajectories by 7/2016
- The LSU model based automatic controller followed M_w target trajectories by 8/2016
- LSU group developed and implemented an Extended Kalman Filter (using ACOMP data) to predict all the state variables on real-time has been initiated.
- A basic principles automatic controller for following target copolymer composition trajectories was developed by Tulane/Fluence and used by 9/2016
- A combined basic principles controller for simultaneous control of M_w, conversion, and copolymer composition was achieved by 10/2016
- The CEO of APMT, Inc. (Alex Reed) was listed by Forbes as one of America's thirty leading entrepreneurs under the age of thirty in the area of industry and manufacturing for 2016.
- A 60 MHz NMR was integrated into the ACOMP system in 11/2016
- First terpolymerization reaction monitoring using combined NMR and UV in the ACOMP system was made in 2/2017
- First terpolymerization composition control achieved using combined NMR and UV in ACOMP
- Active manual control of conversion in an industrial type inverse emulsion polymerization was achieved in 1/2017
- The polymerization of acrylamide in water solution using potassium persulfate (KPS) as initiator is studied to demonstrate the effectiveness of the module and framework.
- Fluence Analytics has contracted with an industrial ACOMP client to provide a beta version of the basic principles Tulane/Fluence M_w controller along with the ACOMP
- Fluence Analytics is in discussions with over 30 chemical companies in a range of polymer applications, and many are interested in the future availability of the molecular weight controller technology for their applications.

I. The ACOMP/CI instrumentation

Fluence Analytics (formerly APMT) designed and built the prototype ACOMP/CI in the first seven months of the project, and transferred this to Tulane University where it was commissioned. As part of its cost share, Fluence built a second ACOMP/CI, identical in all respects, except it has a 64 liter pilot reactor and full scale industrial fast loop with heavy duty gear pump, while the Tulane

ACOMP/CI has a 2 liter reactor with a small gear pump and miniature fast loop. Figure 5 shows the two ACOMP/CI systems with the ACOMP cabinet marked, and the separate Control Interface cabinet labeled 'Reactor Control rack'.

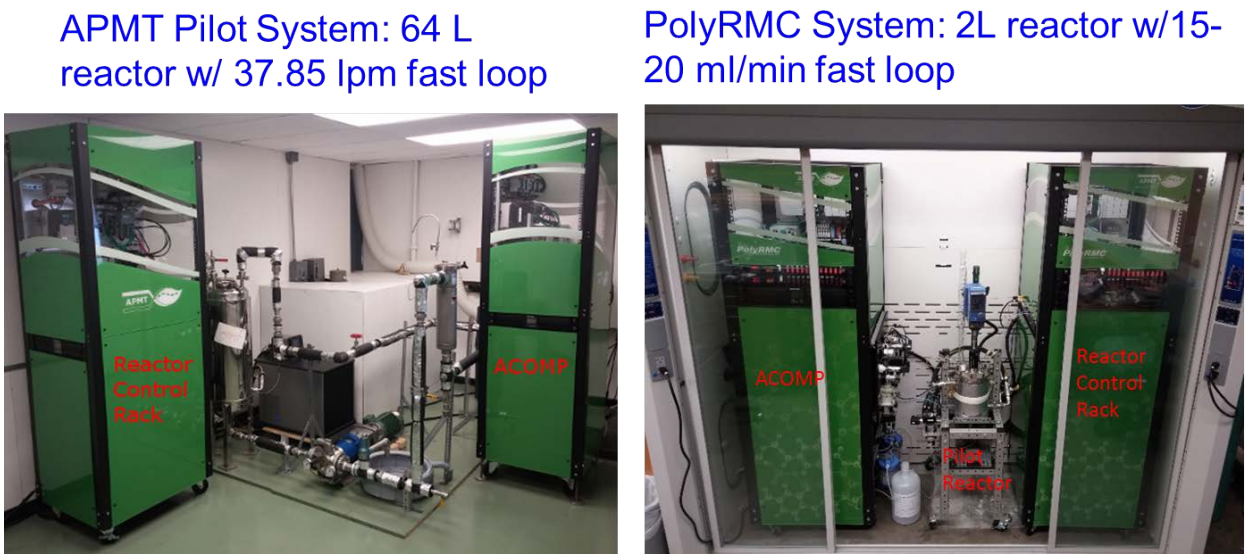

Figure 5. Photographs of the two ACOMP/CI units built by Fluence Analytics. The one on the left was built as partial Fluence Analytics cost-share and is housed at Fluence. The one on the right is housed at Tulane University.

The active manual controller projects continuous, live polymer and reaction characteristics on a computer screen, together with a target trajectory for these characteristics, and an operator manually controls process variables such as temperature and reagent flows to steer the actual reaction trajectory as close to the target trajectory as possible. In the active manual computer assisted mode, a computer processes the characteristics and recommends control actions to the operator to take concerning temperature, reagents flow and other process variables. In the fully automatic controller the controller directly commands pumps, heaters, and all other process variables according to its computations from the ACOMP data stream characteristics.

The operator interacts with the ACOMP/CI system through a custom designed Human-Machine Interface (HMI), built using the Rockwell Factory Talk View SE environment over the Logix5000 programming software. This was interfaced with all ACOMP hardware through a Rockwell Control Logix PLC. All sensor and detector signals were compiled into the Rockwell database tables locally, which were then sent to the ACOMP Analysis package over an Open Platform Communications gateway (OPC). The ACOMP Analysis software was programmed in C^{++}, which interprets all appropriate sensor and detector signals for characterization of the reaction and polymer properties. The ACOMP Controller software, which receives the online analyses data and sends control signals to regulate different process variables, was developed in Python 3.5 which also communicates with the Rockwell automation through the OPC gateway. In the current application the fully automatic active controller regulated the flow rate of Am from the concentrated reservoir into the reactor.

II. Prelude: Active manual control

The plan for ramping up to fully automatic active control involved the preliminary step of active manual control. In this, the operator observes the trajectory of one or more reaction process characteristics and tries to match the ongoing reaction trajectory to a pre-determined target trajectory by controlling one or more process variables.

Figure 6 shows the first achievement in the control of M_w. This met and surpassed the criterion for the go/no-go decision at the end of year one of the project (December 2015). In figure 6 the target trajectory (black) for M_w was established by increasing the reactor temperature from 45°C to 65°C during Am polymerization. This causes M_w to drop more rapidly than in a batch reaction. In a subsequent reaction the operator held the reaction temperature constant at 45°C and manually increased the initiator concentration in order to produce a trajectory (blue) as close to the target trajectory as possible. Increasing initiator has a similar effect on the reaction as increasing temperature; it leads to increased reaction rate and decreased M_w. The two curves in figure 6 represent an 'isomorphic reaction pair in M_w'. They are isomorphic because they have the same shape but are produced by two different means; one by increasing T and holding initiator concentration constant, and the other by holding temperature constant and increasing initiator concentration.

The trajectory of the second reaction followed the target trajectory to within 10% or less during the entire reaction. The original DoE SOPO for the go/no-go decision called for agreement within 35%. Hence, this experiment on 12-21-2015 exceeded the go/no-go criterion and fell within the projected timeline.

This paved the way for fully automatic control, described below.

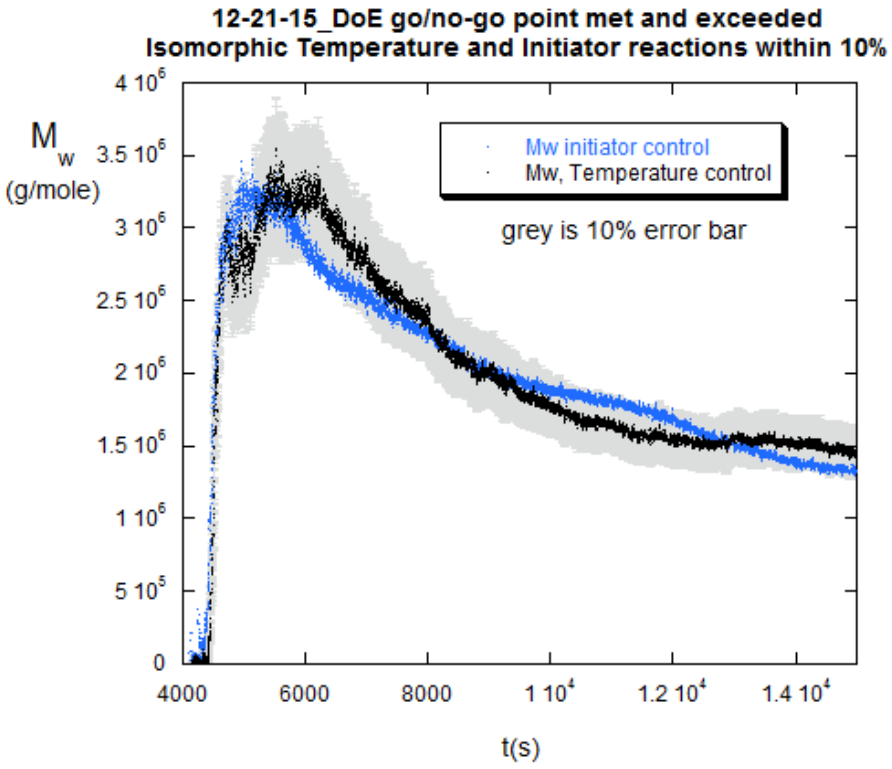

Figure 6. The first active manual control of M_w during Am polymerization

III. The basic principles Tulane/Fluence automatic controller

In parallel with the model based non-linear control developed by the LSU group, a basic principles approach was taken that seeks to maximize the benefit of the continuous ACOMP stream of polymer and reaction characteristics, and minimize dependence upon any specific kinetic models.

1. Conversion and M_w control

III.1.1 Approach to the basic principles Tulane/Fluence controller

It is evident that a specific trajectory of M_w vs time will yield a specific MWD, because each small interval of M in the MWD is visited by the trajectory during the production of an interval of polymer concentration. Conversely, given a desired MWD a multitude of trajectories can be found which will yield it. In this work the subject of the optimal trajectory is not addressed, and the focus is on proving that, once a specific target M_w trajectory is established, $M_{w,t}(t)$, it can be followed by the controller during the polymerization reaction. Later work will focus on specific MWDs and optimization of trajectories. Optimization of chemical processes, in general, is a highly developed field.[31,32]

The term 'trajectory' needs explanation. Time is the natural independent variable during a reaction and ACOMP measures the relevant quantities of monomer and polymer concentration and weight average molecular weight, C_m, C_p, and M_w, respectively, directly in time. However, having these quantities at each instant means that any of them can be used as a variable against which the others can be mapped. The specification of MWD depends on how instantaneous weight average molecular weight, $M_{w,inst}$, builds with C_p, so that C_p is the natural variable to be used against which to measure the trajectory of M_w; i.e. $M_w(C_p)$ is the favored representation of trajectory. Concretely, for polymerization reactions for which the time to produce a polymer chain is much shorter than the total reaction time, e.g. free radical polymerization, the relationship between $M_w(C_p)$ and $M_{w,inst}(C_p)$ is, by definition

$$M_w(C_p) = \frac{\int_0^{C_p} M_{w,inst}(C_p')dC_p'}{C_p} \tag{1}$$

$M_w(C_p)$ is measured directly from light scattering and concentration detectors in the ACOMP system. $M_{w,inst}(C_p)$ can be computed from the ACOMP value of $M_w(C_p)$ according to equation 1 by

$$M_{w,inst}(C_p) = \frac{d\left[C_p M_w(C_p)\right]}{dC_p} \tag{2}$$

Computation of $M_{w,inst}$ from the primary ACOMP values of M_w and C_p allows the instantaneous weight average of the MWD to be followed, and a histogram representation of the MWD to be made as synthesis proceed. The histogram, however, does not take the instantaneous MWD into account. Up to this point all quantities are model-independent and based on primary detector measurements. While the histogram representation is very useful to gauge the width and to detect multi-modal populations, it will underestimate the polydispersity that results from the full MWD, since it includes no information on the instantaneous MWD or polydispersity. Below, it will be shown that if a model-dependent assumption on the form of the instantaneous MWD is made, e.g. the Flory-Schulz distribution, then the $M_{w,inst}$ histogram can be used to estimate the polydispersity indices M_w/M_n, M_z/M_w and others, and to also make continuous MWD representations, if desired, similar to those obtained by GPC or other separation methods.

It is important to note that from *any* cumulative property measured by ACOMP, $Y(C_p)$, the instantaneous value $Y_{inst}(C_p)$ can be computed by

$$Y_{inst}(C_p) = \frac{d\left[C_p Y(C_p)\right]}{dC_p} \tag{3}$$

$Y(C_p)$ can include such properties as comonomer composition, reduced or intrinsic viscosity, diffusion coefficient, polymer dimensions, etc. Some of these will be considered in the results below.

Now, the ACOMP controller is based on two basic principles and does not involve any detailed kinetic or inferential models with many parameters. These principles are:

i) *The instantaneous kinetic chain mass M_ν is proportional to C_m, and $M_{w,inst}$ is proportional to the kinetic mass M_ν*

$$M_{w,inst} = aM_\nu = pC_m \tag{4}$$

This is a fundamental principle of linear free radical chain growth polymerization. The proportionality constant p subsumes all the complex parameters that constitute the relationship in equation 4, without the need to explicitly know any of them. In a typical standard free radical kinetic model, for example, p would be given by

$$p = d\,\frac{k_p}{k_t[R] + k_3[CTA]} \tag{5}$$

where k_p is the propagation constant, k_t is the termination constant, k_3 is the chain transfer constant, [R] is the free radical concentration, [CTA] is the concentration of chain transfer agent , and d is a dimensionless constant on the order of unity that depends on what percentage of termination is by disproportionation and what by recombination, as well as the instantaneous relationship between the weight average chain length and most probable (kinetic) chain length.

Each of these parameters can be steep functions of temperature and to further increase the complexity of p, [R] is composed of additional terms. In the free radical polymerization quasi-steady state approximation (QSSA),[33] for example,

$$[R] = \sqrt{\frac{2Fk_d[I_2]}{k_t}} \tag{6}$$

where F is the initiator efficiency, k_d is the initiator decomposition rate constant, and $[I_2]$ is the initiator concentration. These can also have steep temperature dependences, and $[I_2]$ is generally time dependent.

The robustness of the ACOMP controller in its current form derives from the fact that none of these many parameters, and how they change during the reaction, need be known. After having an Ansatz value of p, e.g. from a previously monitored batch reaction, p can be re-computed at intervals during a reaction and the new value will subsume changes in all the parameters into this single, experimentally measured parameter, without requiring any specific kinetic model. The first re-computation of p during the reaction will also correct errors in the Ansatz value.

ii) *The rate of polymerization of monomer is proportional to the concentration of monomer*. That is

$$\frac{dC_m}{dt} = -\alpha(t)C_m \tag{7}$$

This is the standard first order or pseudo-first order expression that controls myriad processes in nature, from radioactive decay and spontaneous atomic emission spectra, to biological populations. The proportionality parameter $\alpha(t)$ may change in the course of time so that equation 7 yields an

exponential solution only when α is constant in time. For free radical polymerization $\alpha(t)$ subsumes several other parameters. For example, in a typical kinetic model

$$\alpha(t) = k_p[R] \tag{8}$$

where [R] can change in time due to changes in parameters, for example, those in equation 6, and k_p can change both due to temperature, chain length, viscosity of the reaction milieu, and other quantities.

Again, the robustness of the ACOMP controller resides in the fact that after an Ansatz value of $\alpha(t)$ is used, e.g. as determined in a previously monitored batch reaction, α can be re-computed at intervals during a reaction and the new value will subsume changes in all the parameters into this single, experimentally measured parameter, without requiring any specific kinetic model. The re-computation of $\alpha(t)$ during the reaction will also correct errors in the Ansatz value. It is noted that the controller makes no assumption of a simple exponential first order reaction, since $\alpha(t)$ can change during the reaction.

III.1.2 Instrumentation and data analysis background

The ACOMP Process Flow Diagram was shown in Figure 4. The sample is continuously extracted from the reactor recirculation loop at a rate between 0.25 and 0.50 cm^3/minute, depending on the experiment, by the Extraction Pump and is immediately quenched and diluted 80x with solvent (distilled water in these experiments) from the Solvent Pump, and homogenized in the Mixing Chamber, from which the sample flows through a 4 wavelength UV/Vis detector UV/Vis 159 detector by Gilson, (Middleton, WI.), which continuously monitors the absorption of the monomer during the polymerization. Polymer conversion was calculated using the 245 nm wavelength. After flowing through the UV/Vis detector, a fraction of the sample stream is diverted by an Isocratic Pump to achieve a continuous and pulse free flow through the remaining detector train comprising a custom built Multi Angle Laser Light Scattering (MALS) detector, with four angles; 65^o, 90^o, 115^o, 130^o , and a custom built single capillary Viscometer. Based on the reaction and polymer characteristics determined by the ACOMP/CI the reactor temperature, nitrogen, monomer or initiator feeds can be adjusted to control the desired aspects of the polymerization; in this work the trajectories of the total C_m and M_w were controlled by manual active control using temperature and initiator flow in batch mode, and full active automatic control of C_m and M_w was achieved with monomer flow in semi-batch mode.

The delay from the reactor to the first detector, the UV, is 85 seconds. To correct for this delay time in the control computations, forward linear regression from the previous 30 seconds to the current instant, t, of real-time was used for C_m, which controls $M_{w,inst}$ via equations 4 and 5.

Use of UV absorption, viscosity, and MALS to compute monomer and polymer concentration, reduced viscosity, η_r, M_w and z-average mean square radius of gyration $\langle S^2 \rangle_z$ have been detailed in previous ACOMP publications.[32,33] For the latter, the usual Zimm equation was used,[34,35] where $I_R(\theta)$ is the excess Rayleigh scattering ratio from the polymer solution at scattering angle θ

$$\frac{KC_p}{I_R(\theta)} = \frac{1}{M_w}\left(1 + \frac{q_s{}^2 < S^2 >_z}{3}\right) + 2A_2C_p \tag{9}$$

where, C_p is polymer concentration, q_s is the magnitude of the scattering vector

$$q_s = \frac{4\pi n}{\lambda}\sin(\frac{\theta}{2}) \tag{10}$$

K is an optical constant, given for vertically polarized incident light by

$$K = \frac{4\pi^2 n^2 (dn/dC_p)^2}{N_A \lambda^4} \tag{11}$$

where dn/dC_p is the differential index of refraction for the polymer in a solvent of refractive index n, N_A is Avogadro's number and λ is the vacuum wavelength of the incident laser. For Am in water $dn/dc=0.181 cm^3/g$ was used, n=1.333, and λ=660nm from a 35mW Laser Max linearly polarized miniature diode laser.

In equation 9 A_2 is a complex average of the second virial coefficient. It was found on end products to be $3.29x10^{-4}$ cm^3-Mole/g^2 +/- 20% and was only weakly dependent on M_w, and was hence used as a constant correction factor. The maximum concentration of pAm in the detector train was $4x10^{-4}$ g/cm^3, which leads to a correction factor in equation 9 of $2A_2M_wC_p$~0.26, for a value of M_w~10^6g/mole in the estimate. With an error bar of 20% on A_2 this leads to a maximum systematic error of 5% for M_w at maximum concentration and high M_w.

III.1.3 Details of the conversion controller

In this first version of an automatic feedback ACOMP controller a single control variable is used, the flow rate of monomer from a concentrated monomer reservoir (51% Am) into the reactor; i.e. semi-batch operation is used. This flow rate is designated Q(t), and it is the automatic computation of Q(t) and the automatic setting of the reservoir pump to the computed value that provides the M_w control needed to follow the target trajectory $M_{w,t}(t)$. The ACOMP extraction rate from the reactor is q(t), which is usually small, between 0.25 and 0.5 cm^3/min, and held constant. It is treated as negligible in the following. This outflow from the reactor provides the continuous sample stream that is diluted and conditioned for the ACOMP measurements. V(t) is the volume of liquid in the reactor and V_o is the initial volume.

The change in monomer concentration dC_m over an interval dt is given by

$$dC_m = \left(-\alpha(t)C_m + \frac{C_m'}{V(t)}Q(t) \right)dt \tag{12}$$

where the rate principle of equation 7 is used together with the addition of monomer to the reactor via the pump rate Q(t). C_m' is the concentration of monomer in the reservoir and V(t) the reactor volume as a function of time.

Monomer concentration control. Equation 12 allows $C_m(t)$ to be the controlled process characteristic, which can frequently be valuable in its own right, and is just one step away from control of M_w, once p is introduced. Let $C_{m,t}(t)$ be the target trajectory for $C_m(t)$. The object will then be to make $C_m(t)$ in a reaction follow $C_{m,t}(t)$

The controller now breaks the reaction up into finite control intervals Δt_i, where Δt_i is the duration of the i^{th} control interval, and Δt_i is very short compared to the duration of the entire reaction, which allows changes in variables and characteristics to be approximated as linear over the short intervals. At the beginning of control interval i, which starts at t_i, the required amount of

monomer change over this interval, $\Delta C_{m,t,i}$, is the target trajectory value at $t_i+\Delta t_i$ minus the current measured value $C_m(t_i)$, that is

$$\Delta C_{m,t,i} = C_{m,t}(t_i + \Delta t_i) - C_m(t_i) \tag{13}$$

Expanding dt to Δt_i in equation 12, and using equation 13, $Q(t_i)$ is computed by

$$Q(t_i) = \frac{V(t_i)}{C_m'}\left[\frac{\Delta C_{m,t,i}}{\Delta t_i} + \alpha(t_i)C_m(t_i)\right] \tag{14}$$

The ACOMP controller then sets the monomer feed pump to $Q(t_i)$ at t_i. $C_m(t_i)$ in equation 14 is the measured value of $C_m(t)$, not the target trajectory value.

In equation 14 $\alpha(t_i)$ is the latest value of $\alpha(t)$. $\alpha(t_i)$ can be computed over any previous time interval $\Delta\tau$ during the reaction as follows. The rate at which polymer is produced is

$$\frac{dC_p}{dt} = \alpha C_m \tag{15}$$

so that the polymer concentration at any time, by mass balance, is

$$C_p(t) = C_{m,o} - C_m(t) + \frac{C'}{V(t)}\int_0^t Q(t')dt' \tag{16}$$

where $C_{m,o}$ is the initial amount of monomer in the reactor. $C_m(t)$ is measured directly by ACOMP, $\int_0^t Q(t')dt'$ is known by automatic integration of the pump flow rate and V(t) is given by

$$V(t) = V_0 - qt + \int_0^t Q(t')dt' \tag{17}$$

where q is the constant ACOMP withdrawal rate. Hence, $\alpha(t_i)$ can be computed over any previous time interval $\Delta\tau$ before t_i by

$$\alpha(t_i) = \frac{\Delta C_p(\Delta\tau)}{C_m(t_i - \Delta\tau)\Delta\tau} \tag{18}$$

The actual value of $\Delta\tau$ used depends on signal/noise considerations and does not have to correspond to the control interval values Δt_i.

Figure 7 shows an example of monomer concentration control using the above approach. In this it was decided that a non-monotonic trajectory for $C_{m,t}(t)$ would be interesting, to set it apart from a simple exponential decay in a corresponding batch reaction. A sinusoid of the form

$$C_{m,t}(t) = 0.010 + 0.002\sin(\omega t) \quad (\mathrm{g/cm^3}) \tag{19}$$

was used, where $\omega=2.5\times10^{-4}\pi$ radians/s. The reaction was carried out at T=55°C.

The controller result is quite excellent and falls well within a 2% error bar from the target trajectory, and is in fact indistinguishable from the target trajectory in the first half of the cycle. Also shown in Figure 7 for contrast is the monomer concentration trajectory in an equivalent pure batch

reaction with no monomer feed; i.e. the controller follows a conversion trajectory very different from the natural batch trajectory.

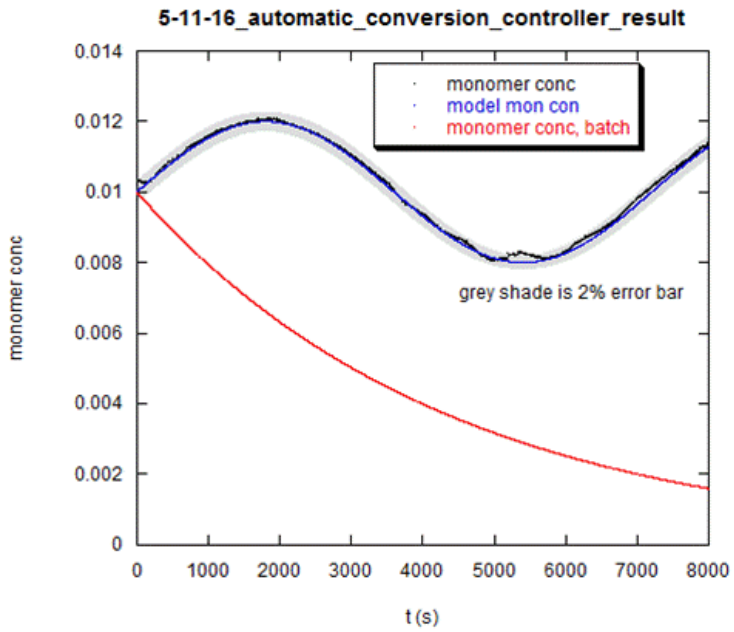

Figure 7. Automatic control of conversion (black) along a sinusoidal target trajectory (blue). Also shown is the uncontrolled batch trajectory (red).

While the purpose of the reaction was to control C_m it is interesting to see the corresponding result for M_w and $M_{w,inst.}$. These are shown in Figure 8. $M_{w,inst}$ follows roughly the sinusoidal form of $C_m(t)$, whereas M_w has a damped sinusoidal form.

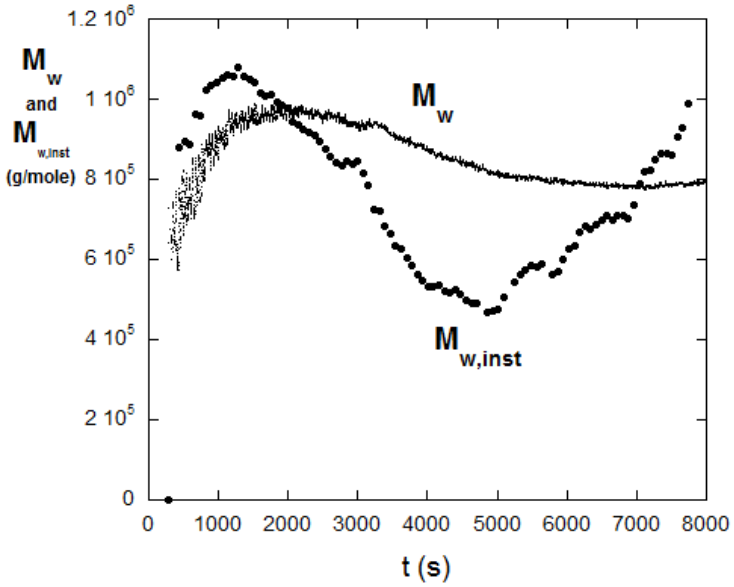

Figure 8. M_w and $M_{w,inst}$ for the reaction shown in figure 7.

III.1.4 M_w control and results

The previous section has set the stage for M_w control, including a description of how $\alpha(t_i)$ is computed. To control M_w requires use of the proportionality parameter p(t) introduced in equation 4. First, a target trajectory for $M_{w,inst}$ or $M_w(t)$ is decided upon. For the former, the target trajectory is denoted $M_{w,inst,t}(t)$. In further practice this is better represented in terms of C_p, $M_{w,inst,t}(C_p)$, as discussed above. The $M_{w,t}(C_p)$ control trajectory is then determined according to equation 1. Since $C_p(t)$ is known the representation in terms of $M_{w,inst,t}(t)$ will be used in the following. The subscript 'i' in t_i and Δt_i will also be dropped for ease of notation.

Consider that from a time t to a time Δt in the future $M_{w,t}(t+\Delta t)$ can be written as

$$M_{w,t}(t+\Delta t) = \frac{\int_0^t M_{w,inst,t}\,dC_p + \int_t^{t+\Delta t} M_{w,inst,t}\,dC_p}{C_p + \Delta C_p} \approx \frac{\left(\int_0^t M_{w,inst,t}\,dC_p + \int_t^{t+\Delta t} M_{w,inst,t}\,dC_p\right)}{C_p}\left(1-\frac{\Delta C_p}{C_p}\right) \tag{20}$$

where $M_{w,t}(t+\Delta t)$ is the value the experimental $M_{w,e}$ should be at $t+\Delta t$, where $M_{w,e}(t)$ is the experimentally measured value from ACOMP, and the approximate expression on the right is the expansion of $1/(C_p+\Delta C_p)$ to first order. This will apply after some C_p has been accumulated, to justify the series truncation; i.e. when $C_p >> \Delta C_p$. It is also necessary to accumulate a finite C_p in order to get an accurate measurement of $M_{w,e}(t)$ from the ACOMP light scattering detector.

Now, the first integral is what the target $M_{w,t}(C_p)$ *should* be at t, whereas it is desired that the target $M_{w,t}(t+\Delta t)$ be reached at $t+\Delta t$. Hence, the trajectory has to be corrected over t to $t+\Delta t$ to achieve this, and the interval starts at the real, experimentally measured $M_{w,e}(t)$. Hence, the first integral from 0 to C_p is replaced by $M_{w,e}(t)$. Further, calling $<M_{w,inst,t}>$ the average $M_{w,inst}$ over the concentration interval $C_p(t)$ to $C_p(t+\Delta t)$ allows the theorem of the mean to be invoked for the second integral in equation 20, so that, again to first order in $\Delta C_p/C_p$,

$$M_{w,t}(t+\Delta t) = M_{w,e}(t)\left(1-\frac{\Delta C_p}{C_p}\right) + \frac{< M_{w,inst,t} > \Delta C_p}{C_p} \tag{21}$$

where $\Delta C_p = C_p(t+\Delta t) - C_p(t)$, and the experimental instantaneous weigh average $M_{w,inst,e}$ is used to define $M_{w,e}(t)$ according to

$$M_{w,e}(t) = \frac{\int_0^t M_{w,inst,e}\,dC_p}{C_p} \tag{22}$$

Now, $\Delta M_{w,t}(t)$ is defined to be the increment in M_w that must occur over time Δt in order for $M_{w,e}(t+\Delta t)$ to be equal to $M_{w,t}(t+\Delta t)$

$$\Delta M_{w,t}(t) = M_{w,t}(t+\Delta t) - M_{w,e}(t) \tag{23}$$

This allows equation 21 to be re-written as

$$\Delta M_{w,t}(t) = \left(< M_{w,inst,t} > - M_{w,e}(t)\right)\frac{\Delta C_p}{C_p} \tag{24}$$

using the relationship between $<M_{w,inst,t}>$ and the average monomer concentration $<C_m>$ over the interval t to $t+\Delta t$

$$< M_{w,inst,t} >= p(t) < C_m > \tag{25}$$

and

$$\Delta C_p = \alpha(t) < C_m > \Delta t \tag{26}$$

leads to the quadratic equation

$$< C_m >^2 - \frac{M_{w,e}(t)}{p(t)} < C_m > - \frac{\Delta M_{w,t}(t) C_p}{p(t)\alpha(t)\Delta t} = 0 \tag{27}$$

This yields the solutions

$$< C_m >= \frac{M_{w,e}(t)}{2\,p(t)} \pm 0.5 \left(\left(\frac{M_{w,e}(t)}{p(t)} \right)^2 + \frac{4 C_p \Delta M_{w,t}(t)}{\alpha(t)\, p(t) \Delta t} \right)^{1/2} \tag{28}$$

This controller assumes that control intervals are short enough that the quantities change linearly over the control intervals Δt, which are much shorter than the duration of the reaction. Hence

$$< C_m >= \frac{C_m(t + \Delta t) + C_m(t)}{2} \tag{29}$$

so that

$$C_m(t + \Delta t) = 2 < C_m > - C_m(t) \tag{30}$$

and the required change in C_m over the control interval Δt is

$$\Delta C_m(t) = 2\left[< C_m > - C_m(t) \right] \tag{31}$$

Using $\Delta C_m(t)$ and Δt in place of dC_m and dt, respectively, in equation 12 gives the flow rate Q(t) to which the monomer feed pump should be set over the entire control interval Δt

$$Q(t) = \frac{V(t)}{C'} \left(\frac{2\left[< C_m > - C_m(t) \right]}{\Delta t} + \alpha(t) C_m(t) \right) \tag{32}$$

where $<C_m>$ is from equation 28.

As mentioned after the Ansatz value of p is used it is re-computed over any interval $\Delta\tau$ before t by

$$p(t) = \frac{1}{C_m(t)} \left(M_{w,e}(t) + \frac{C_p(t) \Delta M_{w,\exp}(t)}{\alpha(t) C_m(t) \Delta \tau} \right) \tag{33}$$

where $\Delta M_{w,exp}(t)$ is the difference between $M_{w,e}(t)$ and $M_{w,e}(t-\Delta\tau)$

$$\Delta M_{w,\exp}(t) = M_{w,e}(t) - M_{w,e}(t - \Delta\tau) \tag{34}$$

There are several physical limits that constrain the solutions to the addition of monomer to the reactor. One of these is that $M_{w,e}(t)$ cannot fall faster than the batch rate that occurs when Q(t)=0. This limit can be extended if the controller adds extra initiator or the temperature increases, or if a

controller that includes chain transfer agent (CTA) is incorporated. In this latter case the CTA does not affect the reaction kinetics and can cause much larger reductions in M_w than either initiator or temperature increases. Extension to CTA is currently underway.

Considering the limits imposed by equation 28 leads to three cases to distinguish.

1) If $\Delta M_{w,t}(t)>0$ then the positive root of equation 28 must be used, otherwise an unphysical negative $<C_m>$ would be obtained ; i.e.

$$< C_m >= \frac{M_{w,e}(t)}{2\,p(t)} + 0.5\left(\left(\frac{M_{w,e}(t)}{p(t)}\right)^2 + \frac{4C_p\Delta M_{w,t}(t)}{\alpha(t)\,p(t)\Delta t}\right)^{1/2} \quad \text{for } \Delta M_{w,t}(t) > 0 \qquad (35)$$

2) Equation 24 shows that $<M_{w,inst}>$ can become negative if $\Delta M_{w,t}(t)$ is sufficiently negative. $<M_{w,inst}><0$ is unphysical and such an $\Delta M_{w,t}(t)$ cannot be achieved over the control interval Δt, and the only recourse is to set the pump flow rate to zero, Q(t)=0, and wait until $M_{w,e}(t')=M_{w,t}(t')$ at some point t' which is greater than $t+\Delta t$. The condition for setting Q(t)=0 over the control interval Δt is, if

$$\Delta M_{w,t}(t) < -\frac{\alpha C_m \Delta t M_{w,e}(t)}{C_p}, \text{ then Q(t)} = 0 \qquad (36)$$

As mentioned, this limit can be extended if other control variables, such as CTA, temperature, or initiator are used.

3) The square root in equation 28 will be negative and hence the solution will be imaginary and unphysical, so that no monomer will be added over the control interval and so Q(t)=0 over the control interval when

$$\Delta M_{w,t}(t) < -\frac{M_{w,e}(t)^2\,\alpha\Delta t}{4pC_p}, \text{ then Q(t)} = 0 \qquad (37)$$

4) The negative root of equation 28 is used as follows:

If

$$-\frac{\alpha C_m \Delta t M_{w,e}(t)}{C_p} \le \Delta M_{w.t}(t) < 0 \text{ and } -\frac{M_{w,e}(t)^2\,\alpha\Delta t}{4pC_p} \le \Delta M_{w,t}(t) < 0 \qquad (38)$$

then

$$< C_m >= \frac{M_{w,e}(t)}{2\,p(t)} - 0.5\left(\left(\frac{M_{w,e}(t)}{p(t)}\right)^2 + \frac{4C_p\Delta M_{w,t}(t)}{\alpha(t)\,p(t)\Delta t}\right)^{1/2} \qquad (39)$$

It is noted that this is not a simple 'bang-bang controller', such as are found, for example, in a thermostat controlled heating system, where the heating element is either switched on or off.

M_w controller results for linearly increasing M_w vs t, at T=45^{o}C. Figure 9 shows an example result for an application of the M_w controller. For this an $M_{w,t}(t)$ target trajectory was

chosen as linearly increasing in time with a slope of 50.00 g/mol-s and an $M_w(0)$ of $3.5x10^4$ g/mole. The reaction was carried out at T=45°C and had a starting monomer concentration $C_{m,0}$=0.005 g/cm^3. The control interval was kept uniform at $\Delta t_i=\Delta t$=120s. This increasing M_w gives good contrast to a corresponding batch reaction in which $M_w(t)$ decreases, which is also shown in Figure 9. The overall slope for the controlled M_w was 50.02 g/mol-s, less than 0.1% away from the target slope. The target trajectory was met by the controller within a 6% error bar. The early oscillatory swings about the model path are due to the use of Ansatz values for α and p deliberately far from the actual values, which allowed these latter values to self-correct and hence bring the reaction very close to the control trajectory. The A_2 term in equation 9 was negligible through most of the reaction, increasing at the end to 8%.

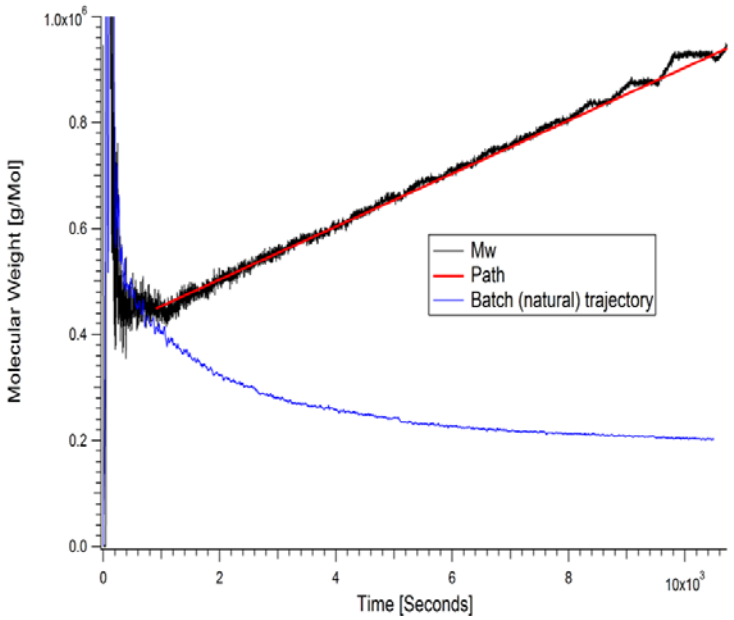

Figure 9. Linearly increasing target M_w trajectory (red), and the reaction that followed it (black). Also shown is the uncontrolled, batch trajectory for M_w.

Equation 2 was used to compute the experimental values of $M_{w,inst}$, denoted $M_{w,inst,e}$, from $M_{w,e}(t)$. The results are shown in figure 10, with $M_{w,e}$ also shown to contrast the two quantities. Using equation 1 the target trajectory for $M_{w,inst,t}$ can be computed from the target trajectory $M_{w,t}(t)=M_{w,o}+st$, where M_w is in g/mole, and t in seconds, and $M_{w,o}=3.5x10^4$ and s=50.0 g/mole-s. This yields

$$M_{w,inst,t}(t) = M_{w,t}(t) + s\frac{\left(t + st^2/2M_{w,o}\right)}{\left(1 + st/M_{w,o}\right)} \tag{40}$$

The curve of $M_{w,inst,t}$ through $M_{w,inst,e}$ in figure 10 follows equation 46 and is not a fit

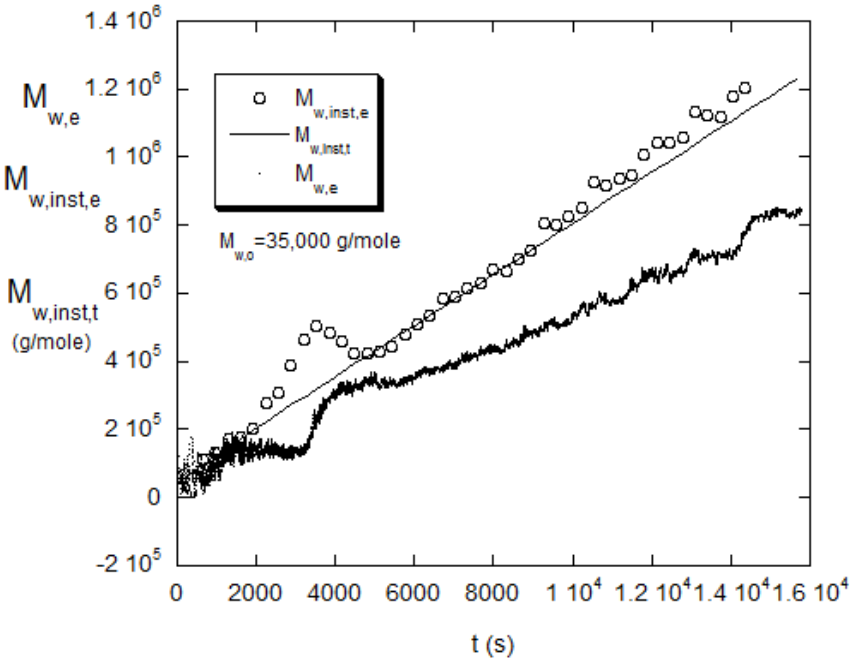

Figure 10. $M_{w,inst,e}$ computed from $M_{w,e}$ via equation 2 is shown, together with $M_{w,e}$. Also shown is the target trajectory for $M_{w,inst,t}$ given by equation 46

Figure 11 shows both $C_m(t)$ and $C_p(t)$ from the reaction of figure 9. The fluctuations in C_m that lead to the fluctuations in M_w and $M_{w,inst}$ seen in figure 10 are apparent. Also shown in figure1 are the pump flow rates, where the granularity corresponds to the finite width of the control interval, 120s. Compared to the total reaction time of 15,800s, $\Delta t/t_{total}=0.0076$. The oscillations in C_m are directly correlated to the spike-like behavior of the flow rate Q(t); Q(t) is at its maximum when C_m is at its minimum and the controller is requesting a large increase in C_m, after which Q(t) tapers off as C_m increases and when C_m reaches a local maximum it instructs the pump to shut off, Q(t)=0. Technical refinements in controller response can be made to reduce the oscillations, but the net M_w fidelity to the control path is already very good. The oscillations in C_p are largely suppressed because, while C_m is an instantaneous measurement from the UV detector, C_p integrates the flow of monomer into the reactor to give total accumulated polymer, as seen in equation 16.

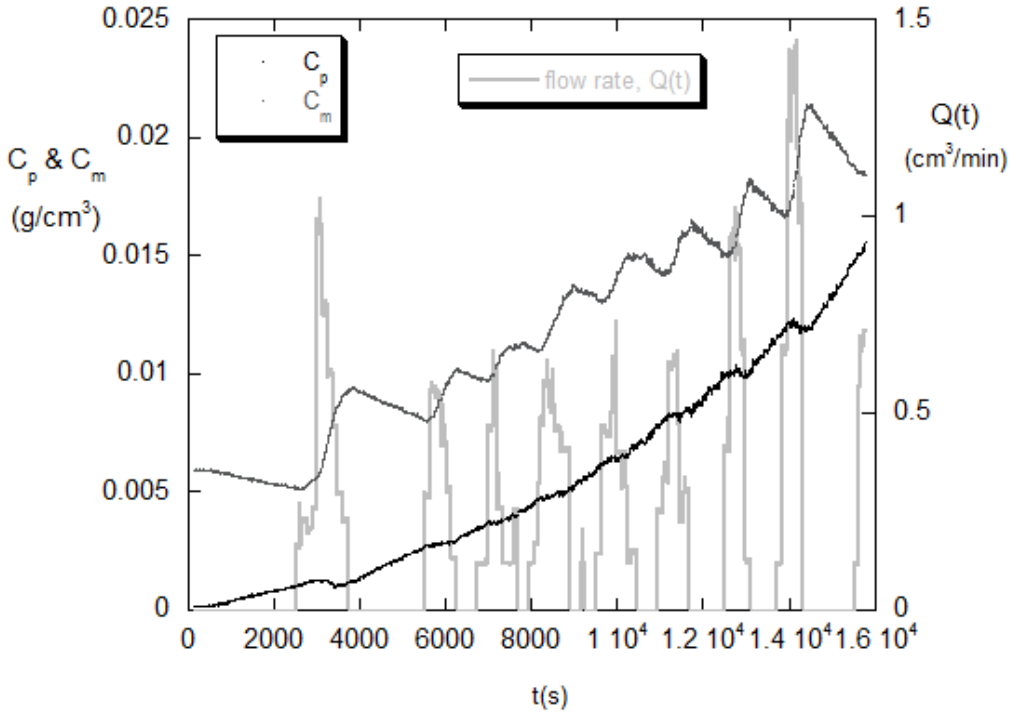

Figure 11. C_p and C_m in the reactor (g/cm^3) during the reaction of figure 5. Also shown is the flow rate as modulated by the automatic controller. The control interval is 120s.

III.1.5 Associated reduced viscosity results for linear M_w vs t at T=45^{o}C

There are cases where it may be difficult to obtain the good, continuous $M_{w,e}$ data needed for this type of controller. Such cases include significant particulates in the sample stream, such as in the case of inverse emulsion polymerization,[36] where aggregates are present, or where turbidity is high, even in dilute solutions. In such cases the reduced viscosity offers a powerful alternative because it is not very sensitive to dense particulates, since these have low intrinsic viscosities, and is not sensitive to turbidity and other optical effects. Since it is related to molecular weight, often by a Mark Houwink relationship it can serve as a useful replacement for direct measurements of M_w. Vega et al. used periodic manual measurements of intrinsic viscosity on reaction aliquots, together with densitometer measurements for conversion to achieve a closed loop controller via an experimentally determined Mark Houwink relation.

Figure 12 shows η_r and instantaneous $\eta_{r,inst}$ computed by the general equation 3 for the reaction of figures 9 and 10. The two curves are reminiscent of $M_{w,e}$ and $M_{w,inst,e}$ in figure 10, and an η_r controller can be constructed by re-tracing the steps in the above M_w controller. The major difference is that η_r is not generally directly proportional to C_m, so that a polymer-specific relationship might be used based on a Mark-Houwink relationship between (instantaneous) intrinsic viscosity $[\eta]_{inst}$ and $M_{w,inst.}$

$$[\eta]_{inst} = aM^{\beta} = p'C_m^{\beta} \tag{41}$$

Where β ranges from 0.5 for an ideal random coil to 0.8 for a coil with excluded volume. Figure 13 shows $\eta_{r,inst}$ vs $M_{w,inst}$. The power law obtained, β=0.72, falls within the expected range. It is noted that C_p in the detector train is low enough that the reduced viscosity is essentially equal to the intrinsic viscosity; i.e. $\eta_r \cong [\eta]$.

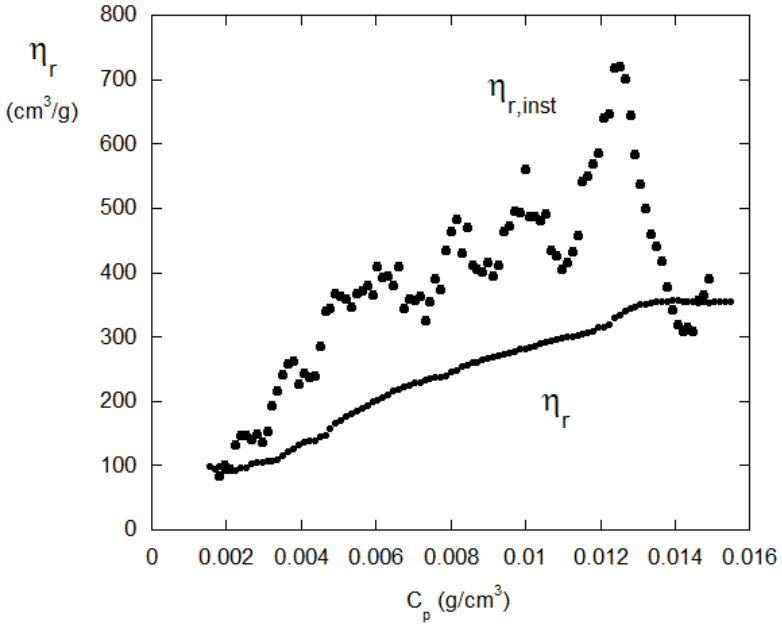

Figure 12. Data for η_r and $\eta_{r,inst}$ corresponding to the reaction of figure 9.

Associated $<S^2>_z$ results for linear M_w vs t at T=45°C

The angular extrapolation of the MALS data allowed $<S^2>_z$ in equation 9 to be computed. Using equation 3 $<S^2>_{z,inst}$ was also computed and is shown in figure 9 vs $M_{w,inst,e}$. A power law of the form

$$R_g \equiv < S^2 >^{1/2} = bM^{\gamma} \tag{42}$$

is expected, where R_g is defined as the root mean z-squared radius of gyration of the polymer. For random coils γ is expected to fall in the range 0.50 (ideal coil) to 0.60 (with excluded volume). γ=0.51 is in this range.

If the relation holds that hydrodynamic volume is proportional to R_g^3 then, because $[\eta] \propto R_g^3/M$ the exponents for R_g and $[\eta]$ are expected to have the relationship $\beta = 3\gamma - 1$. The exponents γ=0.51 and β=0.72 are within 25% of this. The extrapolations shown do not cover a full order of magnitude so are not expected to yield highly precise exponents, rather good estimates which might be useful in qualitatively determining features such as branching and cross-linking in future reactions on branching/cross-linking systems, especially those where branching/cross-linking agents might be used as control variables.

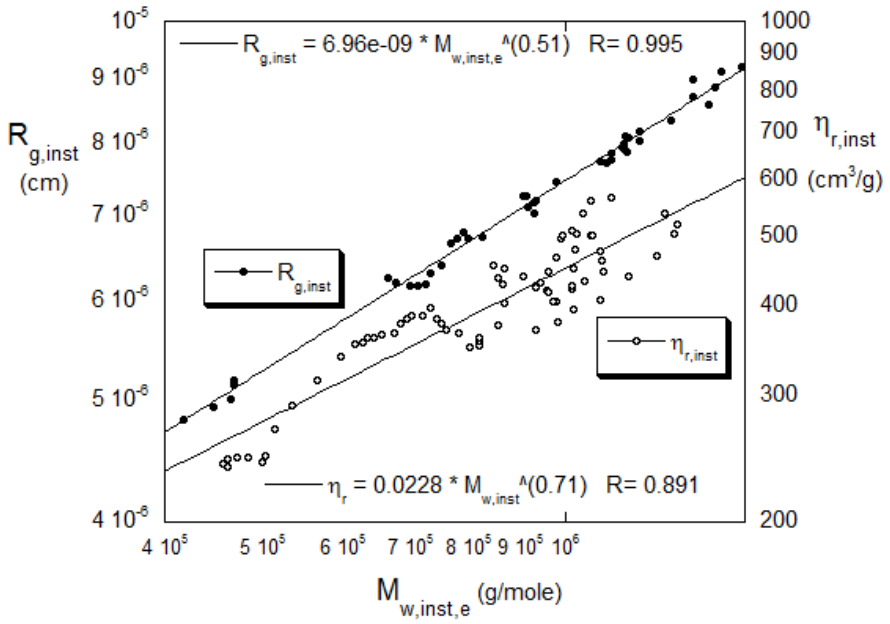

Figure 13. Power law plots of $R_{g,inst}$ and $\eta_{r,inst}$ vs $M_{w,inst}$

To test the robustness of the M_w controller the same linear M_w vs t as in the reaction at T=45°C (figures 9 and 10) was requested but with a rising T. In the isothermal experiment above p and α remained approximately constant throughout, as expected for constant temperature and very slowly dissolving initiator. With changing temperature, however, these parameters are no longer constant and the ability to successfully re-compute them during the reaction is a strong test of the 'free of kinetic model' nature of the controller. In other words, the effects of T are entirely subsumed into p and α and their re-computations, which make no model assumptions about their temperature dependence.

Figure 14 shows a target trajectory with the same slope s=50.0 g/mole-s as in figure 9, but with temperature increasing by steps from 45°C to 57°C during the reaction. The re-computation of p and α during the rising temperature reaction yielded performance comparable to the isothermal reaction of figure 9. Values of α ranged from 1.0×10^{-4} s^{-1} to 2.5×10^{-4} s^{-1}, while p ranged from 4.0×10^{7} to 9.0×10^{7} These data demonstrate how the controller can continue to function even when reactor temperature changes significantly during the reaction, without requiring a detailed kinetic model.

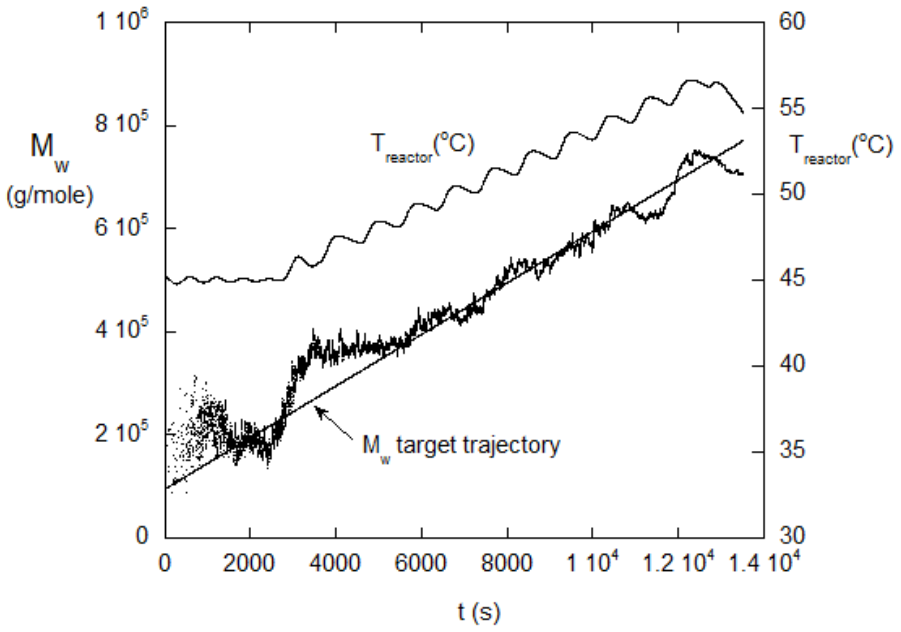

Figure 14. Automatic M_w controller results when the reactor temperature is changing.

III.1.6 Conclusions on basic principles automatic controller for conversion and M_w

Direct automatic control of monomer concentration and of M_w during linear chain growth free radical polymerization has been achieved for the first time. The controller does not depend on a detailed kinetic model and uses two proportionality constants based on fundamental rate and free radical polymerization principles, $\alpha(t)$ and $p(t)$. It is the first step in extending the automatically, actively controlled variables to include chain transfer agents, initiator, temperature, branching agents, quenchers, inert and non-inert gases, and other variables, as well as to extension to composition control in copolymerization.

It is noted that ACOMP is frequently used in reactions with high solids contents[37,38,39] including emulsion[40,41] and inverse emulsion[36] reactions and the current controller is directly applicable to such cases without modification. The only difference in using ACOMP with high solids is that a higher dilution level is used. Whereas 80x dilution is used here, yielding on the order of $5x10^{-4}$ g/cm^3 in the detector train, an industrial type reaction with 50% solids would be diluted 1,000x. The controller itself is unaffected by the amount of dilution.

Extension to copolymerization will follow a similar strategy; there will be proportionalities in the rates, α_A and α_B , for comonomers A and B, which can be frequently re-computed during the copolymerization, so that composition trajectories can be determined without recourse to a model, so that concepts such as reactivity ratios, while quite useful, are not required for the controller. The ratio of feed rates of comonomers A and B can be determined by the current values of α_A and α_B in order to follow a desired composition trajectory. The molecular weight can be simultaneously controlled by the total rates of A and B feed, where p can now be a function of instantaneous comonomer concentrations, and can also be re-computed if and as it changes during copolymerization. ACOMP has been used extensively for monitoring copolymerization reactions,[42,43,44,45,46,47,48] so that the underlying methodology needed to provide composition information to the copolymerization controller already exists.

The current controller is for linear chain growth and so is not directly usable for branching growth. ACOMP has already been utilized, however, to monitor molecular weight and intrinsic viscosity during branching and cross-linking reactions,[49] so that the basic data stream needed to develop a branching controller has been demonstrated.

The current work forms a basis for extending polymerization reaction control, which will involve much concerted extra effort and additional approaches, to many types of reactions of current interest. Areas where control may offer intriguing new opportunities include controlled radical and other living type reactions that underlie much progress in stimuli responsive polymers of unique compositions, MWD, and architectures,[50,51,52,53,54,55] nucleobase polymers[56,57] , and information containing polymers,[58,59] On the other end of the spectrum, high volume industrial polymers, such as polyolefins, can benefit from direct active control approaches. The complexities of synthesizing these polymers has recently been highlighted[60] and an extensive literature exists.[61,62,63]

While this work has not used any formal engineering principles, efforts are currently underway to use non-linear control algorithms and optimization procedures derived from the vast area of process control theory and practice.

2. Production of multimodal MWD

In batch and semi-batch polymerization reactions it is typical to end up with a final polymeric product that has unimodal distributions as concerns molecular weight, comonomer composition, and branching. The types and shapes of these distributions can be varied by many different control variables, including reagent concentrations, temperature, and, in the case of semi-batch production, flow rate of reagents into the reactor.

The molecular weight distribution (MWD) of a polymer is one of the single most important characteristics defining its usefulness for applications. MWD controls mechanical properties and processability, as lower M_w fractions are easier to process when a fraction of higher M_w is present.[64,65,66] There is often an advantage to having two or more distinct polymer sub-populations. The production of multimodal polymers is frequently achieved by blending polymers made in separate reactions,[67,68,69] often in separate reactors.[70,71,72]

This work concerns the production of two or more modes (or sub-populations) during a polymerization process. Production of multi-modal molecular weight distributions is the focus with free radical homopolymerization of linear (unbranched) chains. The instrumentation used to achieve this is ACOMP (Automatic Continuous Online Monitoring of Polymerization reactions), [73] together with a feedback control interface: ACOMP/CI. A weight average molecular weight controller (M_w controller) was recently introduced and used in conjunction with an ACOMP/CI to follow target monomer concentration and molecular weight trajectories, producing specific final MWDs.[74] The M_w controller does not require any detailed kinetic models. Rather, it uses two fundamental principles: 1) The rate of monomer conversion to polymer is proportional to monomer concentration, C_m, at any instant, which is a universal rate concept. 2) For free radical growth of linear chains the instantaneous value of weight average molecular weight, $M_{w,inst}$, is also proportional to C_m.

This work using the M_w controller with the new ACOMP/CI allows multimodal polymer populations to be built up in successive stages in a single reactor. Here, the automatically controlled flow of monomer into the reactor is used together with one or more automatically controlled discrete additions of chain transfer agent (CTA) to achieve two or more sub-populations in the final polymer product.

III.2.1 Use of a chain transfer agent to control M_w automatically

In considering the ways in which molecular weight can be changed quickly in a minimally disruptive manner during free radical polymerization, chain transfer agents (CTA) are superior for several reasons: 1) an immediate, calculated large decrease in M_w can be made by adding a specific amount of CTA, 2) the CTA does not change the reaction rate 3) the CTA does not require changing temperature or adding any additional reagents, such as monomer, and 4) use of CTA provides a wider dynamic range of M_w control than any of the other readily available methods.

CTA can be contrasted with the other means of changing M_w, such as controlling temperature, or initiator or monomer concentration. Temperature is a blunt means of controlling M_w. Raising T reduces M_w and increases the reaction rate, and lowering T increases M_w while slowing the reaction. Increasing initiator concentration $[I_2]$ decreases M_w at approximately 1/sqrt$[I_2]$, but also accelerates the reaction proportionately to sqrt$[I_2]$. Increasing C_m gives an increase in $M_{w,inst}$ since this latter is directly proportional to C_m. Hence, adding monomer cannot be used to lower M_w in a multi-modal population, but could be used for one or more upwards jumps of M_w to produce multi-modes. One aspect to be cautious of in such an approach is causing a large increase in reactor viscosity, as well as possible strong exothermicity which can lead to reactor gelation.

Figure 15 shows fractional monomer conversion, f, vs time. The reaction rates are the same with two different concentrations of CTA and without any CTA, for all three reactions at 45°C. The rates are so close it is difficult to distinguish the data from the separate reactions. In contrast, the reaction rates are significantly increased when T is increased to 55°C and then further to 65°C.

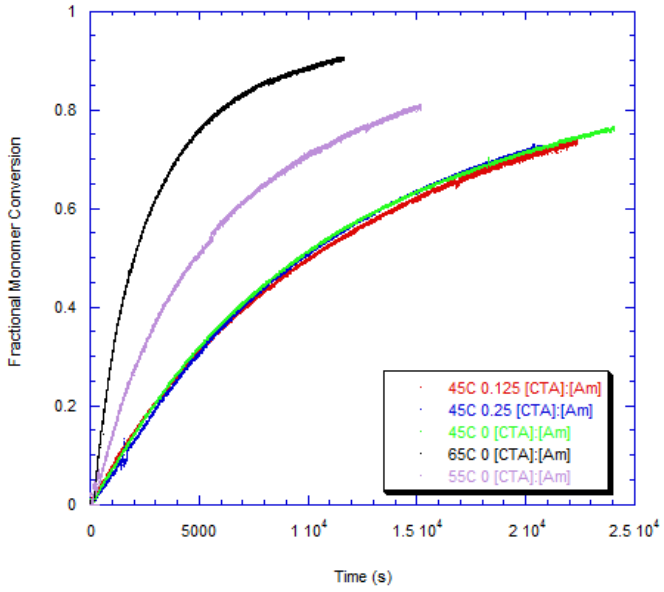

Figure 15. Fractional monomer conversion versus time for varying [CTA]/[monomer], and for three different temperatures: 45°C, 55°C, and 65°C. The CTA does not affect conversion kinetics, whereas increasing T substantially accelerates conversion.

In this work CTA was used to decrease M_w by as much as a factor of thirty. To achieve this effect with initiator would require an impractical increase of one hundredfold in the initiator concentration. Figure 16 shows measured M_w (f=0.75) in a batch reaction as a function of temperature from 45C to 65C, and as a function of the concentration of CTA, expressed as the molar

ratio of [CTA]/[monomer]. Also shown is final M_w computed from increasing initiator concentration at fixed T=45°C. Clearly, the CTA offers a much broader dynamic range of M_w control, while leaving the reaction rate unchanged.

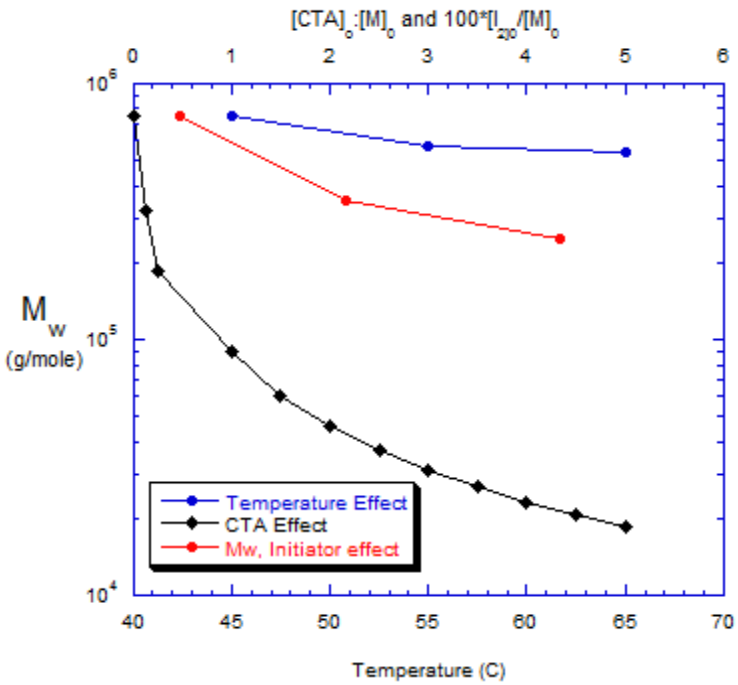

Figure 16. Effects on final M_w of changing $[CTA]_0/[M]_0$, T, and $100*[I_2]_0/[M]_0$. For the latter, the actual $[I_2]_0/[M]_0$ was multiplied by 100 in order to fit on the same x-axis as $[CTA]_0/[M]_0$.

As a prelude to multimodal control, the chain transfer constant, k_3, was determined for pAm synthesized using KPS as initiator and NaOOCH as chain transfer agent. The chain transfer constant (CTC) had been previously determined by ACOMP for other types of CTA.[75]

The chain transfer constant was determined within the context of the weight average molecular weight M_w and weight average chain length $X_w=M_w/M_{Am}$ (where M_{Am} is the molar mass of Am, 71.08 g/mole), since that is the moment of the molecular weight distribution (MWD) measured by light scattering and used as the basis for control.

$$X_{w,inst} = d\frac{k_p}{k_t[R]Y + k_3[CTA]}[M] \tag{43}$$

where k_p, k_t, and k_3 are the propagation, termination, and chain transfer rate constants, respectively, and [M], [R], and [CTA] are molar concentrations of monomer (Am), free radical, and chain transfer agent, respectively. Y is a dimensionless constant that varies from 1 for pure recombination to 2 for pure disproportionation, with value between 1 and 2 when both processes occur. For Am polymerization disproportionation dominates[76]. The dimensionless constant d is the polydispersity index M_w/M_n.

The reciprocal of equation 43 leads to a linear relation with [CTA]/[M], where all values are taken at the outset of the reaction; i.e. where monomer conversion f is in the limit of f=0. This allows use of the known initial ratio of chain transfer agent to initial monomer concentrations,

$[CTA]_0/[M]_0$, and is also the moment in the reaction when polydispersity is the lowest; i.e. near f=0 the polydispersity indices, such as M_w/M_n and M_z/M_w are close to their instantaneous values. For free radical polymerization $M_z:M_w:M_n$ = 3:2:1. It is typical in standard, non-ACOMP methods to determine chain transfer properties at low conversion.

$$\frac{1}{X_{w,inst}(f=0)} = \frac{1}{X_{w,inst}(f=0;[CTA]=0)} + \frac{k_3}{k_p d}\frac{[CTA]_0}{[M]_0} \tag{44}$$

When plotted vs $[CTA]_0/[M]_0$ the slope of this equation yields $k_3/k_p d$. This dimensionless quantity is the chain transfer constant, CTC_w, where the subscript 'w' indicates it is based on M_w:

$$CTC_w = \frac{k_3}{k_p d} = \frac{d\left(X_{w,inst}(f=0)\right)^{-1}}{d\left(\frac{[CTA]_0}{[M]_0}\right)} \tag{45}$$

$X_{w,inst}(f=0;[CTA]=0)$ is the weight average chain length at f=0 when there is no CTA. It subsumes the cluster of constants $k_t[R]Y/k_p d$ in equation 43, so that none of these needs to be individually known to find CTC. The standard CTC is based on M_n and is k_3/k_p, so its relation to CTC_w determined by light scattering is

$$CTC_n = dCTC_w \tag{46}$$

Data for CTC determination was obtained using ACOMP by running batch reactions using KPS as initiator at No CTA, 0.25 and 0.125 [NaOOCH]:[Am]. For these batch reactions, the NaOOCH, Am and DIH_20 were charged to the reactor, then stirred and purged for 0.5 h prior to polymerization. The reactions were carried out at 45°C, 2% starting AM and 0.5% KPS to total mass of monomer.

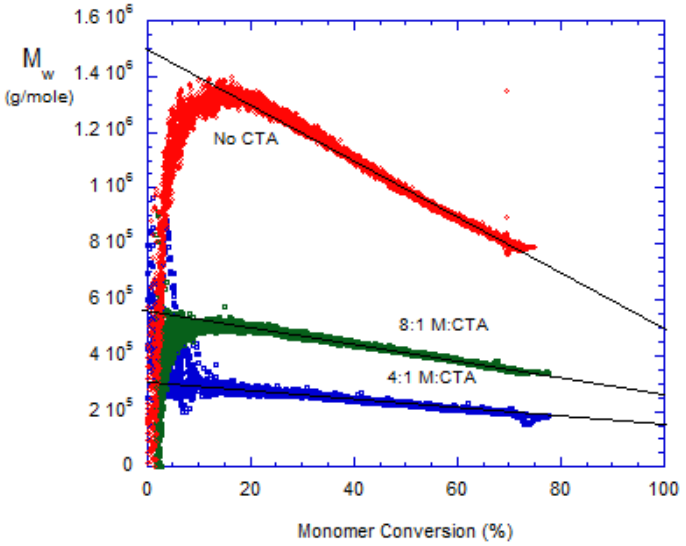

Figure 17: Batch reaction of polyacrylamide with increasing CTA concentration and determination of CTC. Lines show extrapolation to f=0, which are used for $X_{w,inst}(f=0)$ in equation 2. CTC=7.51x10^{-4} using equations 43 and 44.

For determination of the CTC_w, the M_w for $X_{w,inst}(f=0)$ were found from extrapolating the linear portions of the conversion data in figure 17 to f=0, as seen by the line fits. $CTC=7.51x10^{-4}$ (dimensionless) was found. While McCormick et al.[77] used initiator VA-044 at 30C it is still interesting to compare that group's result with the present CTC_n result for KPS. McCormick found $CTC_n=1.06x10^{-3}$ and $d=M_w/M_n=1.5$ by SEC-MALS, and also used $X_n(f=0)$ in equation 2. Applying $M_w/M_n=1.5$ to equation 4 yields $CTC_n=1.12x10^{-3}$ for the data of figure 17, within 4% of McCormick's value despite the different temperature and initiator.

There are cases where it may be difficult to obtain the good, continuous M_w data needed for this type of controller. Such cases include significant particulates in the sample stream, such as in the case of inverse emulsion polymerization,[36] where aggregates are present, or where turbidity is high, even in dilute solutions. In such cases the reduced viscosity η_r offers a powerful alternative because it is not very sensitive to dense particulates, since these have low intrinsic viscosities [η], and is not sensitive to turbidity and other optical effects. Since [η] is related to molecular weight, often by a Mark Houwink relationship, it can serve as a useful replacement for direct measurements of M_w. Vega et al. used periodic manual measurements of intrinsic viscosity on reaction aliquots, together with densitometer measurements for conversion to achieve a closed loop controller via an experimentally determined Mark Houwink relation.[78] In the current ACOMP system the concentration of polymer and shear rate are low enough that the approximation is used that $\eta_r \cong [\eta]$. This approximation is usually made for viscosity measurements made in GPC characterization.

Figure 18 shows [η] vs conversion for the same reactions as in figure 17. The effect of the CTA on [η] is clear, and a similar treatment for chain transfer constant as it relates to [η] can be made, and is briefly considered in Results and Discussion.

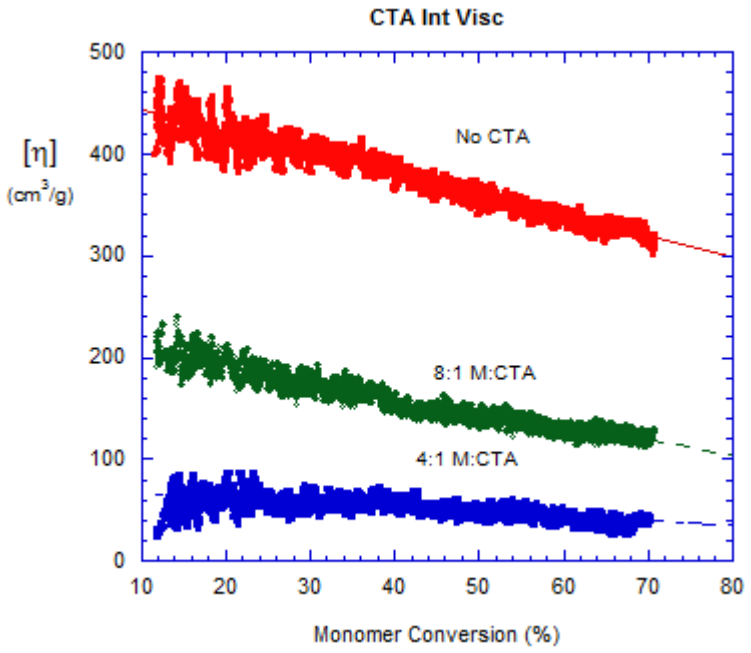

Figure 18. The effect of CTA on intrinsic viscosity [η].

III.2.2 Results for bimodal and trimodal MWD

Figure 19 shows results for automatic production of a bimodal MWD. M_w shows an abrupt change in slope when the CTA is added at C_p=0.0075 g/cm^3, and then smoothly decreases, $M_{w,inst}$ goes through an abrupt drop from an average $M_{w,inst}$ ~ 1.43x10^6 g/mol to M_w ~ 56,000 g/mol. It is noted that to produce a drop of 26x in M_w by using initiator alone would have required an impractically huge increase of 650x in initiator concentration.

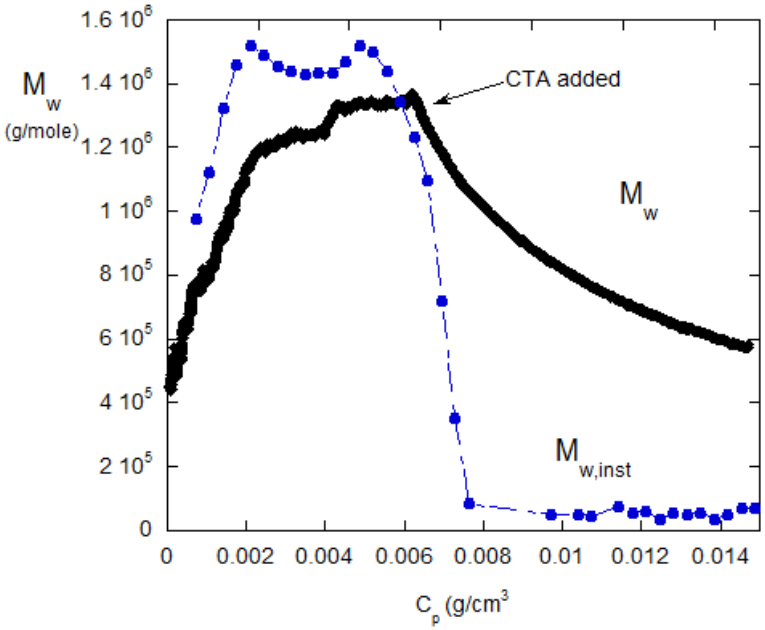

Figure 19. M_w and $M_{w,inst}$ during the production of a bimodal polymer production

Figure 20 shows the automatic flow rate decisions made by the controller, both for the monomer and CTA flow rates from their respective reservoirs.

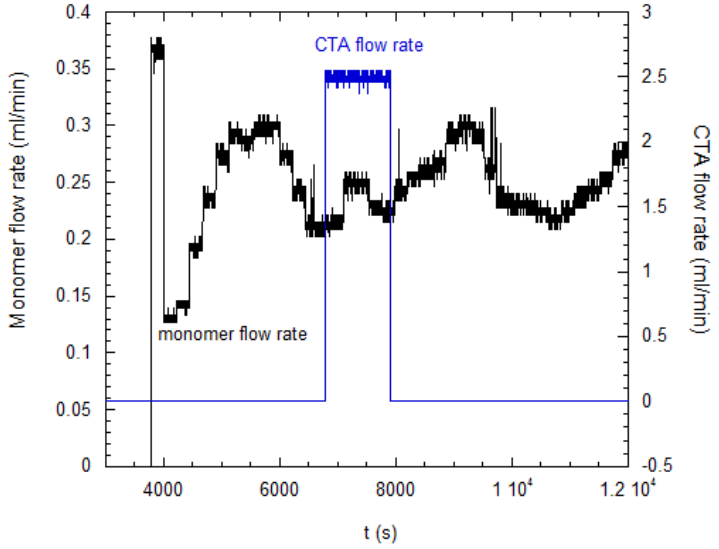

Figure 20. The CTA and monomer flow rates into the reactor during the reaction of figure 19.

There can be situations where MALS is impractical, e.g. in the cases of high particulate content or turbidity. In these cases measurement of reduced viscosity η_r can offer a robust alternative

for control. A single capillary viscometer has no optical components and η_r is normally unaffected by particulates in a polymer solution. Such single capillary viscometers are also inexpensive and need no calibration. Use of single capillary viscometry has been widely discussed in previous work.[37,38,79] Intrinsic viscosity [η] is the limit of η_r at zero concentration. The values of C_p and shear rates in the ACOMP visometer are low enough that $\eta_r \sim [\eta]$. This latter assumption is virtually always made in viscometric analysis of GPC data, where the C_p and shear conditions are comparable.

Figure 21 shows η_r and $\eta_{r,inst}$ where $\eta_{r,inst}$ is computed from the ACOMP data for η_r and C_p according to

$$\eta_{r,inst} = \frac{d(C_p \eta_r)}{dC_p} \tag{47}$$

The data are from the same bimodal reaction of figure 19. The behavior of η_r and $\eta_{r,inst}$ closely mirror the behavior for M_w and $M_{w,inst}$ in figure 19; there is a sudden change in slope of η_r when the CTA is added and $\eta_{r,inst}$ drops abruptly.

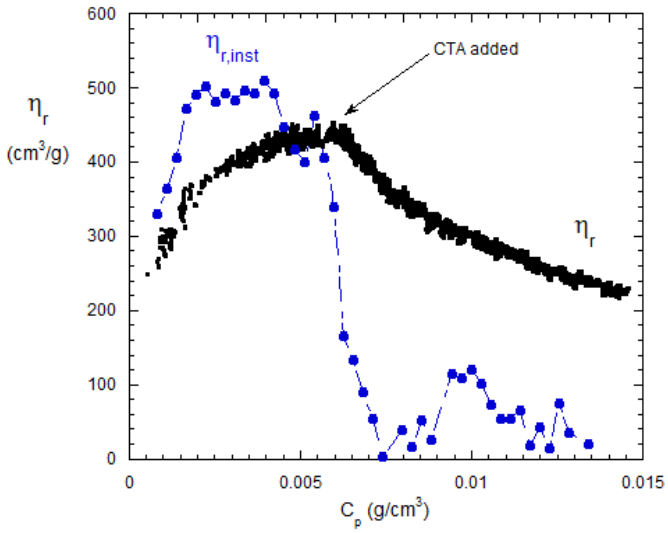

Figure 21. Behavior of η_r and $\eta_{r,inst}$ for the bimodal reaction of figure 6.

The relationship between reduced viscosity and molar mass of the form

$$\eta_{r,inst} = AM_{w,inst}^{\beta} \tag{48}$$

can be used to control $M_{w,inst}$ via measurements of $\eta_{r,inst}$. Figure 22 takes the average values of $\eta_{r,inst}$ and $M_{w,inst}$ in the two bimodal regions of figures 19 and 21, which yields a power law of β=0.594, which is in the normal range of β for random coils (0.5 for an ideal coil and 0.8 for a random coil with high excluded volume). Also shown in figure 22 is η_r vs M_w. Figure 21 shows that there is a much smaller variation in η_r than $\eta_{r,inst}$, and figure 19 shows the smaller variation of M_w compared to $M_{w,inst}$, which yields a significantly different power law for η_r vs M_w.

When using a viscometer instead of light scattering for control, a target trajectory can be established, $M_{w,inst,t}$, and then equation 48 can be used to find the corresponding target path $\eta_{r,inst,t}$.

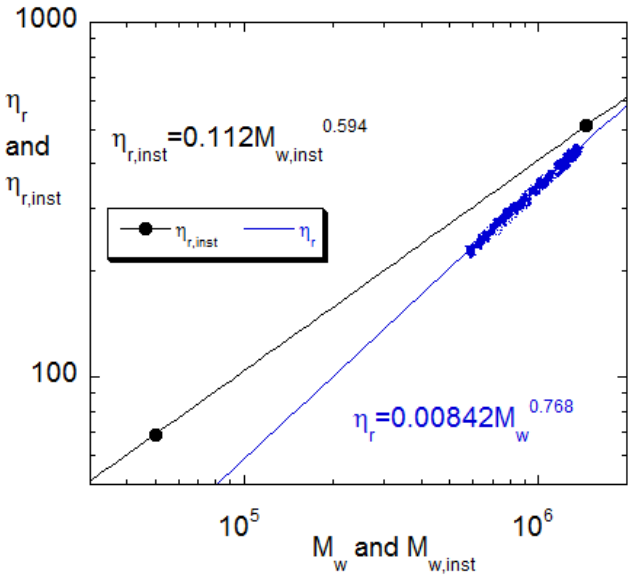

Figure 22. Determination of A and β in equation 48 for $\eta_{r,inst}$ vs $M_{w,inst}$, from the average values of the high and low mass modes.

A trimodal population was produced automatically by stabilizing an initial M_w, followed by a first addition of CTA and then a second addition of CTA. The results are shown in figure 23. The inflection points upon each addition of CTA are noticeable in the cumulative M_w data, but not pronounced. The $M_{w,inst}$ data clearly shows the three molecular weight modes produced.

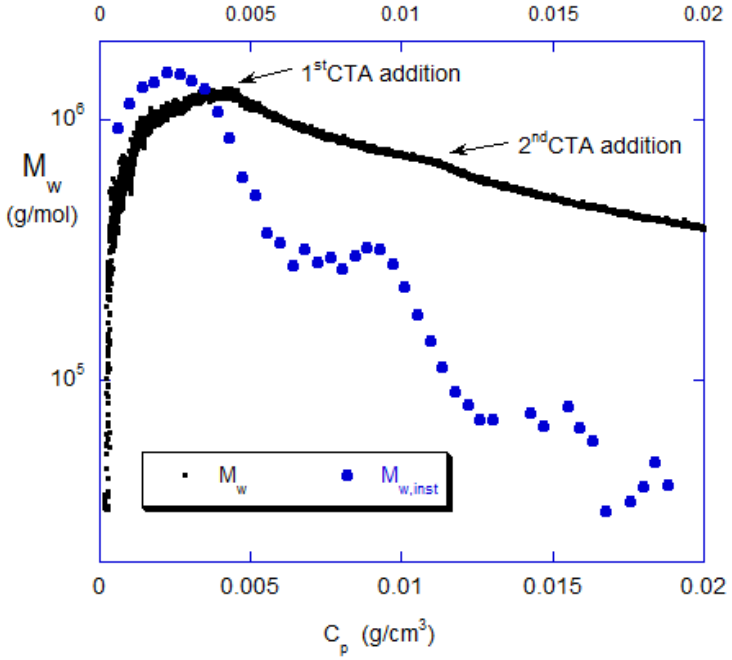

Figure 23. A trimodal population produced by two additions of CTA.

The chromatography-free method of computing MWD developed in this project (discussed in section IV.1) was used with the $M_{w,iinst}$ values shown in figure 23 and the results are shown in figure 24. The instantaneous value of $M_w/M_n=2$ was used together with a log-normal distribution. Also

shown in figure 24 is the GPC chromatogram. The two methods are in remarkably good agreement (there is no fitting used between the two MWD results). They both illustrate that, although there is a trimodal population, clearly seen in the $M_{w,inst}$ in figure 23, the natural instantaneous width of the MWD is enough to smear out the net MWD so that the three sub-modes cannot be resolved by GPC or the chromatograph-free approach. Interestingly then, the $M_{w,inst}$ gives the most direct evidence of the trimodal population, with no model assumptions and no auxiliary chromatographic measurements.

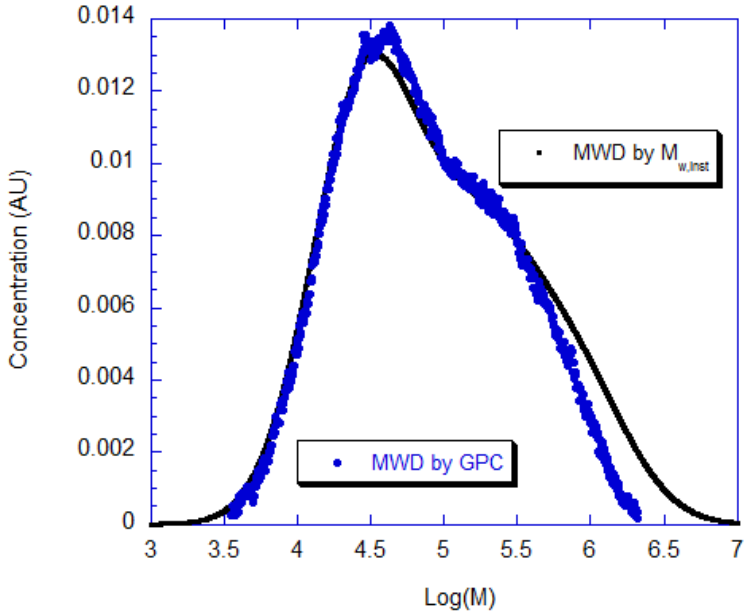

Figure 24. MWD by both the $M_{w,inst}$ data from ACOMP with the log-normal assumption for instantaneous MWD, and by GPC using PEO calibration standards.

Figure 25 is a superposition of normalized MWD for the bimodal distribution of figure 19 and the trimodal distribution of figure 23. 'Normalized' means the integral of the distribution is unity. The MWD based on the $M_{w,inst}$ computations are shown. Both MWD cover the same range of molecular weights, but the bimodal distribution emphasizes the extremes and would be expected to have higher polydispersity.

Table 2 compiles the number, weight, and z-average masses, M_n, M_w, and M_z, respectively, and the polydispersity indices M_w/M_n and M_z/M_w. As expected the M_w/M_n for the bimodal is higher than for the trimodal, by both methods. The agreement between $M_{w,inst}$ and GPC results is better for the bimodal than the trimodal, which is unexpected, since figure 19 for the bimodal shows a seemingly greater disparity between the GPC and $M_{w,inst}$ MWDs than in figure 23 for the trimodal. This may be due to the high M tail on the $M_{w,inst}$ MWDs for the trimodal in figure 23, which weights the M_w and M_z averages towards higher values. It is not certain if the high M deviation between GPC and $M_{w,inst}$ MWDs is due to the GPC column reaching its exclusion limit, where all high M molecules elute at the same elution volume, or to some other effect.

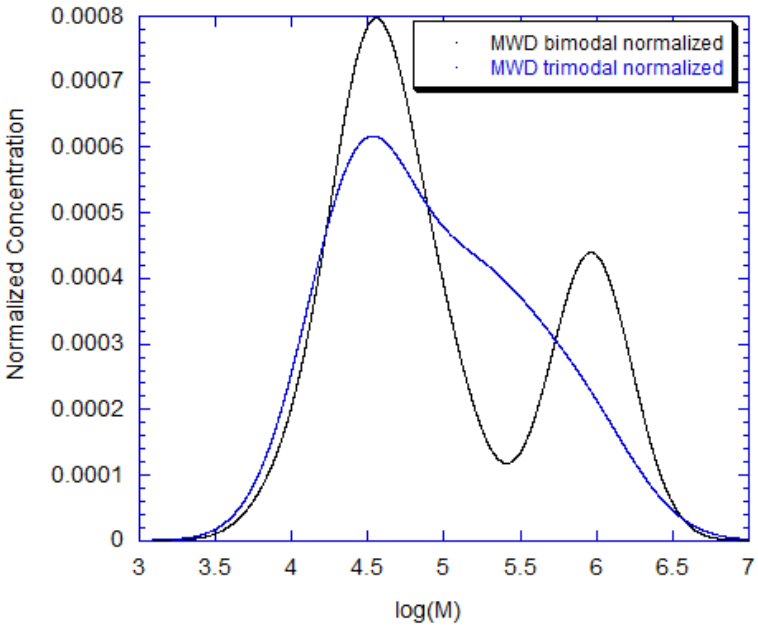

Figure 25. Superposition of normalized bimodal and trimodal MWD from the $M_{w,inst}$ computations.

Table 2. Comparison of molecular weight averages and polydispersities from the GPC and $M_{w,inst}$ determinations of MWD for bimodal and trimodal MWD.

		Bimodal figure 19			**Trimodal figure 23**	
		by $M_{w,inst}$	**by GPC**		**by $M_{w,inst}$**	**by GPC**
Mn		**3.75E+04**	**3.31E+04**		**3.52E+04**	**3.59E+04**
Mw		**3.63E+05**	**2.71E+05**		**2.82E+05**	**1.70E+05**
Mz		**1.43E+06**	**1.07E+06**		**1.60E+06**	**5.60E+05**
Mw/Mn		**9.66**	**8.20**		**8.01**	**4.73**
Mz/Mw		**3.96**	**3.96**		**5.66**	**3.30**

III.2.3 Outlook on automatic production of multimodal MWD

Multimodal molecular weight distributions for unbranched polymers produced in free radical reactions have been created using an automatic feedback controller. The controller continuously monitors polymer M_w and constantly adjusts the monomer flow from reservoir to reactor in order to achieve a specified M_w trajectory, and then adds an amount of CTA to create a second, lower M_w mode, when a target amount of the first M_w mode is reached. The amount of CTA can be predetermined or calculated in real time based on the current weight average molecular weight and the target weight average molecular weight using a previously defined CTC. Further subsequent additions of CTA can be made to produce additional modes.

A non-chromatographic method for determining MWD using ACOMP measurements of $M_{w,inst}$ and an assumed log-normal distribution for the instantaneous MWD yields MWD for the final product in good agreement with PEO-equivalent GPC MWD. Because of the instantaneous width of the MWD neither GPC nor the model-dependent $M_{w,inst}$ method of obtaining final MWD can resolve all sub-populations. In contrast, the model free $M_{w,inst}$ obtained directly from the ACOMP data reveals the multiple modes.

3. Copolymer composition control, and simultaneous M_w and composition control

III.3.1 Basic principles approach to automatic composition control

The ultimate goal of the controller is to lead the reaction along simultaneous target trajectories for instantaneous weight average molecular weight, $M_{w,inst,t}(t)$, and for instantaneous composition, which can be represented as the instantaneous average mass fraction of comonomer A incorporated into chains forming at any instant t, $F_{A,inst,t}(t)$. The instantaneous average mass fraction of comonomer B incorporated into the chain is simply $F_{B,inst}(t)=1-F_{A,inst}(t)$. In some cases it will be preferable to use polymer concentration C_p as the independent variable, instead of t, especially in cases where the endproduct should have specific composition distributions.

In the homopolymer controller case a single rate constant α and a molecular weight proportionality constant, p, were needed to control the trajectory of M_w, each of which can be re-computed during the reaction.[21] To extend to a copolymer system the rates α_A and α_B are introduced, such that, over an interval Δt the amount of A and B converted to polymer are

$$\Delta C_{A,p} = \alpha_A C_A \Delta t$$

$$\Delta C_{B,p} = \alpha_B C_B \Delta t \qquad (49a,b)$$

where C_A and C_B represent the concentration of monomers A and B in g/cm^3. In reality α_A and α_B are subtly complex; for any given composition they embody the relative reactivities of A and B as well as the concentrations of A and B. Hence, there is a stronger requirement to re-compute α_A and α_B during even isothermal reactions, compared to re-computation of α in the homopolymer case. Although it is explicitly acknowledged that α_A and α_B can change throughout the reaction, and hence should be re-computed during the reaction, cases have been found where α_A and α_B remain constant.[24]

The issue of the relationship between monomer concentration and instantaneous weight average molecular weight $M_{w,inst}$ is also more complex than in the homopolymer case, where the single, measurable proportionality constant p was used

$$M_{w,inst} = pC_m \qquad (50a)$$

where C_m is the monomer concentration in g/cm^3 and all molecular weights in this work are expressed in g/mole. It is noted that '$M_{w,inst}$' is the general term for 'instantaneous weight average molecular weight', whereas '$M_{w,inst,t}$' is the term for 'target instantaneous weight average molecular weight'. While no model was needed for p, since it is frequently measured during the reaction, it implicitly subsumes factors such as polymerization, termination, and initiator decomposition rates, k_p, k_t, k_d, respectively, initiator efficiency, chain transfer, and initiator concentration.[19]

For the copolymer case p is dependent on reactivity ratios and hence on F_A; i.e. $p=p(F_A)$ so that

$$M_{w,inst}(F_A) = p(F_A)C_m \qquad (50b)$$

where F_A is abbreviated notation for the instantaneous average mass fraction of comonomer A incorporated into polymer chains formed at any instant, $F_{inst,A}$, and is given by

$$F_A \equiv F_{A,inst} = \frac{dC_{A,p}}{dC_{A,p} + dC_{B,p}} \qquad (51)$$

Since $p(F_A)$ can be computed and re-computed during a reaction, two independently chosen composition and molecular weight trajectories, $F_{A,t}(t)$ and $M_{w,inst,t}(t)$ can be followed simultaneously.

There are monomer reservoirs and feed pumps for monomer A and monomer B, at concentrations C_A' and C_B', with independently controlled feed rates into the reactor of $Q_A(t)$ and $Q_B(t)$, respectively. The goal of the controller is to automatically control $Q_A(t)$ and $Q_B(t)$ to follow both the chosen target trajectories $F_{A,t}(t)$ and $M_{w,inst,t}(t)$. The ratio of the feed rates at any instant will generally control $F_A(t)$, whereas the sum of the rates will generally control $M_{w,inst}(t)$.

For the copolymer case the total monomer concentration m is given by

$$C_m = C_A + C_B \tag{52}$$

It is noted that computation of M_w by light scattering for copolymers becomes significantly more complex if the comonomers in the copolymer have significantly different dn/dc in the solvent used when there is significant breadth to the composition distribution. This problem has been solved using ACOMP, but requires specific implementation.[25] . In the current case dn/dc of Am and SS in water are close enough to each other that a constant value of 0.180 cm^3/g was used. Details on dn/dc and its treatment for SS and Am were given previously.[26]

The instantaneous average fractional compositions F_A and F_B=1-F_A are required for the controller. The primary quantity that the ACOMP system measures in terms of conversion is the concentration of each monomer C_A and C_B. The concentration of each monomer in polymeric form $C_{A,p}$ and $C_{B,p}$ at any point in the reaction is found from mass balance by

$$C_{A,p}(t) = C_{A,0} - C_A(t) + \frac{C_A'}{V(t)}\int_0^t Q_A(t')dt'$$
$$C_{B,p}(t) = C_{B,o} - C_B(t) + \frac{C_B'}{V(t)}\int_0^t Q_B(t')dt' \tag{53a,b}$$

where V(t) is the volume in the reactor at time t, C_A' is the concentration of monomer (g/cm^3) in the A reservoir, and $Q_A(t)$ is the flow rate (cm^3/s) of A from the reservoir into the reactor. The same notation applies to comonomer B. The cumulative fraction of polymer consisting of A is f_A, and of B is f_B

$$f_A(t) = \frac{C_{A,p}}{C_{A,p} + C_{B,p}} = \frac{C_{A,p}}{C_p}$$
$$f_B(t) = \frac{C_{B,p}}{C_{A,p} + C_{B,p}} = \frac{C_{B,p}}{C_p} \tag{54a,b}$$

where $f_A(t)+f_B(t)=1$ and the total concentration of polymer is

$$C_p = C_{A,p} + B_{B,p} \tag{55}$$

The instantaneous most probable fraction of A in polymer chains produced at any time t is F_A given by equation 51. Since dA_p=-dA=α_AAdt, F_A can be written as

$$F_A = \frac{\alpha_A C_A}{\alpha_A C_A + \alpha_B C_B} \tag{56}$$

Equation 56 shows the power of α_A and α_B, since they not only determine the consumption of each comonomer, but also the instantaneous most probable composition F_A, and F_B=1-F_A. There is, of course, a distribution of compositions around the most probable value. Here, the most probable

instantaneous value of F_A will be referred to as the 'average value of instantaneous composition'. Model distributions were previously used in ACOMP to compute full composition distributions from the most probable values.[27] A similar method is illustrated in one of the cases below.

III.3.2 Combined, simultaneous controller for M_w and copolymer composition

The goal of the controller is to follow simultaneous target trajectories for molecular weight and composition, $M_{w,inst,t}(t)$ and $F_{A,t}(t)$, respectively, in order to produce a final composition distribution $C_p(F_A)$ where $C_p(F_A)dF_A$ is the concentration of polymer chains that have a fractional composition of monomer A, F_A, within the interval F_A to F_A+dF_A, and a molecular weight distribution $C_p(M_{w,inst})$ where $C_p(M_{w,inst})dM_{w,inst}$ is the concentration of chains that have $M_{w,inst}$ in the interval $M_{w,inst}$ to $M_{w,inst}+dM_{w,inst}$. The controller uses a control interval Δt starting at time t, over which the required changes in C_A and C_B are made with the monomer feed pumps in order to obtain $M_{w,inst,t}(t+\Delta t)$ and $F_{A,t}(t+\Delta t)$.

At a given time, t, a control interval begins, where $C_A(t)$, $C_B(t)$, $F_A(t)$, $C_{A,p}(t)$, $C_{B,p}(t)$, $C_p(t)$, $f_A(t)$, and $M_w(t)$ are all known from the ACOMP data stream. The target trajectory for F_A is denoted by $F_{A,t}(t)$. By the end of a control interval of length Δt the composition should be $F_{A,t}(t+\Delta t)$. This places the following requirement on $\Delta C_A(t+\Delta t)$ and $\Delta C_B(t+\Delta t)$: Using equation 56

$$F_{A,t}(t+\Delta t) = \frac{1}{1+\dfrac{\alpha_B\left[C_B(t)+\Delta C_B(t+\Delta t)\right]}{\alpha_A\left[C_A(t)+\Delta C_A(t+\Delta t)\right]}} \tag{57}$$

where α_A and α_B are the current values that have been directly measured from the ACOMP data stream. Equation 57 specifies only the ratio of the required $\Delta C_A(t+\Delta t)$ and $\Delta C_B(t+\Delta t)$, but not the sum. The sum is the change in total monomer concentration $\Delta C_m(t+\Delta t)=\Delta C_A(t+\Delta t)+\Delta C_B(t+\Delta t)$, and this is a degree of freedom. This degree of freedom is used to simultaneously fulfill the target molecular weight, as follows.

From equation 50b the target for the total monomer concentration at any time must be

$$C_{m,t}(t) = \frac{M_{w,inst,t}(t)}{p\left[F_A(t)\right]} \tag{58}$$

where $p[F_A(t)]$ explicitly recognizes that p is dependent on copolymer composition. The method of the first molecular weight controller for homopolymer can then be used. $p(F_A)$ is computed over a previous interval and that value is used over the subsequent control interval, under the premise that F_A changes slowly enough over control intervals to use a previous value. The rest of the procedure in that controller is then followed, including solution of the quadratic equation for determining the necessary average monomer concentration over the control interval, $<C_m>$. Upon further inspection of the M_w controller above, it was found that case iv) leads to non-optimum flowrates, and the solution to case i) should be used for case iv) as well; i.e. use of the negative root solution of case iv above, equations 38 and 39, has been eliminated.

Reaching the target molecular weight over the interval t to $t+\Delta t$, $M_{w,inst,t}(t+\Delta t)$, will fix $\Delta C_m(t+\Delta t)$ to a target value for that interval, $\Delta C_{m,t}(t+\Delta t)$ so that the necessary monomer concentration is reached at the end of the interval t to $t+\Delta t$. The total target concentration of monomer at $t+\Delta t$ is

$$C_{m,t}\left(t+\Delta t\right) = C_A(t) + \Delta C_A\left(t+\Delta t\right) + C_B(t) + \Delta C_B\left(t+\Delta t\right) \tag{59}$$

Then, the target value for change in total monomer concentration over the interval t to t+Δt, $\Delta C_{m,t}(t+\Delta t)$, is the required difference in total monomer concentration from t to t+Δt, in order to reach $C_{m,t}(t+\Delta t)$.

$$\Delta C_{m,t}(t+\Delta t) = C_{m,t}(t+\Delta t) - C_m(t) = \Delta C_A(t+\Delta t) + \Delta C_B(t+\Delta t) \tag{60}$$

So, the required change in C_A by the end of the control interval is

$$\Delta C_A(t+\Delta t) = \frac{\alpha_B\left[C_B(t) + \Delta C_{m,t}(t+\Delta t)\right]F_{A,t}(t+\Delta t) - \alpha_A C_A(t)\left[1 - F_{A,t}(t+\Delta t)\right]}{\alpha_A\left[1 - F_{A,t}(t+\Delta t)\right] + \alpha_B F_{A,t}(t+\Delta t))} \tag{61}$$

and $\Delta C_B(t+\Delta t)$ is

$$\Delta C_B(t+\Delta t) = \Delta C_m(t+\Delta t) - \Delta C_A(t+\Delta t) \tag{62}$$

Now, the total change ΔC_A over Δt is due to the loss of A due to polymerization over Δt and the amount of A pumped in over Δt

$$\Delta C_A(t+\Delta t) = \left(-\alpha_A C_A(t) + \frac{C_A'}{V(t)}Q_A(t)\right)\Delta t \tag{63}$$

which yields the sought after automatically set pump rate $Q_A(t)$

$$Q_A(t) = \frac{V(t)}{C_A'}\left(\frac{\Delta C_A(t+\Delta t)}{\Delta t} + \alpha_A C_A(t)\right) \tag{64a}$$

Similarly, the pump rate $Q_B(t)$ from monomer B reservoir is automatically set to

$$Q_B(t) = \frac{V(t)}{C_B'}\left(\frac{\Delta C_B(t+\Delta t)}{\Delta t} + \alpha_B C_B(t)\right) \tag{64b}$$

V(t) is the volume of the reactor at time t, and is computed taken into account both the inflow of fluid from reservoirs A and B, and the outflow from the ACOMP withdrawal rate q.

$$V(t) = V_o - qt + \int_0^t Q_A(t')dt' + \int_0^t Q_B(t')dt' \tag{65}$$

where V_0 is the initial volume of the reactor. Pumps A and B are set to $Q_A(t)$ and $Q_B(t)$ at t, the beginning of the control interval.

Limitations

The naturally occurring values of p, α_A and α_B put certain limitations on the target trajectories $M_{w,inst,t}(t)$ and $F_{A,t}(t)$. The changes in these latter two quantities over interval Δt are

$$\Delta M_{w,inst,t}(t+\Delta t) = p(t)\left[\Delta C_A(t+\Delta t) + \Delta C_B(t+\Delta t)\right] \tag{66}$$

and, taking the total differential of F_A in equation 57

$$\Delta F_A(t+\Delta t) = \frac{\alpha_A(t)\alpha_B(t)\left[C_B(t)\Delta C_A(t+\Delta t) - C_A(t)\Delta C_B(t+\Delta t)\right]}{\left(\alpha_A(t)C_A(t) + \alpha_B(t)C_B(t)\right)\left[\alpha_A(t)\left(C_A(t) + \Delta C_A(t+\Delta t)\right) + \alpha_B(t)\left(C_B(t) + \Delta C_B(t+\Delta t)\right)\right]} \tag{67}$$

Or, more compactly,

$$\Delta F_A(t+\Delta t) = \frac{F_A^2(t)\alpha_B(t)}{C_A(t)\alpha_A(t)}\left[\frac{C_B(t)}{C_A(t)}\Delta C_A(t+\Delta t) - \Delta C_B(t+\Delta t)\right] \tag{68}$$

Equations 66 and 68 show that, in addition to p(t), $\alpha_A(t)$ and $\alpha_B(t)$, the achievable value of $\Delta C_A(t+\Delta t)$ further limits $\Delta M_{w,inst}(t+\Delta t)$, and $\Delta F_A(t+\Delta t)$, and hence also $\Delta F_B(t+\Delta t) = 1 - \Delta F_A(t+\Delta t)$. The lowest value of $\Delta C_A(t+\Delta t)$ is when no pumping from the A reservoir to reactor occurs, $Q_A(t)=0$, for which equation 62 becomes the minimum achievable change in C_A, $\Delta C_{A,min}(t+\Delta t)$

$$\Delta C_{A,\min}(t+\Delta t) = -\alpha_A C_A(t)\Delta t \tag{69a}$$

and similarly for the minimum achievable change in B, $\Delta C_{B,min}(t+\Delta t)$ occurs at $Q_B(t)=0$, so that

$$\Delta C_{B,\min}(t+\Delta t) = -\alpha_B C_B(t)\Delta t \tag{69b}$$

This means the maximum negative change in total monomer concentration over Δt is

$$\Delta C_{m,\min}(t+\Delta t) = \Delta C_{A,\min}(t+\Delta t) + \Delta C_{B,\min}(t+\Delta t) \tag{70}$$

The maximum negative change (drop) in $M_{w,inst,t}(t)$ that can be demanded over Δt, $\Delta M_{w,inst,nm}(t+\Delta t)$ is hence at $Q_A(t)=Q_B(t)=0$, and is given by

$$\Delta M_{w,inst,t,nm} = -p\left[\alpha_A C_A(t) + \alpha_B C_B(t)\right]\Delta t \tag{71}$$

This fundamental limit is placed by p(t), $\alpha_A(t)$, $\alpha_B(t)$, and the current abundances of comonomers $C_A(t)$ and $C_B(t)$.

In principle there is no fundamental maximum positive increase in $M_{w,inst}$, since this is governed by equations 59 and 62, which depend on, for a given reactor volume V(t) and abundances of comonomers $C_A(t)$ and $C_B(t)$, reservoir concentrations C_A', C_B', and flow rates Q_A, Q_B, whose maximum values are limited only by technical considerations.

The maximum positive changes in $\Delta F_A(t+\Delta t)$ are similarly limited by the same technical considerations of V(t), C_A', C_B', and flow rates Q_A, Q_B. Since the $\Delta C_B(t+\Delta t)$ cannot be eliminated, it can only be minimized by setting $Q_B=0$ in achieving the technical maximum of $\Delta F_A(t+\Delta t)$, $\Delta F_A(t+\Delta t)_{technical\ max}$, in which case

$$\Delta F_A(t+\Delta t)_{\text{technical max}} = \frac{F_A^2(t)\alpha_B}{C_A(t)\alpha_A}\left[\frac{C_B(t)}{C_A(t)}\Delta C_A(t+\Delta t) - \alpha_B C_B(t)\Delta t\right] \tag{72}$$

When comonomer B has a high reactivity ratio r_B, the $\alpha_B C_B \Delta t$ term can seriously reduce this technical maximum.

Unlike the fundamentally limited $M_{w,inst,nm}(t+\Delta t)$, given by equation 71, the maximum negative change in $\Delta F_A(t+\Delta t)$, $\Delta F_A(t+\Delta t)_{technical\ mn}$, is technically limited. The way to produce $\Delta F_A(t+\Delta t)_{technical\ mn}$ is to set $Q_A=0$ and maximize the feed of B into the reactor, subject to its technical limitations. In this case

$$\Delta F_A(t+\Delta t)_{technical,nm} = -\frac{F_A^2(t)\alpha_B}{C_A(t)\alpha_A}\left[\frac{C_B(t)}{C_A(t)}\alpha_A C_A(t)\Delta t + \Delta C_B\left(t+\Delta t\right)\right] \quad (73)$$

When establishing target trajectories $M_{w,inst,t}(t)$ and $F_{A,t}(t)$ the above limitations can be used to make sure the trajectories lie within both the fundamental and technical limitations of the system. When establishing target trajectories *simultaneously*, further constraints appear on the range of allowable simultaneous trajectories. This is because, while equation 59 connects the $\Delta C_m(t+\Delta t)$ necessary to achieve a target $\Delta M_{w,inst,t}(t+\Delta t)$ over interval t to the necessary $\Delta C_A(t+\Delta t)$ and ΔC_B $(t+\Delta t)$ over the interval, these latter two quantities depend on $C_A(t)$ and $C_B(t)$ at the beginning of the interval, as well as the most recent values of p(t), $\alpha_A(t)$, and $\alpha_B(t)$, and are hence trajectory-dependent.

One way to attempt to ensure viable simultaneous trajectories is to start with known values of $C_A(0)$ and $C_B(0)$ and Ansatz values for p(0), $\alpha_A(0)$, and $\alpha_B(0)$, and then compute the maximum changes in $\Delta M_{w,inst}(t+\Delta t)$ and $\Delta C_A(t+\Delta t)$ possible over the first interval, producing the extrema for these latter two quantities, thus setting envelopes in which the target trajectories $M_{w,inst,t}(\Delta t)$ and $\Delta F_t(\Delta t)$ must lie over the first interval. Computing the subsequent extrema from these latter extrema yields the new boundaries for $M_{w,inst,t}(2\Delta t)$ and $\Delta F_t(2\Delta t)$, and so on. Case 4) below is an example where the last part of the trajectories for $M_{w,inst,t}(t)$ and $F_t(t)$ could not be met simultaneously, and in this case control reverted to an active manual form. Applying the latter iterative procedure to $M_{w,inst,t}(t)$ and $F_t(t)$ before starting a synthesis could avoid this problem. Because $p[F_A(t)]$, $\alpha_A(t)$, and $\alpha_B(t)$ can vary in complex ways during a reaction, however, it will not be possible to employ the iterative procedure without some knowledge or estimates of these latter values. Without complete knowledge, alternatively, hierarchical rule based controllers can be used, which set acceptable bounds for deviation from the target trajectories $M_{w,inst,t}(t)$ and $F_t(t)$ and make control decisions based on maintaining trajectories within these bounds

Finally, the method can be extended to N comonomers, with the requirement that the concentration of each be measurable. This will not normally be possible with UV spectra alone, so other detectors, such as conductivity, refractometry, polarimetry (for chiral molecules, such as in natural products) NMR, FTIR, NIR, and Raman scattering may be required. In the case of N monomers, whose rates $\alpha_1, \alpha_2....\alpha_N$ are measured via measurement of each comonomer concentration, the target composition trajectory for each one, $F_{i,t}$, can be established, where the current value of $F_i(t)$ is given by

$$F_i(t) = \frac{\alpha_i(t)C_i(t)}{\sum_{k=1}^{N}\alpha_k(t)C_k(t)} \quad (74)$$

III.3.3 Results for the simultaneous copolymer composition and M_w controller.

Figure 26 shows a reaction where the target trajectory for copolymer composition $F_{A,t}(t)$ was held constant, by holding constant the total monomer concentration as well as the instantaneous fraction of SS, F_{SS}. The total monomer concentration is within 4.6% of the target, with an average error of 2.9%. The F_{SS} converges on the trajectory ~900 seconds after control begins, and remains within 4.5% of the trajectory with an average error of 1.7%. Also shown in figure 26, for contrast, is the trajectory that F_{SS} follows in a batch (uncontrolled) reaction. Because $r_{SS}>>r_{Am}$ the SS is consumed rapidly and F_{SS} dies off.

Figure 27 shows the pump rates for SS and Am, $Q_{SS}(t)$ and $Q_{Am}(t)$, continuously adjusted by the automatic controller according to equations 64a and 64b during the controlled reaction. It is noted that it is not sufficient to simply feed SS in order to compensate its more rapid consumption than Am, rather, Am must also be fed into the reactor to compensate for its differential loss.

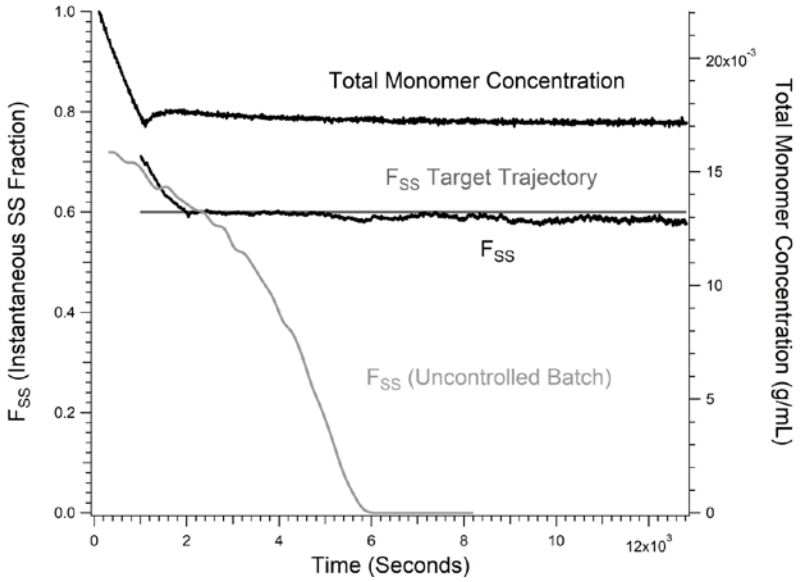

Figure 26. Copolymer control for constant composition and monomer concentration, together with target composition and monomer concentration trajectories, $F_{A,t}(t)$ and $m_t(t)$, respectively (gray scale). The F_{SS} target trajectory is the horizontal gray line. The experimental trajectory straddles the target trajectory. Also shown is total monomer concentration (right hand y-scale), which was kept constant.

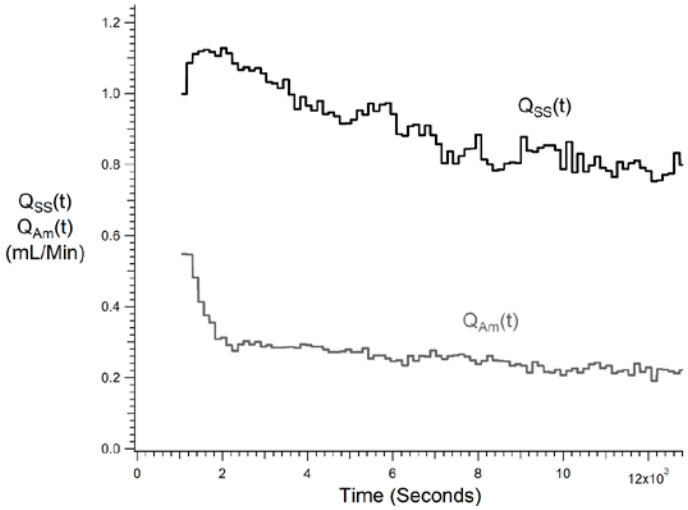

Figure 27. Pump rates $Q_{SS}(t)$ and $Q_{Am}(t)$ for Case 1, the reaction of figure 26.

Figure 28 shows the results for the case where both target composition and M_w trajectories are held constant, $F_{SS,t}(t)=0.64$ and $M_{w,t}(t)=52{,}000$ g/Mol, respectively. The average of F_{SS}, $\langle F_{SS} \rangle$ =

0.615, is slightly lower than the 0.64 desired F_{SS} trajectory. The M_w is within 10% of the 52,000 g/Mol trajectory after ~35 minutes of the control being active and steadily converges closer to the value as the reaction proceeds.

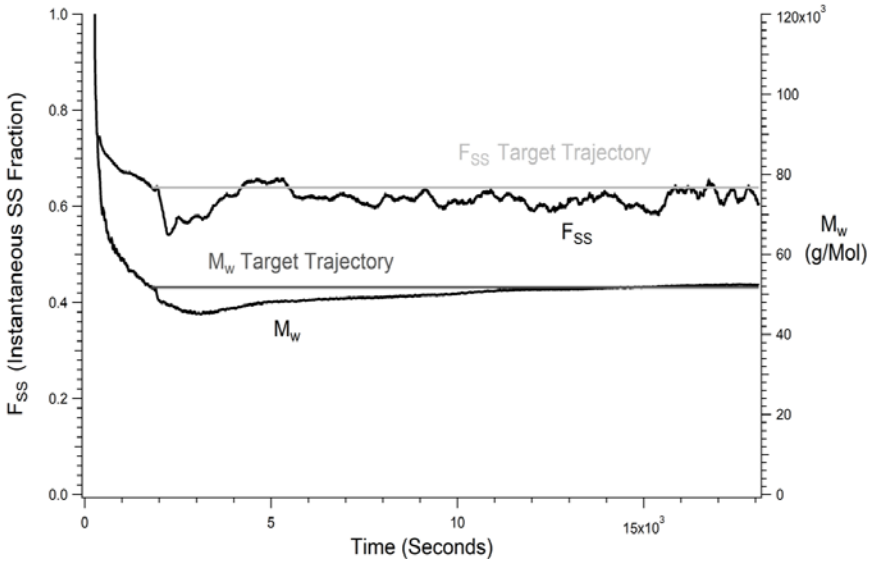

Figure 28. Both composition and M_w are held constant. The horizontal gray lines show the target trajectories for composition, $F_{SS,t}(t)$, and for $M_{w,t}(t)$.

Figure 29 shows the results when both SS and M_w are targeted to rise linearly in time. Due to the much higher reactivity ratio of SS, F_{SS} would decrease quickly in a batch reaction, as shown in the grey curve of figure 26, so an increasing F_{SS} path is a dramatic opposite of the uncontrolled case. While both M_w and F_{SS} have a systematic offset from the target trajectory, they both follow the target linear increase well, and are far different from the batch trajectories.

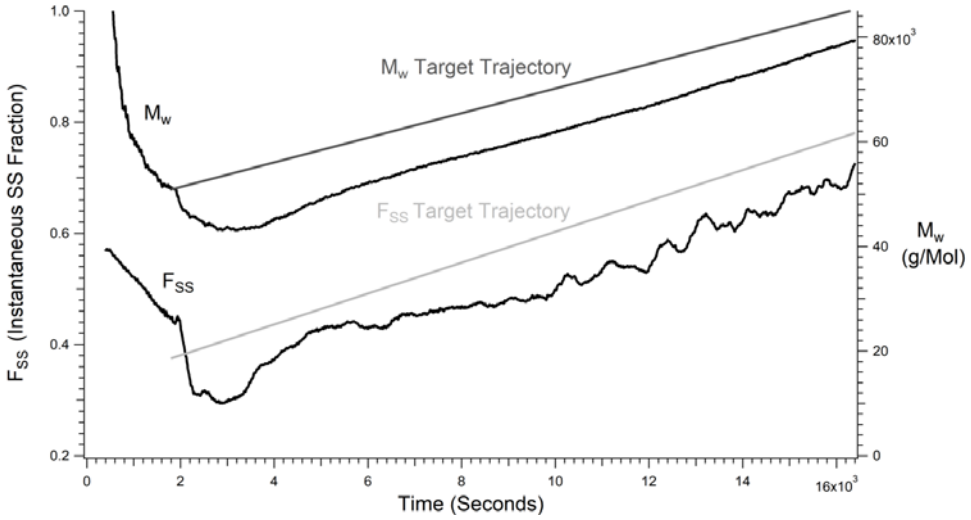

Figure 29. M_w and composition F_{SS} are both targeted to rise linearly. The composition and target trajectories $F_{SS,t}(t)$ and $M_{w,t}(t)$ are shown in gray scale.

Figure 30 shows the target composition trajectory $F_{SS,t}(t)$ (gray scale lines) for producing a trimodal composition distribution and the corresponding experimental result. The representation for figure 30 is versus C_p. The resulting polymer has similar amounts of high SS content chains (F_{SS}~0.75), mid-content SS chains(F_{SS}~0.5), and low content SS chains (F_{SS}~0.25). The target M_w trajectory was set to be constant at $M_{w,inst,t}(t)=3.65x10^4$ g/mole, and this was met to within 7% and had an average error of 2.9%.

This is an example of 'hybrid automatic control'; control switched from fully automatic to active manual control in the final F_{SS}=0.25 stage of the trimodal production. The automated controller did well to control both the composition and molecular weight in the first two stages until it reached the final stage at F_{SS}=0.25. After this, M_w was too high to allow monomer to be pumped in, causing the SS fraction to continue to drop. Thus the operator switched to active manual mode to maintain the desired SS fraction despite the molecular weight rising slightly above the desired path. This is a case of 'operator discretion', where the decision was made to allow the M_w to rise above the target path in order to maintain F_{SS}=0.25. In future controllers hierarchical decisions based on priorities can be programmed in when certain limits are reached; e.g. maintain the trajectory of composition at the expense of M_w, or vice versa, or automatically follow a path that uses a weighted compromise of allowable deviations from the target trajectories.

Figure 31 shows the variation of p with the ratio of SS and Am concentrations; $p(F_{SS})$. These values were obtained from averages of the values of $p(F_{SS})$ on the three $F_{SS}(C_p)$ plateaus in figure 32, and from homopolymer pSS and pAm reactions. The explicit dependence of p on F_{SS} was introduced in equation 50b. Significantly, $p(F_{SS})$ drops by over an order of magnitude from its maximum at $p(F_{SS}=0)$~$2.5x10^7$ cm^3/Mol to its minimum at approximately $p(F_{SS}=0.5)$~1.75×10^6 cm^3/Mol , before climbing after this and ending at $p(F_{SS}=1)$~$7x10^6$ cm^3/Mol . As the automatic controller tried to switch from 50% SS polymer to 25% SS polymer, $p(F_{SS})$ increased by ~50%, causing the M_w to increase. The operator, being able to see these data live, was able to identify that the M_w and composition trajectories for the third phase were not simultaneously achievable. Thus, by switching to active manual mode, the operator was able to maintain the desired SS polymer fraction by allowing M_w to be slightly above the set path. Figure 32 shows the details of how $p(F_{SS}(t))$ (t), $\alpha_A(t)$, and $\alpha_B(t)$ vary as the reaction proceeds. It should be noted that there are artefactual undulations that occur when calculating instantaneous values, such as F_{SS}, α, and $p(F_{SS})$, which are due to the time required for the reactor contents to reach equilibrium when monomer flowrates are changed. Due to mixing residence times in both the reactor and detector train mixing chamber, it takes 10's of seconds for the full signal to appear in the detectors. These artefactual undulations are most prevalent during manual control when the operator toggled the pumps on/off to achieve the trajectory rather than the smooth changes produced by the automatic controller. However, the average values of these instantaneous quantities are accurate and useful.

The above section on Limitations outlines fundamental limits on how much decrease in $M_{w,inst}$ is possible over a control interval, and also treats technical limitations on the minimum decrease in F_A over a control interval, and the technical limitations on the maximum increases in $M_{w,iinst}$ and F_A over a control interval. The third phase of figure 30, as described in the preceding paragraph, is a good example of this. Due to $p(F_{SS})$ rising significantly, the controller does not need any additional monomer to reach the desired molecular weight. Due to the much higher reactivity ratio of SS compared to Am, the composition portion requires the addition of SS

monomer to maintain the desired SS polymer fraction. In cases such as this, the live data displayed by the controller allow the user to intervene when the paths cannot be physically achieved.

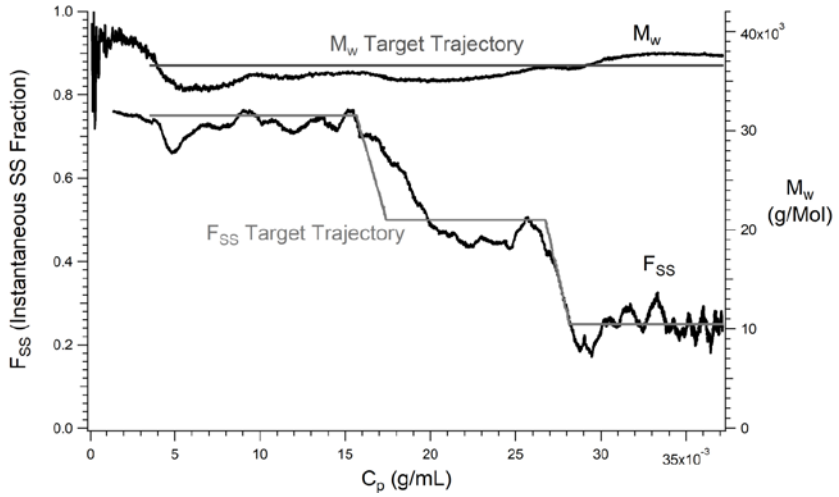

Figure 30. Production of a trimodal composition distribution, while holding M_w constant.

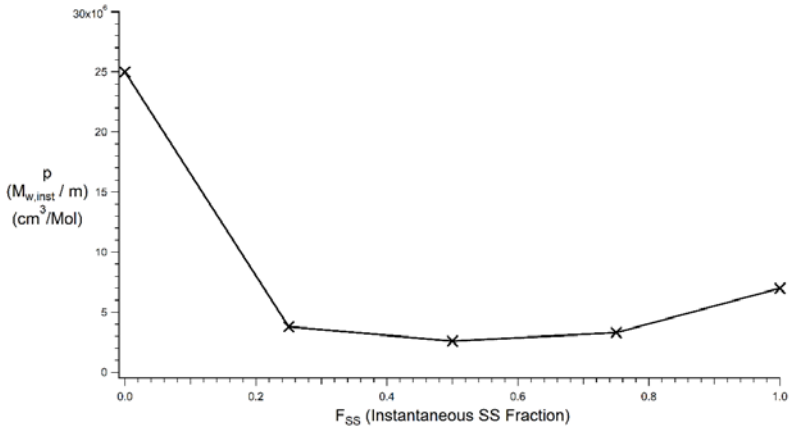

Figure 31. Dependence of p on F_{SS}; p(F_{SS}), as first defined in equation 50b.

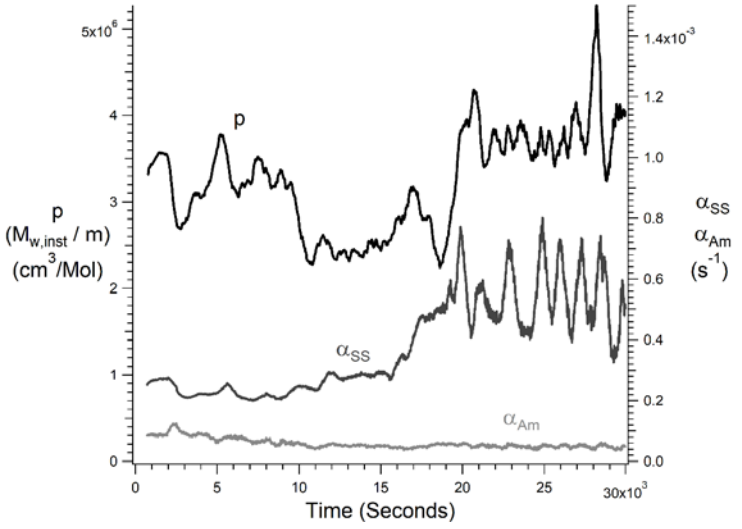

Figure 32. shows the computed values of p, α_{SS}, and α_{Am} for production of the trimodal distribution of figure 30

III.3.4 Instantaneous composition distributions

The instantaneous fractional composition provided by ACOMP is the average composition of polymer being produced at a given instant. The Stockmayer bivariate distribution is invoked to provide the distribution from which that average comes. Let L_{inst} be the instantaneous number-average length of live radical chains,

$$L_{inst}=M_{w,inst}/\langle m\rangle \tag{75}$$

where $\langle m\rangle$ is the average molecular weight of the monomers producing polymer at that instant,

$$\langle m\rangle=F_A m_A+F_B m_B \tag{76}$$

where m_A and m_B are the molar masses of monomers A and B, respectively. Because the molecular weight distribution is computed with its own distribution function, the Stockmayer distribution $w(u)$ is simplified to focus solely on the composition distribution u centered around the average instantaneous fraction of monomer species A, $u=F-F_A$

$$w(u) = L_{inst}\frac{1}{\sqrt{2\pi\beta / L_{inst}}}\exp\left(-\frac{u^2 L_{inst}}{2\beta}\right) \tag{77}$$

where $\beta=F_A F_B\sqrt{1+4F_A F_B(r_A r_B-1)}$, where the reactivity ratios r_A and r_B are r_{ss} = 2.0 ; r_{Am} = 0.085 respectively. *W(u)* is then normalized.

The instantaneous composition distribution w_i is summed with the previous distributions $w_0,\ldots,w_{i-1}$, each weighted by the change in polymer concentration increase over which it was computed so that the cumulative composition distribution is

$$CCD=\sum \Delta(c_p)_i w_i \tag{78}$$

Figure 9 shows the composition distribution from the ACOMP values of F_{SS}, together with the computations for full composition distributions based on the Stockmayer approach.

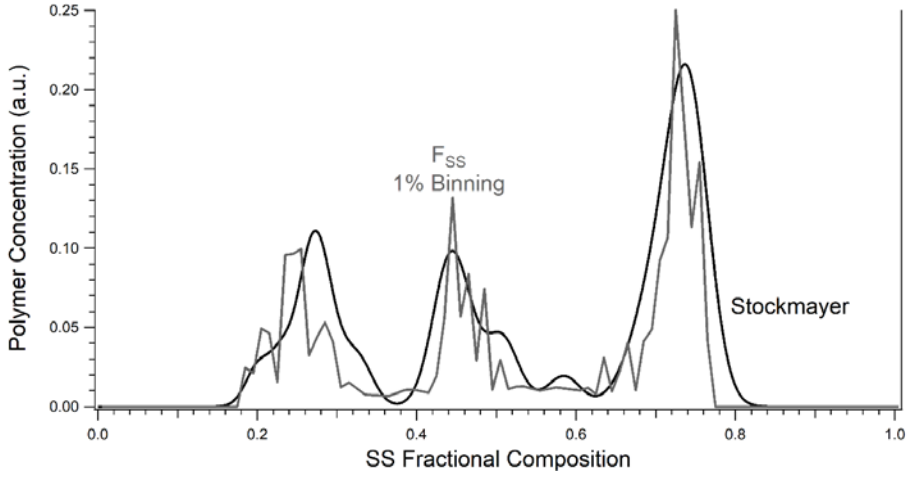

Figure 33. Average and full model based composition distributions for the trimodal composition distribution

III.3.5 Summary and outlook for simultaneous copolymer composition and M_w control

A fully automatic controller was developed which can simultaneously follow target trajectories for copolymer composition and M_w. The controller does not require a detailed kinetic model. Instead, the individual conversion rates of both comonomers, α_A and α_B are measured, in addition to the proportionality constant, p, between total comonomer concentration and $M_{w,inst}$. These three measurable parameters allow the pump rates from reservoirs containing monomers A and B to be constantly readjusted in order to follow the target trajectories. The three parameters can also be re-measured as frequently as required during the process to follow changes in their values as reaction concentrations and conditions change. Figure 32 gives an example of the changing values of α_A, α_B, and p during a controlled reaction.

The controller was demonstrated for target trajectories that 1) maintain constant composition and comonomer concentration with no M_w control, 2) Maintain both composition and M_w constant, 3) increase both M_w and F_{SS} (instantaneous fraction of SS), both of which tend to naturally decrease in uncontrolled batch reactions, and 4) produce a trimodal composition distribution while maintaining M_w constant.

Fundamental and technical restrictions on the latitude of choice for simultaneous composition and molecular weight trajectories have been considered, including switch over from fully automatic to active manual control when limits are surpassed. The idea of hierarchical priorities and decision making for such cases as a future part of the controller is raised.

Without using models, the ACOMP data produce results for the average values M_w, f_A, and f_B, as well as the average instantaneous values $M_{w,inst}$, F_A, and F_B. As such, average distributions can be built, but the full distributions are not directly measured. If well known distributions are invoked then the average distributions can be turned into full distributions, in a model dependent procedure. This was demonstrated for composition using the Stockmayer composition distribution.

The controller can find use in several contexts. One is to assure that desired average compositions and molecular weights are obtained consistently in polymer manufacturing. Another is to produce controllable composition and molecular weight distributions that can imbue the final product with unique properties. While an exploration of the relationship between specific distributions and final properties is beyond the scope of this work, an initial demonstration of the polyelectrolyte behavior of two different end products was made using ACM. Interestingly, the end products of polymers unimodal and trimodal in composition, with approximately the same overall average M_w and composition, gave very similar polyelectrolyte behavior. Future work could include a deeper exploration of the connection between the distributions and final properties, including film forming, solid state, thermal, and other properties.

Another application for the composition controller, without the molecular weight control portion is for the production of controlled comonomer gradients in living type copolymerizations, such as RAFT and NMP.[1,80,81,82,83,84,85,86,87,88,89,90,91 33,34, 35,36,37, 38, 39, 40, 41] Any type of gradient, such as a 'taper', or simply constant average composition can be programmed. In these cases it is not necessary to control the molecular weight since the conditions of the living polymerization determine the MWD. However, the molecular weight controller could be used to correct for deviations from ideal living behavior, by automatically feeding the necessary reagents into the reactor, controlling temperature, etc.

Finally, as long as the concentration of each comonomer can be measured then it is possible to control the composition distribution of three or more comonomers.

4. Active manual conversion control in industrial type inverse emulsion polymerization

This is a particularly important milestone because it is the first time in the project that a reaction, exactly as used in the polymer manufacturing industry, was run and controlled on the ACOMP/CI.

The inverse emulsion system consisted of a continuous oil phase, an aqueous phase containing Am, surfactant stabilizer, and initiator. The total Am content was 30%, which is an industrial concentration level. This is contrasted with all the previous experiments where Am was at 3% in water. Extensive changes in the ACOMP system were carried out to accommodate the higher viscosities, flow rates, and breaker surfactant dilution solvents used. Considerable effort was invested in these changes and in arriving at proper reaction conditions and continuous sample handling.

Three reactions were performed to evaluate the efficacy of controlling inverse emulsion polymerization reactions using initiator feed as the control variable. These are shown in figure 34. A batch reaction carried out at 51 C was performed to establish the natural trajectory of the reaction (black trace). The second reaction established a target conversion trajectory by increasing the reactor temperature by 2 degrees C every 30 minutes starting one hour after adding initiator (blue trace). The reactor was held at 51C for the third reaction while the operator used initiator feed to steer the conversion along a similar path as the increasing temperature reaction (red trace). Hence, an isomorphic reaction pair in conversion for temperature and initiator was achieved (red and blue traces).

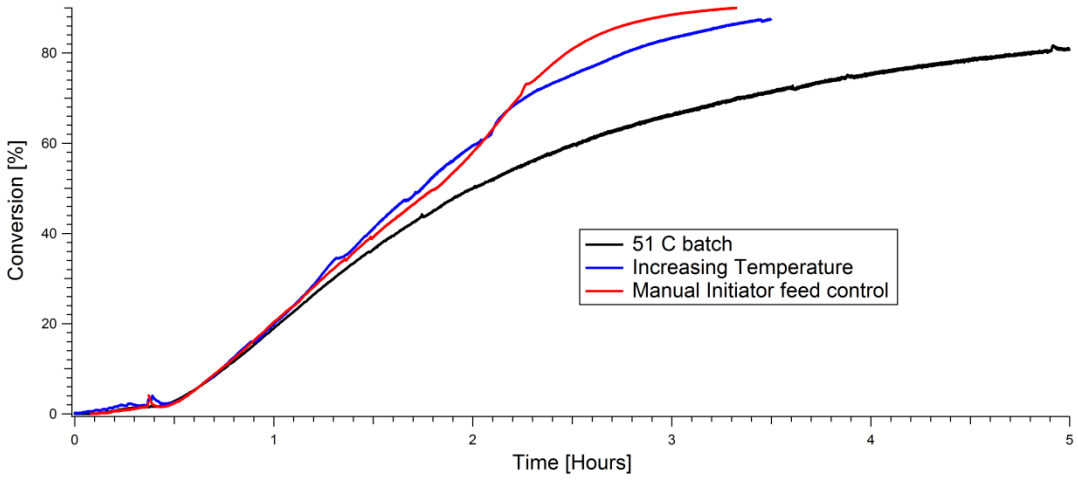

Figure 34. The black trace shows monomer conversion for Am in inverse emulsion at fixed T. The target trajectory obtained by changing T (blue) and the active manual control result (red) are shown.

Figure 35 shows the temperature profile used to produce the target trajectory of figure 34 (blue trace in figure 34). The initiator flow rate sequences provided by the operator in order for the actively controlled reaction to follow the target trajectory are also shown in figure 35.

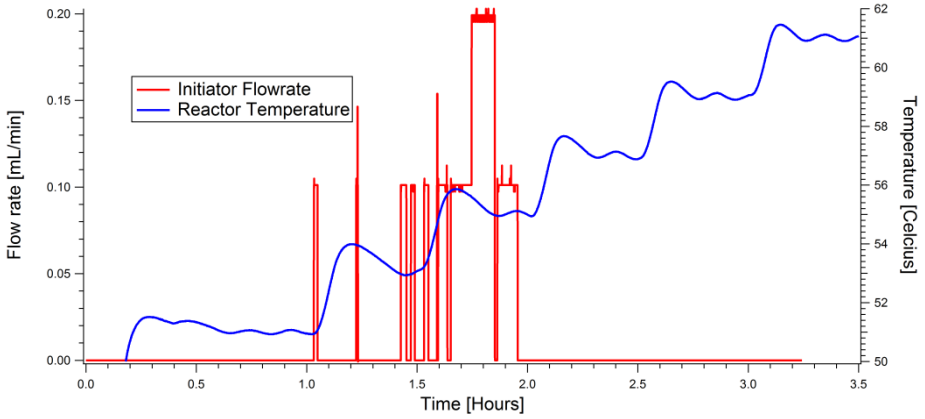

Figure 35. The rising temperature sequence from 51C to 61C used to produce the target conversion trajectory in figure 34 (blue). Also shown is the initiator flow sequence controlled by the operator to produce the trajectory in figure 34 (red) that follows the target trajectory.

Figure 36 shows the raw dilute viscosity signals for all three reactions. As expected, whereas the conversion trajectories for the isomorphic pair are very close (red and blue traces in figure 34), the viscosity traces do not overlap. This is because the conversion rate is proportional to the square root of initiator concentration whereas the molecular weight is inversely proportional to the square root of initiator concentration, so that following a conversion trajectory with initiator will not follow the corresponding viscosity trajectory for that reaction. Hence, a separate active control reaction is needed, whereby the target viscosity trajectory is matched via active manual control of initiator feed. This will be done in the next quarter.

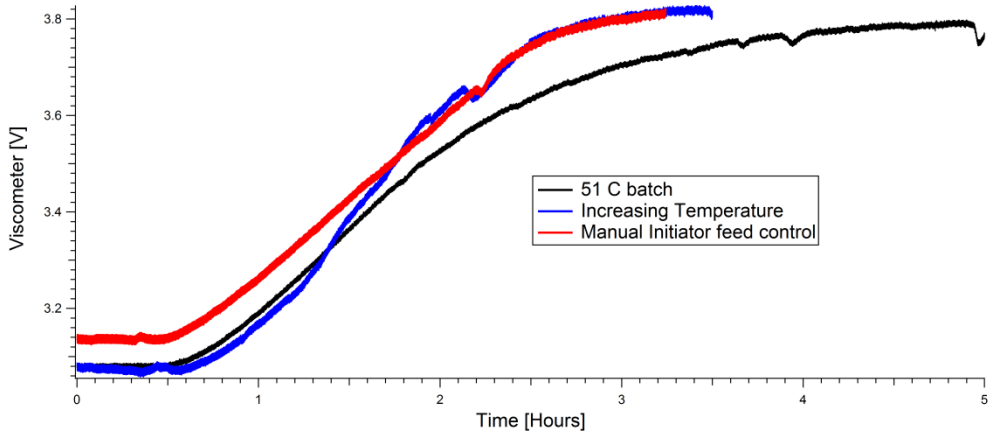

Figure 36. Raw dilute solution viscosity traces for the three experiments.

5. Terpolymerization: first results with NMR/ACOMP†

UV absorption has been used to separate and follow co-conversion of two different comonomers. To separate three or more with UV alone is very difficult. In order to extend the project to terpolyomerization – i.e. with three comonomers- a 60 MHz process NMR (Cosa-Xentaur) was purchased at a very steep discount and integrated into the ACOMP system, receiving a continuous flow of dilute reactor liquid. This allowed first steps in monitoring and control of terpolymerization. For this the monomer Am, SS and sodium acrylate (Ac) were used.

† A manuscript based on these results is still in preparation for peer reviewed publication as of 10/10/17

III.5.1 First time coupling of NMR to ACOMP

NMR analysis was performed using a COSA Xentaur Aspect AI60 high-resolution FT-NMR equipped with a temperature controlled flow cell. Data collection was performed using the manufacturer supplied software. The NMR was coupled to the ACOMP system using a recirculating pump operating continuously at 10 ml/min which withdrew sample directly from the ACOMP reactor for introduction to the NMR flow cell. Withdrawn sample was recirculated back to the reactor and no dilution or conditioning of the sample was performed prior to NMR analysis. The flow cell was heated using an Omega 4" 200W tube heater coupled to a filtered and metered air flow operating at 0.7-1.0 SCFM. Sample temperatures within the flow cell were monitored by thermocouple and maintained to within 40 ± 1.0 ºC during the course of the reactions. (10/20/2016 , 10/26/2016, and 11/4/2016 did not have NMR heating)

NMR data collection was performed continuously during the reaction using a 45º pulse with D1 = 3 sec, P1 = 15 µsec, DT = 20 µsec and AT = 2 sec. A graphical representation of the pulse sequence is shown in Figure 37. Automated shimming of the instrument was performed via the Aspect software immediately prior to the beginning of data collection.

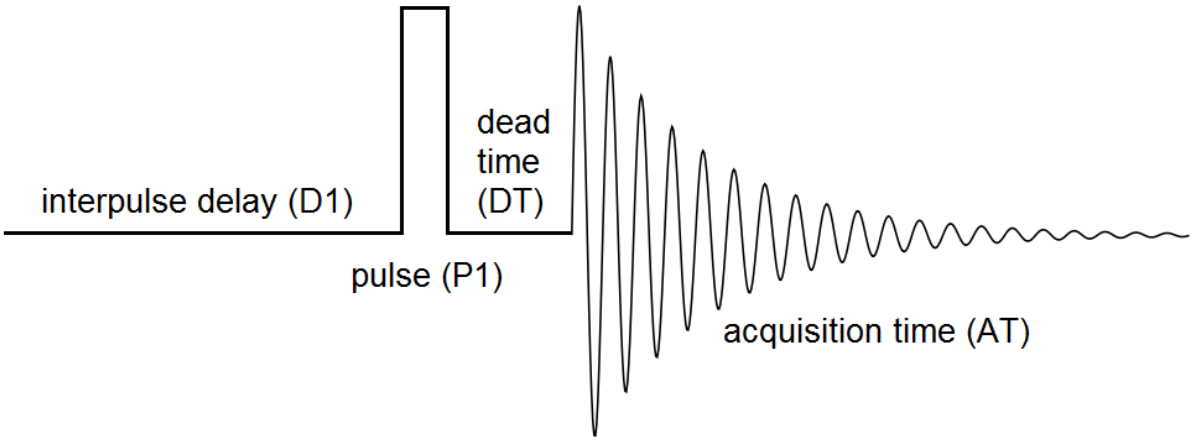

Figure 37. Graphical representation of the NMR pulse sequence used for reactions.

NMR spectra were collected using the "Woody Correction" method in the Aspect software. This method was developed by Woody Conover of Acorn NMR for use in automated, on-line systems. Briefly, the Woody Correction method uses multiple spectra, with each individual pulse transformed then signal averaged in the frequency domain, as opposed to the time domain. The method was developed to reduce field drift broadening which was observed in older permanent magnet NMRs. The Woody Correction in the Aspect software also allows for setting a total number of pulses collected before averaging, along with a rejection criteria based on signal RMS quality threshold. For example, the software can be set to average 6 out of 8 pulses with an RMS threshold of 80%. This method helps to correct for problems often seen in on-line/flow cell systems where bubbles, precipitates, phase separation, etc. can interfere with the quality of individual spectra.

The first step in processing the NMR data is to normalize scans. An example of multiple NMR scans during a batch (uncontrolled) terpolymerization reaction of Am, SS, and Ac is shown in figure 38.

The spectra were normalized to the water peak area from 3.7 to 5.3 ppm. Normalization to the total signal intensity as well as to the water peak intensity was also performed, but was found to be less accurate. Normalizing to the total signal intensity had errors due to baseline noise. Normalizing to the water peak intensity lead to inconsistent results due to varying levels of viscosity broadening across the different experiments. Once normalized, each spectra has the x-axis (ppm) shifted so that the spectral features are in the same ppm location for each scan. When present in the reaction, sodium formate was used as a reference shift. For reactions without sodium formate, the water peak as the reference. Normalization and reference shifting of the data was done using MestReNova.

Several methods of integrating the monomer peak intensities were examined. Processing methods were developed using Mnova software using signal smoothing, reference shifting for formate followed by deconvolution and peak picking for analysis. The available standard processing methods were found to be inadequate, so an a processing method was developed in-house. A linear background subtraction was performed using the spectra values at 5.98 ppm and 6.55 ppm for the linear fit. These points were chosen by looking the evolution of the NMR spectra for many reactions, and observing the spectra is generally flat in these regions and does not contain peaks. Once the linear fit is subtracted, the NMR spectra is integrated from 6.36 – 6.535 ppm for Am and 6.11 – 6.278 ppm for Ac. The region were chosen to maximize the signal from the monomer of interest while minimizing the contribution from the other monomer. Several integration ranges were attempted, all giving very similar results once normalized to all scans. Prior to initiation, the monomer concentrations are known, thus the integral areas are proportional to the monomer concentration. As the reaction proceeds, the loss of integral area is directly proportional to the monomer concentration.

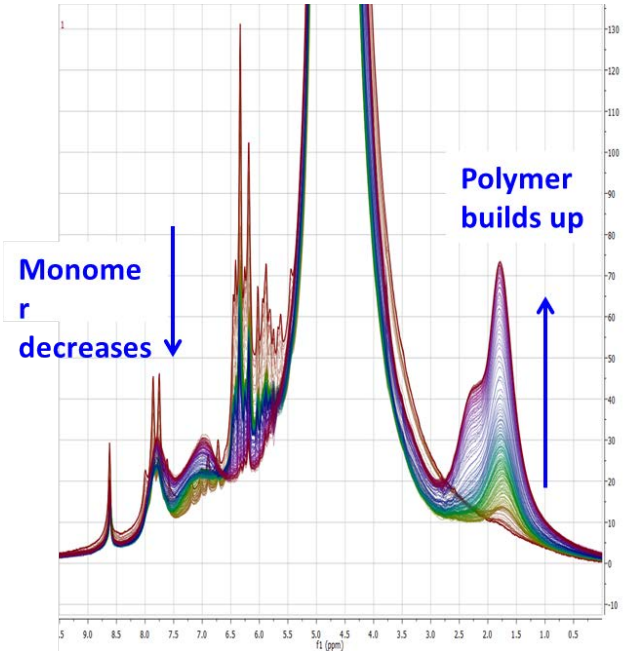

Figure 38. NMR data for the batch (uncontrolled) terpolymerization of Am, Ac, and SS.

III.5.2 Results on terpolymerization with combined NMR and UV in ACOMP

Figure 39 shows the instantaneous mass fractions of the three comonomers during the reaction

shown in figure 38. The NMR separated the Am and Ac signals to give the respective fractions and instantaneous fractions, while the UV was used to separate out the average and instantaneous mass fractions for SS.

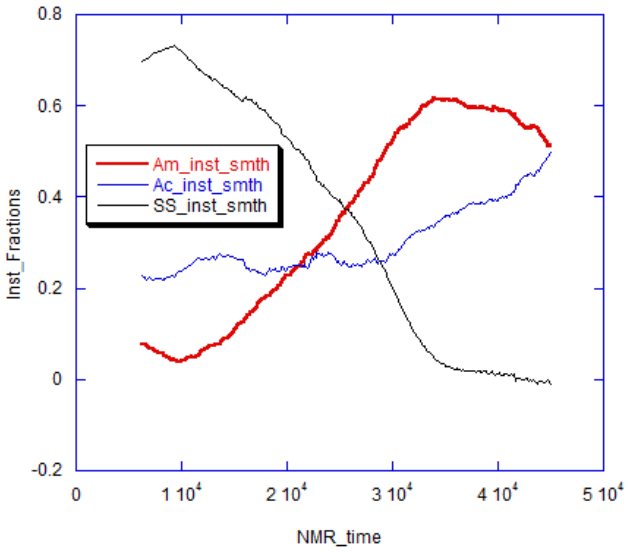

Figure 39. The instantanous mass fractions of Am, SS and Ac from combined NMR and UV data from ACOMP for the batch terpolymerization of figure 38..

Figure 40 shows the corresponding M_w and reduced viscosity data for the batch (uncontrolled) terpolymerization of figure 38.

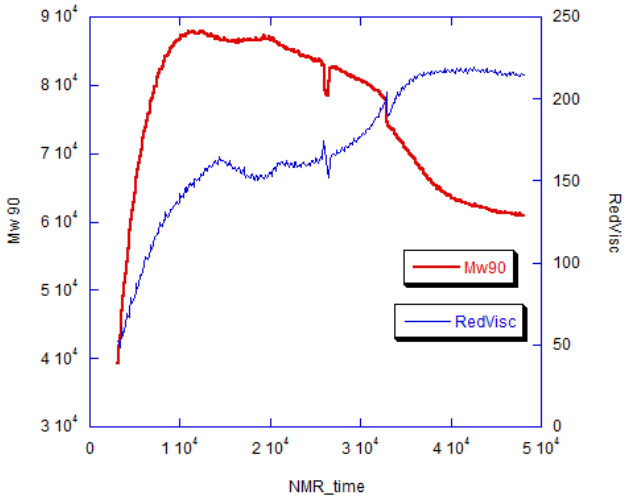

Figure 40. The M_w and reduced viscosity behavior associated with the batch terpolymerizatoin reaction of figure 38.

A first attempt at active, automatic terpolymerization composition control was made using a constant SS mass fraction as the target trajectory. The results are seen in figure 41. It took over two hours to get close to the target $F_{inst,SS}$=0.65 target trajectory, and this was held within about 15% for over 12 hours. At 62,000 seconds control action ceased and the reaction returned to uncontrolled batch mode, with the expected results that SS, which has the highest reactivity ratio of the three comonomers was most rapidly consumed. The results, while not showing the precision of the

copolymer results above, are certainly promising and improvements can lead to monitoring of copolymerization involving four or more comonomers. Such multiple comonomer reactions are commonly used in paint, coating, and adhesive industries.

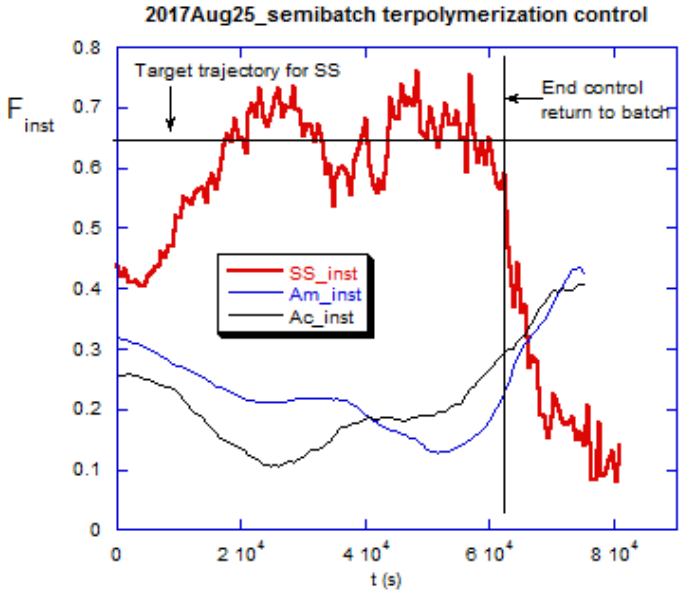

Figure 41. First results for composition control of a terpolymerization reaction using combined NMR and UV data from ACOMP.

IV. Additional groundbreaking

1. Chromatography-free MWD obtained by ACOMP during polymerization

The quantities measured directly by ACOMP are model free. Equation 2 shows the relationship between the cumulative weight average molecular weight $M_w(t)$ measured directly by ACOMP and the derivative yielding the instantaneous weight average molecular weight $M_{w,inst}(t)$. These two characteristics can be quite different from each other, as seen in figure 42.

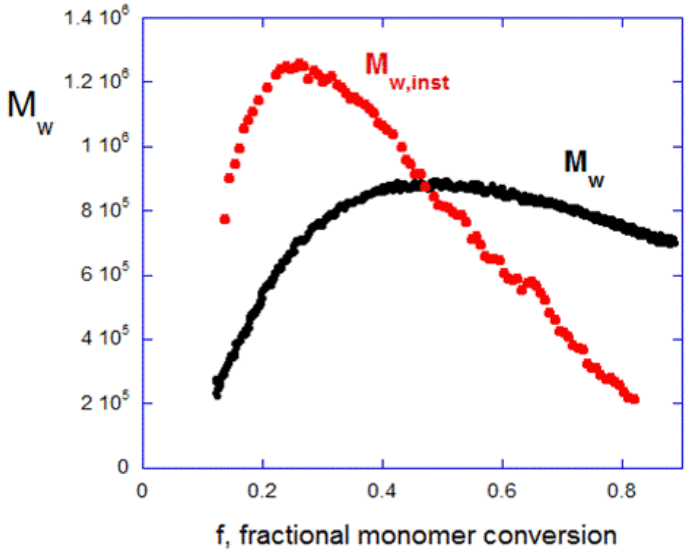

Figure 42. Contrast between M_w and $M_{w,inst}$, both of which are model-free characteristics determined by ACOMP during polymerization reactions.

The basic principles T/F controllers presented above do not require detailed models for their robust performance. Since ACOMP also yields a model-free $M_{w,inst}$ there is an opportunity to combine this latter with model instantaneous distributions to enable chromatography-free complete MWD.

There is a long historical body of work on polymer MWD, with some of the seminal works presented in the mid 20th century,[92,93] with the resulting and widely used Flory-Schulz MWD[94,95], Stockmayer bivariate composition/MWD for copolymers,[96] and others. A comprehensive review of instantaneous MWD and their applications was recently given by Soares.[97]

Before invoking a model, $M_{w,inst}$ itself tracks the 'model free polydispersity', $\left.\frac{M_w}{M_n}\right|_{mfp}$ due to the changes in $M_{w,inst}$ over the course of the polymerization reaction, without any assumptions of instantaneous polydispersity.

$$\left.\frac{M_w}{M_n}\right|_{mfp} = \frac{\left(\sum C_i / M_{w,inst,i}\right)\left(\sum C_i M_{w,inst,i}\right)}{\left(\sum C_i\right)^2} \tag{79}$$

Now, for any instantaneous width $M_{w,inst}$, there will necessarily exist a dimensionless number w_i that relates $M_{w,inst}$ to $M_{n,inst}$,

$$M_{w,inst,i} = w_i M_{n,inst,i} \tag{80}$$

For the Flory-Schulz distribution, which is a specific case of the geometric distribution, and which is expected in the long chain limit for free radical polymerization, w_i=2. (There similarly exists other constants relating other moments to each other, such as M_z, but this is not pursued here). The total weight and number averages M_w and M_n are

$$M_w = \frac{\sum C_i M_{w,inst,i}}{\sum C_i} \tag{81}$$

where the C_i are the histogram heights in figure 43.

$$M_n = \frac{\sum C_i}{\sum C_i / M_{n,inst,i}} = \frac{\sum C_i}{\sum C_i w_i / M_{w,inst,i}} \tag{82}$$

Which gives the polydispersity index M_w/M_n based on the model instantaneous MWD

$$\frac{M_w}{M_n} = \frac{\left(\sum C_i M_{w,inst,i}\right)\left(\sum C_i w_i / M_{w,inst,i}\right)}{\left(\sum C_i\right)^2} \tag{83}$$

In the case where a specific w is presumed to hold for all w_i then

$$\frac{M_w}{M_n} = w\frac{\left(\sum C_i / M_{w,inst,i}\right)\left(\sum C_i M_{w,inst,i}\right)}{\left(\sum C_i\right)^2} = w\frac{M_w}{M_n}\bigg|_{mfp} \tag{84}$$

Table 3 shows the molecular weight averages and polydispersities from GPC using molecular weight standards and $\frac{M_w}{M_n}\bigg|_{mfp}$ from the histogram inset in figure 43, using w=2. The polydispersities are in very good agreement, and the molecular weight averages are in good agreement, considering that ACOMP provides the MALS values and the GPC in this case gives the 'PEO equivalent MWD'.

Table 3. Molecular weights from GPC with PEO standards and from ACOMP $M_{w,inst}$ with w=2

	ACOMP	GPC/standards
M_n	3.13E+05	3.59E+05
M_w	8.01E+05	9.08E+05
M_z	1.71E+05	1.98E+05
M_w/M_n	2.53E+00	2.53E+00
M_z/M_w	2.15E+00	2.19E+00

Figure 43 also shows the MWD that results when the instantaneous w=2 is used in conjunction with the continuous log normal distribution of the form

$$C_p'(\ln x) = \frac{\partial C_p}{\partial \ln M} = \frac{\exp[-\left[\ln\left(M / M_0\right)\right]^2 / 2\sigma^2]}{\sigma\sqrt{2\pi}} \tag{85}$$

While the Flory-Schulz is the ideal underlying instantaneous distribution, the log normal distribution is very frequently used in polymer science in conjunction with GPC since the effect of the column is often to convolute the true MWD of the polymer population (normally the geometric distribution) with a Gaussian spread due both to statistical, entropic permeation of polymers through the multitude of serpentine paths available in the column, as well as lateral diffusion traveling through tubing en route to and through the detector(s). It is completely characterized by the most probable (peak) molecular weight M_o and the width of the MWD, σ. The M_n, M_w, and M_z values are related to these two parameters by

$$M_n = M_o e^{-\sigma^2/2}$$
$$M_w = M_o e^{\sigma^2/2} \tag{86a,b,c}$$
$$M_z = M_o e^{1.5\sigma^2}$$

Using w=2 leads to $\sigma^2=\ln(2)=0.6931$, which allows the instantaneous M_o to be related to $M_{w,inst}$ by

$$M_0 = 0.7071 M_{w,inst} \tag{87}$$

The close match of the MWD by GPC and by ACOMP $M_{w,inst}$ in conjunction with the log normal in figure 43 is striking. While the use of the log normal distribution to produce a continuous MWD resembling the GPC result provides an aesthetically pleasing shape familiar to practitioners of GPC, it contains no additional information beyond the molecular weight averages and polydispersity indices that result from the assumption of w=2, shown in Table 3.

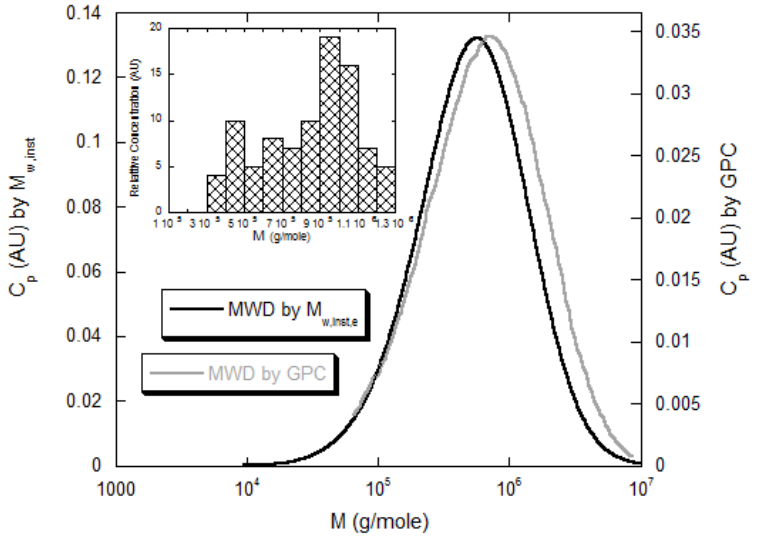

Figure 43. The MWD using GPC with PEO standards (grey) and MWD computed from $M_{w,inst}$ histogram (inset) using w_i=w=2 and the use of the corresponding log normal distribution.

2. Oxygen as a potential process control variable

The project used the following process control variables: Temperature, initiator, monomer, comonomer, and chain transfer agent. In the course of the project an interesting new possibility arose; use of O_2 as a powerful control variable. Currently, O_2, or air, is used in industrial free radical polymerization reactions to slow down or quench reactions. It is often used as a sort of 'panic button'; if a reaction begins to run away exothermically rapid additions of O_2 or air can slow or halt the reaction, thus avoiding a potentially explosive event.

Because of the continuous, precise nature of the ACOMP data stream it was possible to monitor quantitatively the effects of O_2 on both conversion rate and M_w in the aqueous free radical polymerization of Am. Figure 44 shows the effects of different levels of O_2 (in mg/L) in the reactor, starting with 0 (orange). It shows that O_2 can slow the conversion and even completely stop it at some threshold. In figure 44 the threshold is between 17 and 37 mg/L. Furthermore, if the O_2 is purged out by N_2 then the reaction resumes at the rate previous to the introduction of O_2; i.e. O_2 does not 'kill' the reaction, rather it reversibly halts the reaction. There are also effects of O_2 on chain composition, but these were not explored in depth here (preliminary FTIR measurements did show some change in composition when using O_2).

Figure 45 shows the effect of O_2 on M_w during the same reactions. It shows that the effect of O_2 is to decrease M_w. When O_2 is purged out by N_2 then M_w increases again. This reversibility leads to the very interesting possibility of using O_2 as a bidirectional M_w control variable; i.e. introducing controlled amounts of O_2 can lead to desired drops in M_w, whereas purging with N_2 can lead to desired increases in M_w. Both initiator feed and chain transfer used as control variables can only irreversibly decrease M_w, whereas monomer feed as a control variable leads to an increase in M_w. Temperature is a reversible variable - increasing temperature decreases M_w and vice versa- but it has only a limited effect on M_w compared to O_2 and it is generally slow to change and reach equilibrium, especially in large reactors of industrial interest.

Hence, a further area of research would be to develop O_2 as a polymerization control variable. Such development was not within the scope of this project.

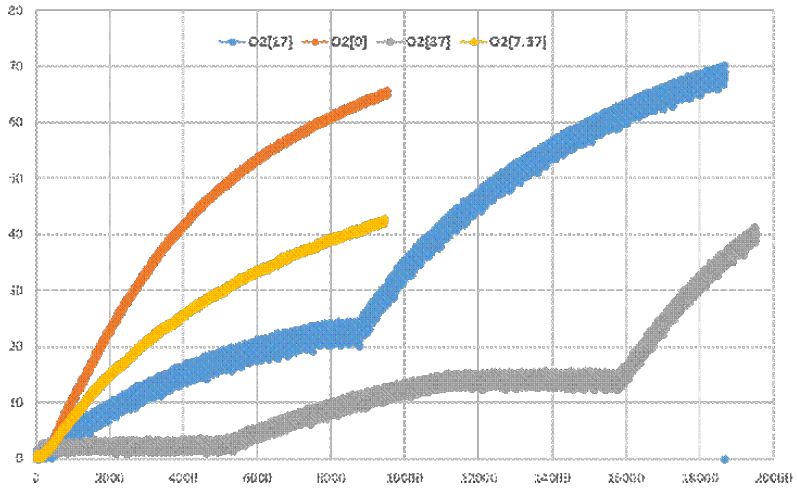

Figure 44. Conversion vs time (s) for different levels of O_2 in the reactor during Am free radical polymerization

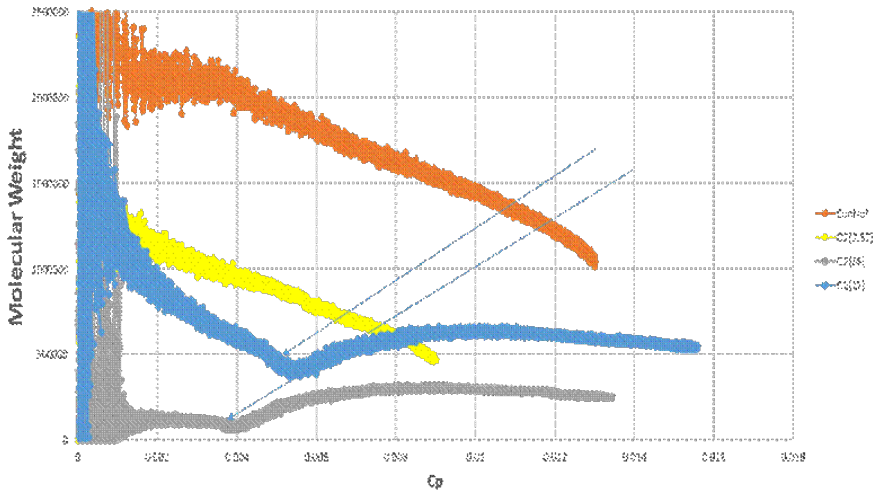

Figure 45. Effect of O_2 on M_w during free radical polymerization of Am

V. LSU developed non-linear reaction control‡

1. Model-Centric Optimal Operation of Polymerization Processes

This report discusses the formulation, implementation and testing of a generic and flexible model centric framework for integrated simulation, estimation, optimization and feedback control of polymerization systems (Figure 46). The modelling work was carried out using gPROMS modelling language and embedded into our model centric framework providing a complete environment for modelling/analysis of complex systems. The core component in the framework is the mathematical model of the system, in this case the batch and semi-batch free radical solution polymerization of Acrylamide in water solution.

Within the scope of the project the following activities were carried out to full completion:

- A first-principles mathematical model was developed by using reaction rate laws available in polymerization literature.
- The model was then validated by comparing the simulations with experimental data.
- The validated model was then used to perform parameter estimation and adjust the kinetic parameters for the proposed system.
- Model-based optimization analysis was conducted to determine the optimal temperature profile in conjunction with the optimal monomer and initiator flow rate in order to reach a final target polymer while minimizing the batch time.
- A nonlinear state estimation strategy was formulated, implemented and tested using experimental facilities.
- Alternative linear and nonlinear control strategies were formulated and tested.
- The polymerization of acrylamide in water solution using potassium persulfate (KPS) as initiator is studied to demonstrate the effectiveness of the module and framework.

‡ This section V was written by the Romagnoli group at LSU. Figure labeling is consecutive with the narrative sequence, but it has its own separate references at the end and its own way of presenting equations

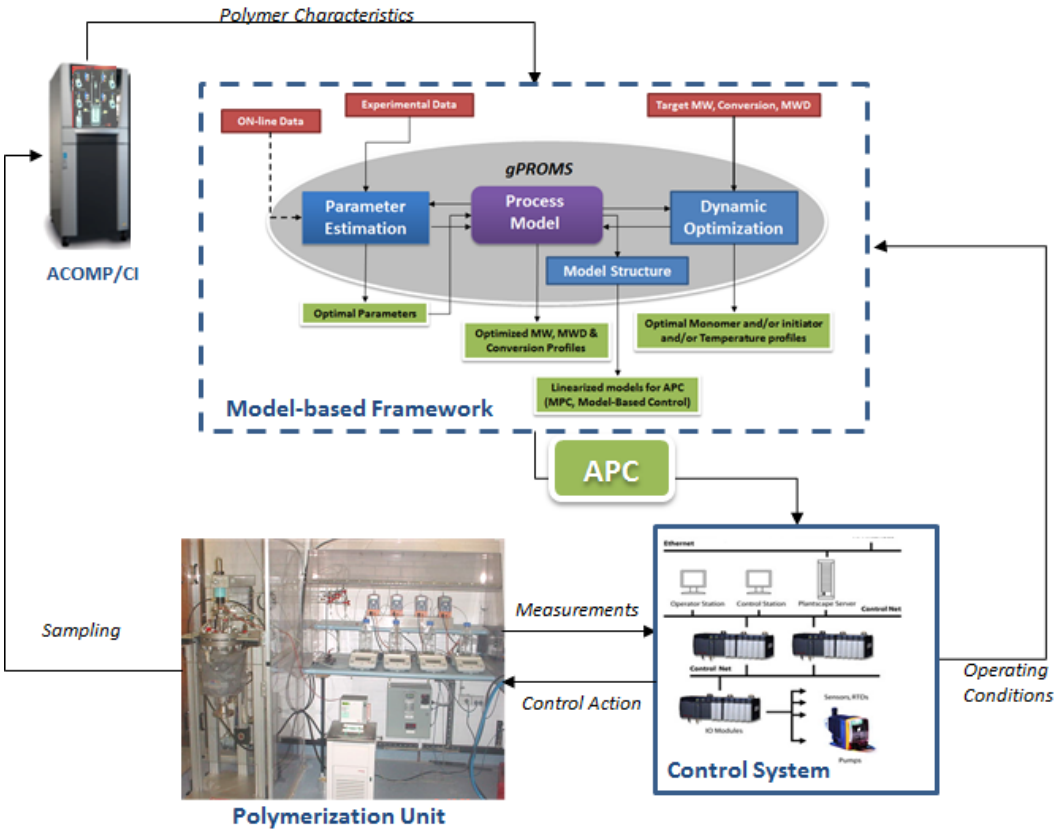

Figure 46: Model centric framework for integrated simulation, estimation, optimization and feedback control of polymerization systems

2. Theoretical Developments

V.2.1 Process Modelling

A detailed mechanistic model for solution polymerization of Acrylamide in batch and semi-batch reactors was developed and tested experimentally. The following set of kinetic and dynamic equations describe the system:

$$\frac{dN_m}{dt} = -(k_p + k_{fm})P_0 N_m + F_m C_{mf} - F_{out} * C_m$$

$$\frac{dN_i}{dt} = -k_d N_i + F_i C_{if} - F_{out} * C_i$$

$$\frac{dN_s}{dt} = -k_{fs} N_s P_0 + F_i C_{sif} + F_m C_{smf} - F_{out} * C_s$$

$$\frac{d(\lambda_0 V)}{dt} = (k_{fm} N_m + k_{td} P_0 V + k_{fs} N_s)\alpha P_0 + \frac{1}{2} k_{tc} P_0^2 V$$

$$\frac{d(\lambda_1 V)}{dt} = \left[(k_{fm} N_m + k_{td} P_0 V + k_{fs} N_s)(2\alpha - \alpha^2) + k_{tc} P_0 N\right] \frac{P_0}{(1-\alpha)}$$

$$\frac{d(\lambda_2 V)}{dt} = \left[(k_{fm} N_m + k_{td} P_0 V + k_{fs} N_s)(\alpha^3 - 3\alpha^2 + 4\alpha) + k_{tc} P_0 V(\alpha + 2) \frac{P_0}{(1-\alpha)}\right] \frac{P_0}{(1-\alpha)^2}$$

Where $N_m = C_m V$, $N_i = C_i V$, $N_s = C_s V$ and:

$$\alpha = \frac{k_p C_m}{k_p C_m + k_{fm} C_m + k_{fs} C_s + k_{tc} P_0 + k_{td} P_0}$$

$$P_0 = \sqrt{\frac{2 f C_i k_d}{k_t}}$$

$$V = \left[1 - \frac{\lambda_1 w_m}{\rho_p}\right]^{-1} \left[\frac{N_m w_m}{\rho_m} + \frac{N_s w_s}{\rho_s} + \frac{N_i w_i}{\rho_i}\right]$$

Monomer Conversion

$$X = \frac{N_{m0} + \int_0^t F_m C_{mf} dt - C_m V - \int_0^t F_{out} * C_m dt}{N_{m0} + \int_0^t F_m C_{mf} dt}$$

Constitutive Equations for the Gel, Glass and Cage Effects

In free radical polymerization, the mobility of the radicals reduces along the reaction due to increase in the viscosity of the reactor as more polymers are produced. This phenomena which is called gel effect causes a reduction in the termination rate constant, k_t, and should be considered in the formulation of the model. At high conversion when even the motion of monomer is severely restricted the propagation rate, k_p, is also decreased. This glassy state in which the solution is highly viscous sets a limiting conversion on the polymerization process. In this work the correlation by Ross and Laurence[9] is used for both gel and glass affect. This can be written as:

$$g_t = \begin{cases} 0.10575 \exp\left(17.15 v_f - 0.01715 (T - 273.15)\right), & v_f > v_{ftc} \\ 2.3 * 10^{-6} \exp(75 v_f), & v_f \leq v_{ftc} \end{cases}$$

$$g_p = \begin{cases} 1, & v_f > v_{fpc} \\ 7.1 * 10^{-5} \exp(171.53 v_f), & v_f \leq v_{fpc} \end{cases}$$

Here, v_f represents the total free volume and v_{ftc} and v_{fpc} are the critical free volumes which are calculated as below:

$$v_{ftc} = 0.1856 - 2.965 * 10^{-4} (T - 273.15)$$

$$v_{fpc} = 0.05$$

$$v_f = \phi_m * v_{fm} + \phi_s * v_{fs} + \phi_p * v_{fp}$$

Where

$$v_{fi} = 0.025 + \alpha_i(T - T_{gi})$$

ϕ_i and T_{gi} are the volume fraction and the glass transition temperature of the polymer, solvent and monomer and α_i is the constant.
The initiator efficiency (f) describes the fraction of initiator free radicals which can successfully initiate the polymerization. Not all primary radicals can produce propagating chains. They execute many oscillations in "cages" before they diffuse apart and start a reaction. During the oscillations the radicals may also form an inactive species. Hence, to account for the two competing phenomena, initiator efficiency is appended in the mathematical model. Initiator efficiency factor also decreases as the viscosity of the reactor solution rises. The free volume theory is used to model this relationship:

$$f = f_0 \exp\left(-C\left(\frac{1}{V_f} - \frac{1}{V_{fcr}}\right)\right)$$

Here f_0 the initial initiator efficiency and C is a constant.

Molecular Weight Distribution

Together with polymer composition, the molecular weight distribution (MWD) can also show drifts that can become critical when reactions are carried to high conversion. In order to obtain complete representation of molecular weight distribution, a similar methodology based on finite weight fractions is applied[11]. However, in our application the approach needs to be modified to account for semi batch operation and the consequent volume changes. It consists of dividing the entire polymer population into discrete intervals and calculating the weight fraction of polymer in each of the discrete intervals. By ignoring the concentration of live polymer given that it is negligible compared with the dead polymer concentration, for each interval the polymer weight fraction is calculated with the following equations:

$$f(m,n) = \frac{\sum_{i=m}^{n} iD_iV}{\sum_{i=2}^{\infty} iD_iV} \quad \text{Or} \quad f(m,n) = \frac{\sum_{i=m}^{n} iD_iV}{\lambda_1 V}$$

The dynamic of weight fraction is then calculated:

$$\frac{d\,f(m,n)}{dt} = \frac{1}{\lambda_1 V}\sum_{i=m}^{n} i\frac{d(D_iV)}{dt} - \frac{1}{\lambda_1 V}f(m,n)\frac{d(\lambda_1 V)}{dt}$$

Where the right-hand side represents the dynamic growth of dead polymers of length n which can be written according to the kinetic rate equation as below:

$$\frac{d(D_iV)}{dt} = \left[k_{fm}C_m + k_{fs}C_s + k_{td}C_p\right]P_nV$$

This can be shown by further simplification as follows:

$$\frac{d(D_i V)}{dt} = k_p C_m V P_i \frac{(1-\alpha)}{\alpha}$$

Substituting we get:

$$\frac{d\,f(m,n)}{dt} = \frac{1}{\lambda_1 V}\, k_p C_m V \frac{(1-\alpha)}{\alpha} \sum_{i=m}^{n} iP_i - \frac{1}{\lambda_1 V} f(m,n) \frac{d(\lambda_1 V)}{dt}$$

The term $\sum_{i=m}^{n} iP_i$ can be represented as:

$$\sum_{i=m}^{n} iP_i = \sum_{i=m}^{\infty} iP_i - \sum_{i=n+1}^{\infty} iP_i$$

Assuming, $P_n = \alpha P_{n-1}$ and $P_n = (1-\alpha)\alpha^{n-1}P$:

$$\sum_{i=m}^{\infty} iP_i = \left[\frac{m(1-\alpha)+\alpha}{(1-\alpha)}\right]\alpha^{m-1}P - \left[\frac{(n+1)(1-\alpha)+\alpha}{(1-\alpha)}\right]\alpha^{n}P$$

And the final form of weight fraction for a semi-batch condition will be:

$$\frac{d\,f(m,n)}{dt} = \frac{1}{\lambda_1}\, k_p C_m \left(\left[\frac{m(1-\alpha)+\alpha}{\alpha}\right]\alpha^{m-1} - \left[\frac{(n+1)(1-\alpha)+\alpha}{\alpha}\right]\alpha^{n}\right)P - \frac{1}{\lambda_1 V} f(m,n) \frac{d(\lambda_1 V)}{dt}$$

Energy balances

One of the most complex features of the free radical polymerization is the exothermic nature of it. Generated energy during polymerization should be removed by a coolant or dissipated to environment. Otherwise, the reactor can thermally run away. Even if run away does not occur, molecular weight can be broaden. To model non-isothermal polymerization, energy balance should be applied to the reactant mixture in the reactor and oil in the bath. From the application of the energy conservation principle, the following equations show the energy balance for a perfectly mixed jacketed semi-batch reactor:

$$\frac{dT_r}{dt} = \frac{(-\Delta H)(k_p + k_{fm})N_m * C_p - UA\left(T_r - T_j\right) + (F_m \rho_m C_{pm} + F_i \rho_s C_{ps})(T_f - T_r)}{\rho_r C_{pr} V}$$

$$\frac{dT_j}{dt} = \frac{F_j \rho_j C_{pj}\left(T_{j,0} - T_j\right) + UA\left(T_r - T_j\right)}{\rho_j C_{pj} V_j}$$

Here T_r and T_j denote the reactor and jacket temperature respectively. It was assumed that both reactor and jacket are perfectly mixed and have a constant temperature. ρ_r and C_{pr} are the average

density and heat capacity of the reactor. C_{pm}, C_{ps} and C_{pj} are the heat capacity of monomer, solvent and coolant flow which consists of water and ethylene glycol. U is the overall heat transfer coefficient and A is the heat transfer area.

Weight Average Molar Mass ($\mathbf{M_w}$) Calculation

Controlling M_w has a high impact on the final distribution of polymers. Thus, it is of interest to investigate the effect of different parameters on M_w as well as determining a formulation which can lead to a certain trajectory. Assuming small chain transfer to monomer and solvent the instantaneous number average of a polymer which is produced at time t is given by:

$$N_{n,inst} = \frac{k_p[C_m]}{Yk_t[P_0]}$$

Where Y is a factor which is equal to 1 when the termination reaction is dominated by recombination, and 2 when disproportionation dominates. The cumulative weight average molar mass $M_w(t)$ can then be obtained by knowing the mass of dead polymer inside the reactor, $m_p(t)$, as follow:

$$M_w(t) = \frac{\int_0^t wM_m N_{n,inst}\, dm_p(t)}{m_p(t)}$$

Here w and M_m are the instantaneous polydispersity and the monomer molecular weight respectively. Assuming constant temperature, which results in constant kinetic rate parameters, the only two terms which are varying during the reaction are the concentration of monomer $[C_m]$ and live radicals $[P_0]$, both of which can be manipulated using the monomer and initiator flow. This gives the opportunity to propose various trajectories of M_w by proper formulation of the optimization problems.

V.2.2 Parameter Estimation

Kinetic rate constants are significant parameters of a polymerization system which have to be determined accurately since only a slight change in them will result in considerable change of the final polymer characteristics. The data regarding the kinetic rate constants may be obtained from literature or determined experimentally. However for some materials the properties are not available in the literature and it may not be possible to measure them through experiments due to lack of experimental facilities. Moreover, there are many criteria that affect the kinetic rate parameters such as reactor operating conditions, presence of inhibitors and purity of the materials which are different for various systems. So, proper values of the rate constants should be determined via a parameter estimation technique. This is an important prerequisite step in order to evaluate these variables and improve the model reliability for optimization and model-based control scheme development. The parameter estimation is often formulated as an optimization problem in which the estimation attempts to determine the values for the unknown parameters in order to maximize the probability

that the mathematical model will predict the values obtained from the experiments. Effective solution of parameter estimation is attainable if the following criteria are met:

1) The nonlinear system should be structurally identifiable which means that each set of parameter values will result in unique output trajectories.

2) Parameters which have a weak effect on the estimated measured variables and the parameters which their effect on the measured output is linearly dependent should be detected and removed from the formulation of the estimation since their affect cannot be either accurately or individually quantified.

For the proposed system, the parameters of the polymerization model which was discussed before can be represented as $z(t) = [X(t), M_w(t)]$ which are the outputs of the parameter estimation model and $u(t) = [T(t), F_m(t)]$ which are the time-varying inputs, and θ the set of model parameters which in this case are $[k_d, k_p, k_t, C_f, f_0]$. The selection of these parameters are justified as the most sensitivity in conversion and weight average molecular weight data is with respect to the termination and propagation rate of a polymeric chain. Proper estimation of the initiator efficiency factor is also important since it controls the effective radical concentration. In this work the parameter estimation scheme is based on maximum likelihood criterion. The gEST function in gPROMS is used as the software to estimate the set of parameters using the data gathered from the different experimental runs. Each experiment is characterized by a set of conditions under which it is performed, which are:

- The overall duration;
- The initial conditions which are the initial loading of initiator, solvent and monomer
- The variation of the control variables. For the batch experiment temperature is the only variable, while in semi batch both temperature and flow rate of monomer or initiator have to be considered.
- The values of the time invariant parameters.

Assuming independent, normally distributed measurement errors, ϵ_{ijk}, with zero means and standard deviations, σ_{ijk}, this maximum likelihood goal can be captured through the following objective function:

$$\phi = \frac{N}{2}\ln(2\pi) + \frac{1}{2}\min_{\theta}\left\{\sum_{i=1}^{NE}\sum_{j=1}^{NV_i}\sum_{k=1}^{NM_{ij}}\left[\ln\left(\sigma_{ijk}^2\right) + \frac{\left(\tilde{z}_{ijk} - z_{ijk}\right)^2}{\sigma_{ijk}^2}\right]\right\}$$

Where N represents the total number of measurements taken during all the experiments, θ is the Set of model parameters to be estimated which may be subject to a given lower and upper bound, NE , NV_i and NM_{ij} are respectively the total number of experiments performed, the number of variables measured in the ith experiment and the number of measurements of the jth variable in the ith experiment. σ_{ijk}^2 is the variance of the kth measurement of variable j in experiment i while $\tilde{z}_{ijk}$ is the kth measured value of variable j in experiment i and z_{ijk} is the kth (model-)predicted value of variable j in experiment i.

The variable σ_{ijk}^2 depends on the error structure of the data which can be constant (homoscedastic) or dependent on the magnitude of the predicted and measured variables (heteroscedastic). If σ_{ijk}^2 is

fixed in the model, the maximum likelihood problem is reduced into a least square criterion. If a pure heteroscedastic model applied, the error has the following structure:

$$\sigma_{ijk}^2 = \omega_{ijk}^2(\tilde{z}_{ijk})^\gamma$$

Which means that as the magnitude of the measured variable increases the variance of $\tilde{z}_{ijk}$ also increases. The parameter ω_{ijk}^2 and γ are determined as part of the optimization during the estimation. In this work we assume the measurement error for both conversion and weight average molecular weight in all the experiments can be described by constant variance models since the errors for both conversion and weight average molecular weight is independent of their magnitude in the measurement. The given upper and lower bounds of the variance are according to the accuracy of the measurement plant and the function gEST specifies the ω_{ijk}^2 value along with X and M_w as part of the optimization.

The capability of the model to properly describe the polymerization system has been investigated by doing a number of experiments in both semi-batch and batch mode using different trajectories for temperature and initiator and monomer flow rate. After the validation of the estimated parameters, the model can then be applied for the dynamic optimization to provide optimum temperature and monomer or initiator flow rate for a desired objective that can be a target conversion or molecular weight distribution. This step will be explained next.

V.2.3 Dynamic Optimization

The objective of the dynamic optimization is to find the optimal control profile for one or more control variables and control parameters of the system that derives the process to the desired final polymer property specification while minimizing the reaction time. The process control variables are selected based on their impact on the product quality and their capability for real time implementation. In this case temperature, monomer and initiator flow rate were selected as the control variables. Temperature plays a very important role in controlling the reaction kinetics which considerably affects the molecular weight distribution while monomer flowrate is also a powerful means of controlling molar mass by affecting the concentration of the main feed to the reactor. The initiator flow also affects both conversion and the molecular weight but offers less straightforward means for controlling molecular weight. The optimization of the model was performed using the gOPT function in gPROMS which applies the control vector parameterization (CVP) approach. Variation of the control variables in this case is considered as piecewise-constant which indicates that the control variables remain constant at a certain value over a certain part of the time horizon before they jump discreetly to a different value over the next interval. The optimization algorithm determines the values of the controls over each interval, as well as the duration of the interval. Optimizer implements a “single-shooting” dynamic optimization algorithm consists of the following steps:

1. Duration of each control interval and the values during the interval are selected by the optimizer

2. Starting from the initial condition the dynamic system is solved in order to calculate the time-variation of the states of the system

3. Based on the solution the values objective function, its sensitivity to the control variables and also the constraints are determined.

4. The optimizer revises the choices at the first step and the procedure is repeated until the convergence to the optimum condition is achieved.

For the proposed system the optimal control problem is formulated as the form below:

$$\min_{t_f, u(t), v} J(t_f)$$

Subject to the process model and the following constraints:

$$x(t_0) - x_0 = 0$$

$$t_f^{min} \leq t_f \leq t_f^{max}$$

$$u^{min} \leq u(t) \leq u^{max}$$

$$v^{min} \leq v(t_f) \leq v^{max}$$

Where J in our case in defined for the general case as

$$J = w_1 \left(\frac{X_f}{X_t} - 1\right)^2 + w_2 \left(\frac{M_{w,f}}{M_{w,t}} - 1\right)^2 + w_3 \sum_{i=1}^{nc} \left(\frac{f_{i,f}}{f_{i,t}} - 1\right)^2 + w_4 \left(\frac{t_f}{t_t} - 1\right)^2$$

Where x_0 is the initial condition of the system including the initial loading in the reactor and t_f stands for the time horizon while $u(t)$ indicates the control variables which are the temperature, monomer and initiator flow rates subjected to their lower and upper bounds. v_t : represents the time variant parameters which in this case is the volume of the contents of the reactor. The formulation of the objective function consists of four terms, whereX_f,$M_{w,f}$ and $f_{i,f}$ are the values of the monomer conversion, molar mass and weight fraction of polymer within a chain length at the final time t_f respectively andX_t,$M_{w,t}$ and $f_{i,t}$ are their corresponding desired values. $w_1 - w_4$ are the weighting factors determine the significance of each term in the objective function. A schematic representation of the optimization problem for the polymerization problem is given in Figure 47.

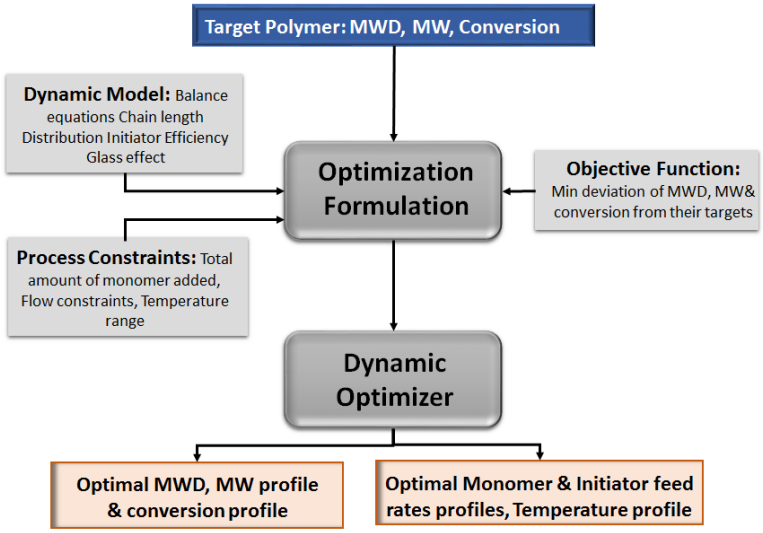

Figure 47: Schematic representation of the optimization problem in polymerization processes

V.2.4 Optimal Nonlinear State Estimation

For nonlinear state estimation, an analogous algorithm to the discrete-time extended Kalman filter (DEKF) is implemented. This method is purely recursive. The sequencing of the algorithm is as follows:

First step - Model and measurements are described in a discretized form for each iteration.

$$\boldsymbol{x_k} = f_{k-1}(\boldsymbol{x_{k-1}}, \boldsymbol{u_{k-1}}, \boldsymbol{w_{k-1}}) \quad \boldsymbol{w_k} \sim N[0, \boldsymbol{Q}]$$

$$\boldsymbol{y_k} = h_k(\boldsymbol{x_k}, \boldsymbol{v_k}) \quad \boldsymbol{v_k} \sim \mathrm{N}[0, \boldsymbol{R}]$$

$$k_\alpha = \frac{\mathrm{t}_\alpha}{\Delta t_\alpha} - 1$$

Here, $\boldsymbol{x}$ represents the state variables, $f(\cdot)$ the nonlinear process model, $\boldsymbol{u}$ manipulated variables, and $\boldsymbol{w}$ the model noise with covariance $\boldsymbol{Q}$. Moreover, $\boldsymbol{y_k}$ represents the measured properties, $h(\cdot)$ the nonlinear measurement and $\boldsymbol{v_k}$ the measurement noise vector with covariance $\boldsymbol{R}$. Both errors$\boldsymbol{w}$ and $\boldsymbol{v}$ are assumed to be independent, with zero mean and white Gaussian noise. Furthermore, k_α is the iteration in which the DEKF is activated, where t_α is the initialization time in [min], andΔt_α is the time interval for nonlinear state estimation in [min].

Second step.- Initialization: For $k = 0$, the nonlinear process model presented initializes and computes current state variables based on the previous states. Additionally, the process model uses real measurements of the controlled variables of system during the calculation of the current states. The initial covariance error matrix $\boldsymbol{P_0}$ and covariance matrices $\boldsymbol{Q}$ and $\boldsymbol{R}$, which contain the DEKF's free parameters, are fixed. State estimation accuracy and data reconciliation ability of the DEKF depend largely on the quality of these parameters.

Third step.- DEKF: For $k > k_\alpha$, notice that the superscripts "+" and "-" denote *a priori* and *a posteriori* states, respectively. *A priori* refers to when the calculation is done before $\boldsymbol{y_k}$ is taken

into account. *A posteriori* refers to when the calculation is after $\boldsymbol{y}_k$ is considered. The following computations occur:

- Derive the model Jacobian matrix of partial derivatives, linearize it around its previous *a posteriori* state estimate and approximate it to a discrete-time approach.

$$\boldsymbol{F}_{k-1} = exp\left(\left.\frac{\partial f(\cdot)}{\partial x}\right|_{\hat{\mathbf{x}}^{+}_{k-1}} \cdot \Delta t_{\alpha}\right)$$

- Calculate the time update of the state estimate and the estimation error covariance matrix, **P**, which is an indicator of the estimation accuracy.

$$\hat{\mathbf{x}}_k^- = f_{k-1}(\hat{\mathbf{x}}_{k-1}^+, \boldsymbol{u}_{k-1}, 0)$$

$$\boldsymbol{P}_k^- = \mathbf{F}_{k-1}\boldsymbol{P}_{k-1}^+\mathbf{F}_{k-1}^T + \mathbf{Q}$$

- Compute the measurement Jacobian matrix of partial derivatives and linearize it around its current a priori state estimate.

$$\boldsymbol{H}_k = \left.\frac{\partial h_k}{\partial x}\right|_{\hat{\mathbf{x}}_k^-}$$

- Calculate the measurement update of the state estimates and estimation error covariance. **K** is the Kalman gain matrix. It computes the amount of correction to incorporate or take from the state variables on their a priori estimation. Notice that the stability properties of the estimation error dynamics can be analyzed through the eigenvalues of the matrix$\mathbf{F} - \boldsymbol{K}\mathbf{H}$.

$$\boldsymbol{K}_k = \boldsymbol{P}_k^-\boldsymbol{H}_k^T\left(\boldsymbol{H}_k\boldsymbol{P}_k^-\boldsymbol{H}_k^T + \boldsymbol{R}\right)^{-1}$$

$$\hat{\mathbf{x}}_k^+ = \hat{\mathbf{x}}_k^- + \mathbf{K}_k[\boldsymbol{y}_k - h_k(\hat{\mathbf{x}}_k^-, 0)]$$

$$\boldsymbol{P}_k^+ = (\mathbf{I} - \mathbf{K}_k\mathbf{H}_k)\boldsymbol{P}_k^-$$

In this formulation, the DEKF has a hybrid implementation. The real-time integration of the nonlinear model computes the state estimates, whereas linear approximation computes the estimate error covariance and the filter gain matrices. The advantages of the filter lie in its nature of estimation and predictive-corrective form. The recursive characteristic allows rapid estimation in real-time, which is mandatory for online deployment. However, a disadvantage is that it cannot take into account bounds on process variables and other constraints.

Tuning the DEKF

For obtaining a robust action of the filter, an adequate tuning of its free parameters is required. The tuning problem addresses the offline minimization of the mean squared errors between the estimated and measured values in each iteration. All measurements have different weights, $\boldsymbol{w}_j$, which aims to normalize the terms by giving them the same importance. To avoid unreal kinetics and unstable behavior of the system, the problem is constrained to only positive values of the *a posteriori* estimated state variables. In addition, the free-parameters search is constrained between an upper and a lower bound vector of $\boldsymbol{p}$ parameters that search the diagonal values $\boldsymbol{P_0}$, $\boldsymbol{Q}$ and $\boldsymbol{R}$. Thus, the dimensionality of the optimization/tuning problem is $r + 2q$, where r denotes the available measurements and q the number of state variables. The selected cost function is.

$$\min \sum_{r=1}^{r} \frac{w_r}{k} \sum_{k=1}^{k} [y_{k,r} - h_{k,r}(\boldsymbol{p}, 0)]^2$$

Constraints:

$$0 < \hat{\mathbf{x}}_k^+$$

$$\boldsymbol{p}^{LB} \leq \boldsymbol{p} \leq \boldsymbol{p}^{UB} \qquad (28b)$$

The algorithm for tuning the DEKF is the Parallel Local Metric Stochastic Radial Basis Function with Restart (*Par*LMSRBF-R) algorithm. This algorithm seeks optimal parameters using a surrogate model, e.g. radial basis function, and evaluates multiple points simultaneously. When no improvement is attested, the algorithm restarts in order to avoid local optimal solutions.

In summary, the algorithm follows a master-worker criterion, assuming that γ processors are available and two function evaluations consume the same computational time. A set of initial points generated by a space filling or other similar experiment design evaluate the cost function. The surrogate model is initially fitted and then updated using the output from each iteration. The function is evaluated with the points obtained from a group of candidate points. *Par*LMSRBF-R performs exploitation of the solution domain by keeping track of the consecutive failed, C_{fail}, and successful, $C_{success}$, iterations. When C_{fail} or $C_{success}$ exceed a predefined tolerance value, the step size is reduced by half or doubled respectively. Later, the recorded values of C_{fail} and $C_{success}$ are reset. Two scored criteria evaluate the next point: the estimated value generated by the response surface model and the minimum distance from points evaluated earlier. A good candidate point should be far from its previously evaluated one, and its estimated function value should be as close as possible to the actual value.

V.2.5 Feedback Control

Linear Feedback Control of M_w

To control the M_w trajectory, a conventional Proportional-Integral (PI) controller is designed where M_w is controlled by manipulating monomer flow rate. The choice of the manipulated variable for the feedback control of the M_w is based on the input effects on the controlled variable, in terms of gain and response time. From the simulation analysis of the response, the monomer flow has been shown to better fit the requirements than initiator flow rate. The feedback control uses a *PI*–like algorithm, which is expressed mathematically as follow:

$$u_n = \bar{u} + k_c \left[e_n + \frac{\Delta t}{\tau_I} \sum_{k=1}^{n} e_k \right]$$

Where $\mathbf{u_n}$ denotes the value for input variables (monomer flow) at each time instant which is sent to the pump. $\mathbf{k_c}$ and τ_i are the proportional gain and integral time constants of the controller.

These parameters are tuned using different simulations with the model, and optimum values for the proportional and integral constants are selected which vary for each experiment.

An alternative approach is to use the velocity form in which the change in controller output is calculated and applied instead of the output value. Writing the equation for the (n-1) sampling time and subtracting, straight forward calculation will lead to the following form:

$$\Delta u_n = k_c \left[(e_n - e_{n-1}) + \frac{\Delta t}{\tau_I} e_n \right]$$

The velocity form has two main advantages over the position form. First it intrinsically contains some provisions for antireset windup since the summation of errors is not explicitly calculated. The antireset windup could be considerably high for M_w because the time constant of the process is rather high and the response is slow. Secondly, for velocity control algorithms, applying the controller in automatic mode, that is, switching it from manual operation, does not require any initialization of the output $\bar{u}$. This is also a prerequisite in this work since all the control experiments start based on the optimization trajectory for the first $15 \sim 20$ minutes of the experiment and then once the data from ACOMP stabilizes, the controller starts to provide corrective actions.

Nonlinear (Linearizing) Control of Monomer Concentration

From previous discussions, it is clear that the main objective in controlling polymerization reactors is to control M_w and indirectly the MMD. However, real-time measurement of monomer concentration is also available by ACOMP. Therefore, an effort was made to control the total amount of monomer and as a result the monomer concentration inside the reactor by manipulating the monomer flow (F_m). The control strategy is based on the input-output linearizing geometric approach which takes into account the nonlinear dynamics of the processes, formalized in the general dynamic model. Unfortunately, due to the complex relationship between M_w and F_m no such formulation can be designed for controlling M_w.

The principle of the linearizing approach is to find a control law such that the tracking error is governed by a pre-specified stable linear differential equation called a reference model. The control algorithm can be explained in three steps. First the input output model should be derived by appropriate manipulation of the general dynamic model. This provides an explicit relation between the manipulated variables and the control objectives which takes the form of an n_{th} order differential equation:

$$\frac{d^n y}{dt^n} = f_0(t) + u(t) f_1(t)$$

With n being the relative degree of the input/output model. Depending on the control and manipulated variables, $f_0(t)$ and $f_1(t)$ could be highly complex functions of the model parameters. However, the relation is always linear with respect to the manipulated variable. Secondly, a stable linear reference model of the tracking error is selected. The model determines how we desire the tracking error to decrease and presented as follow:

$$\sum_{j=0}^{n} \lambda_{n-j} \frac{d^j}{dt^j}[y^*(t) - y(t)] = 0 \qquad \lambda_0 = 1$$

The coefficients λ_{n-j} are tuning coefficients which should be selected so that the differential equation (30) is stable. Finally the control design consists of calculating the control action $u(t)$ such that the input-output model exactly matches the reference model. Using the previous equation and substituting for $\frac{d^n y}{dt^n}$ solution for $u(t)$ can be obtained.

$$u(t) = \frac{1}{f_1(t)}\left[-f_0(t) + \sum_{j=0}^{n} \lambda_{n-j} \frac{d^j}{dt^j}[y^*(t) - y(t)] + \frac{d^n y^*}{dt^n}\right]$$

The formalism of the nonlinear controller using F_m as manipulated variable is considered in this case. The relative degree of F_m with N_m is one thus simplifying the controller formulation. Substituting for $\frac{dN_m}{dt}$, an explicit relation for monomer feed rate $F_m(t)$ can be obtained with respect to known variables:

$$F_m = \frac{\frac{dN_m}{dt}^* - \lambda_p\,[N_m^* - N_{mp}] - \lambda_I[\int (N_m^* - N_{mp})dt] + F_{out}C_m + (k_p)C_p N_m}{C_{mf}}$$

Where N_m^* is the desired/target optimal known trajectory for total amount of monomer obtained from dynamic optimization. It is worth mentioning that similar approach is also possible by using the initiator flow as manipulated variable, however, in this case the relative degree is two thus leading to more complex (although explicit) relationship for the initiator flow.

3. Experimental Implementation

V.3.1 Experimental apparatus and setup

The polymerization pilot plant consists of a 1.5 L reactor monitored by the ACOMP system and different auxiliary fittings and instruments. Pumps driven by encoded stepper motors inject monomer and initiator solutions into the reactor. An external jacket sets the inner temperature of the reactor at certain conditions. From a high flow rate (~40 mL/min) recirculation loop annex to the reactor, the ACOMP extracts a constant sample stream. For pilot scale, a rate of 0.5 mL/min is sufficient. This setup allows minimal time delay from the time new materials are added into the reactor until they are finally detected by the sensor. The ACOMP analyzes the sample by diluting it 80 times with deionized water and homogenizing it in a mixing chamber. Ultraviolet visible absorption spectroscopy, viscometry, and multi-angle laser light scattering detectors measure the sample. The monomer and polymer concentrations are determined by spectroscopy at 245 nm, and the M_w is calculated from the static/multi-angle light scattering data. To ensure stable readings during the experiment, air bubbles are purged from the ACOMP sensors to guarantee precise measurements. Figure 3 illustrates the pilot plant components and its functionality.

Once the experiments are completed, the Gel Permeation Chromatography (GPC) method provides the final MWD with an in-house system. It consists of a Shimadzu LC-10ADVp (Columbia, MD) high-pressure solvent delivery pump that provides a continuous flow of sodium chlorine solution through the GPC column followed by a Shimadzu RID-10A differential refractometer. The sample injector is an IDEX/Rheodyne MX-II with a 50 μL sample loop volume. A series of polyethylene oxide standards ranging from 25,000 to 1 million g/mol are used to create a standard column calibration. The described method refers as GPC standard calibration.

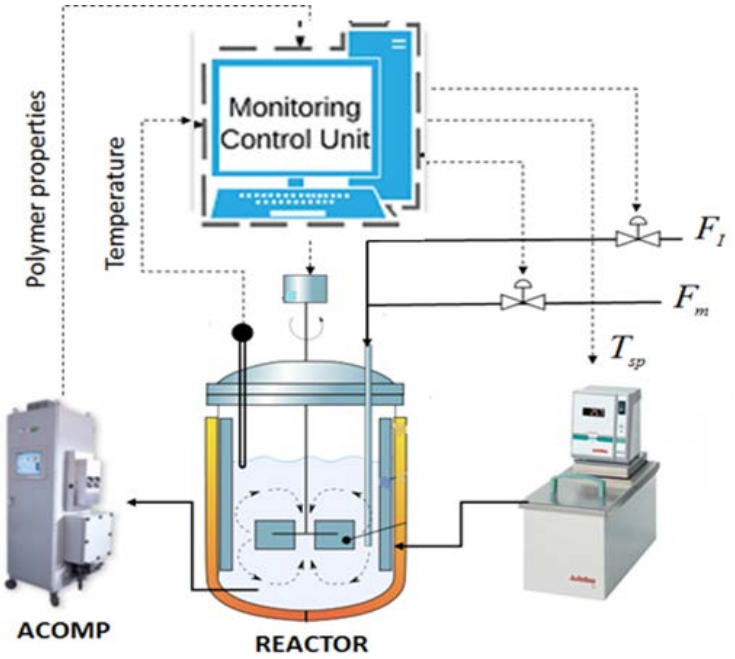

Figure 48: Schematic of experimental setup

V.3.2 Integrated State Estimation and Control Framework

The proposed framework includes the integration of nonlinear state estimation to improve linear control and monitor unmeasured properties. The framework embraces offline tuning of the filter and the dynamic optimization of the system. The filter/controller module is implemented in *python 2.7* environment as it allows full connectivity and has compatibility with the ACOMP server. Figure 49 explains with a flow diagram the functionality of the module. Because the DEKF requires several iterations to converge, a cascade structure improves the resolution of the filter and guarantees an adequate control action. The filter remains in the inner loop at a higher frequency than the outer loop where the control is allocated. Although the DEKF is in the high-frequency loop, it still has a discrete performance. The ACOMP updates measurements every 1 sec; thus, the relation $1\ sec < \Delta t_{\alpha} < \Delta t_{\beta}$ must occur for a satisfactory operation of the module. Narrower time intervals in state estimation bring higher accuracy to the filter action.

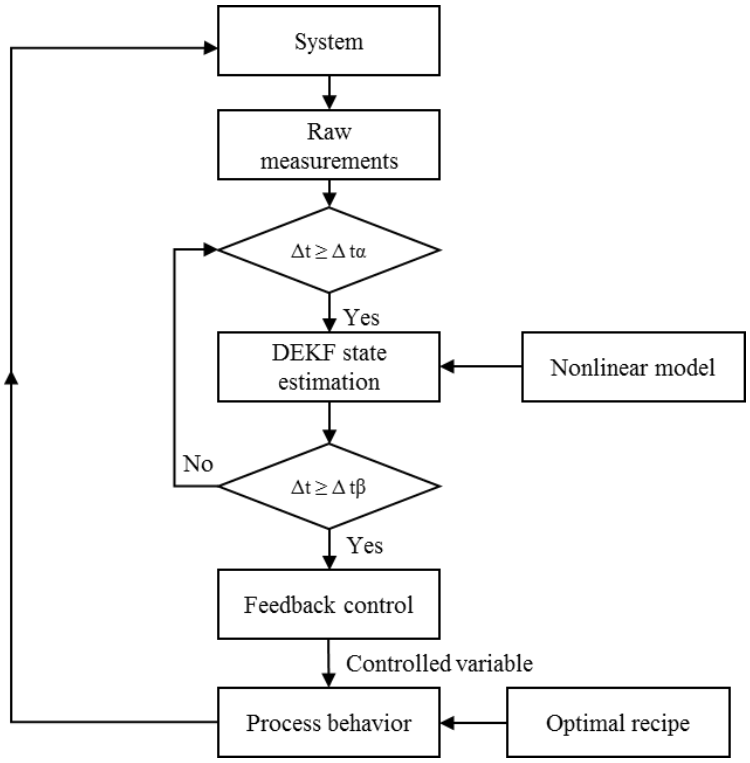

Figure 49: Flow Diagram of DEKF, PID feedback control and process behavior coupled

Figure 50 shows the proposed framework and the idea behind the overall integration. By using gPROMS, optimal recipes through dynamic optimization are generated offline. Similarly, the DEKF free-parameters are tuned using a stochastic global optimization technique. The ACOMP provides online measurements of M_w, C_m, and V which are taken into account for state estimation while reconciling these measurements. The measured control variables F_m, F_i and T are included into the nonlinear model to give more realism to the model. Six state variables are corrected in each iteration based on the attested errors and the Kalman gain matrix. Moreover, the estimated state variables are utilized to calculate unmeasured properties, e.g., MWD and M_n, which allows its monitoring during the reaction. The module starts 20 min after the reaction initiated because the ACOMP requires a prior stabilization of its measurements.

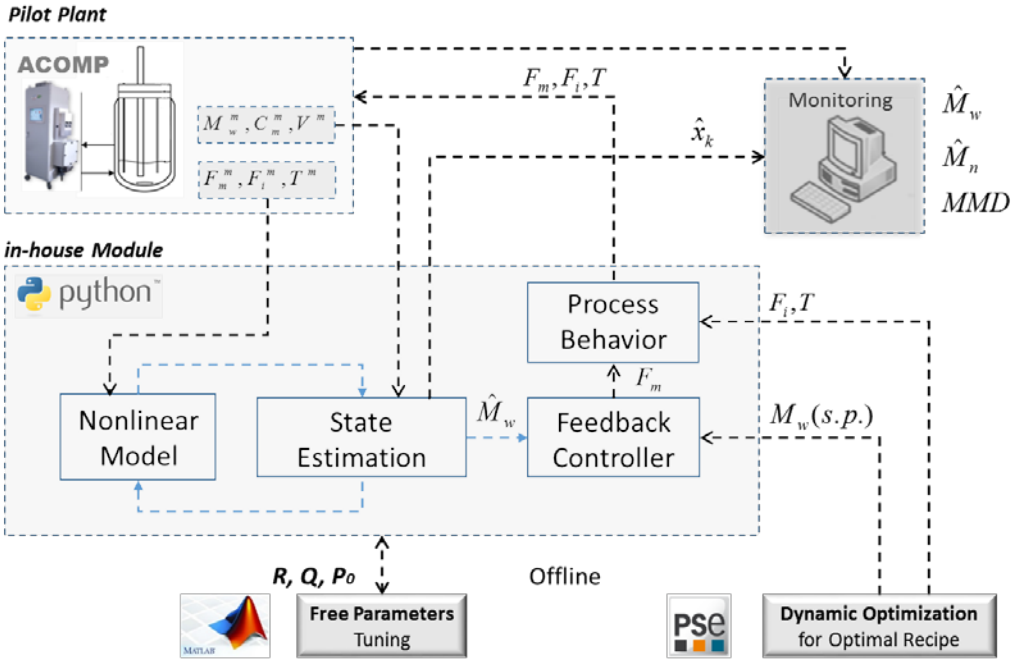

Figure 50: State estimation, monitoring and feedback control framework

4. Results and Discussion

V.4.1 Parameter Estimation

In an initial step, using a set of the experimental data, parameter estimation was performed for the main kinetic parameters. The optimal values of the estimated parameters as well as the uncertainty of the parameter represented as 95% confidence interval (CI) are shown in Table 4. In addition the correlation matrix, given as an 8 × 8 lower triangular matrix (the upper triangular matrix is identical to the lower one), is provided in this table. The most pronounced correlations between the parameters are shown in bold with a threshold value of 0.7.

Most of estimated parameters obtained have narrow confidence intervals indicating that the number of measurements performed for the parameter estimation were sufficient. The normalized covariance matrix shows that although a few parameters are quite correlated, most parameters estimated in the optimization are only weakly correlated and thereby suitable for being estimated simultaneously. The greater correlation coefficients are found between the propagation rate and the termination rate as well as initial initiator efficiency and decomposition rate. Likely, any change in one of these parameters could be compensated by a change in the other ones. For example, the coefficient between *Ap* and *Ad* is 0.94 indicating a strong correlation between them and making it difficult to find a unique estimate for these parameters. Unique parameter estimate means that the parameters shall have an acceptably low correlation to any of the other parameters and a low confidence interval. Thus, in spite of the large covariance above mentioned, a consistent estimation is possible because of the true value of the parameter estimates are located within a very small confidence bands reducing their uncertainty. However the confidence ellipsoids are large including in most cases negative numbers. Thus a second iteration was performed by eliminating two of the correlated parameters *Ad* and *At* and fixing their values to the estimated ones in the first iteration.

The optimal values of the estimated parameters as well as the uncertainty of the parameter represented as 95% confidence interval (CI) are shown in Table 5.

For illustration purposes the confidence regions for the parameter pairs estimated are shown in Fig. 51. Here, the contours correspond to a confidence level of 95%. In other words, there is a probability of 95% that the true values of the parameter pair fall within this ellipsoidal confidence region that is centered in the parameter estimates. The narrow shapes of the joint confidence regions given in Fig. 51 indicate a reliable estimation of the parameters.

Table 4: Original and estimated value of the kinetic rate parameters (first iteration)

Par.	Description	Original value	Estimated value	Confidence Interval			95% t-value	Standard Deviation
				90%	95%	99%		
	Decomposition rate [1/min]	$1.58*10^{15}$	$1.37*10^{15}$	$1.25*10^{14}$	$1.49*10^{14}$	$1.96*10^{14}$	9.19	$7.60*10^{13}$
	Propagation rate [m3/mol.min]	$4.2*10^{5}$	$9*10^{5}$	$5.23*10^{4}$	$6.23*10^{4}$	$8.20*10^{4}$	14.43	$3.17*10^{4}$
	Termination rate [m3/mol.min]	$1.06*10^{8}$	$4.56*10^{8}$	$5.97*10^{7}$	$7.12*10^{7}$	$9.37*10^{7}$	6.40	$3.63*10^{7}$
f_0	Initial initiator efficiency	0.58	0.57	0.048	0.057	0.076	9.84	0.029
	Solvent transition temperature [K]	181	142.61	0.539	0.6431	0.84	221.7	0.327

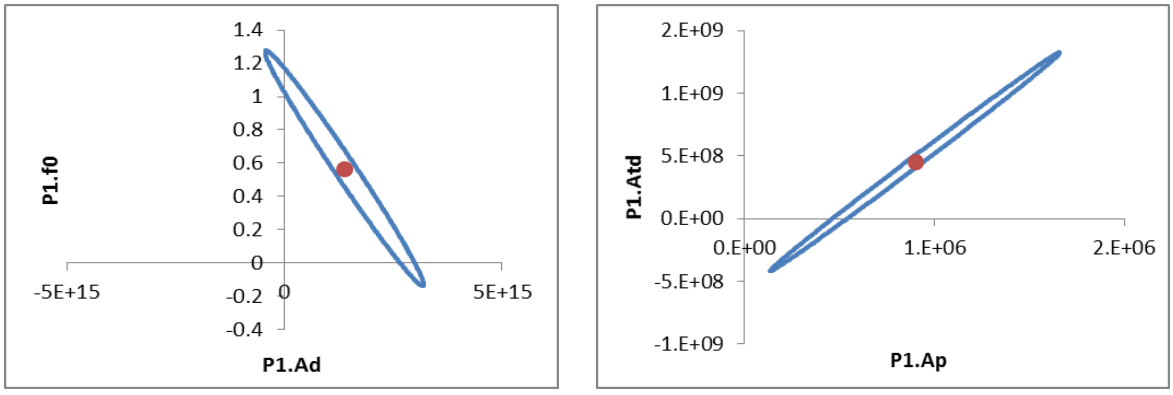

Figure 51: Confidence ellipsoids for *Ad-f0* and *Ap-At*

Table 5: Original and estimated value of the kinetic rate parameters (second iteration)

Par.	Description	Original value	Estimated value	Confidence Interval			95% t-value	Standard Deviation
				90%	95%	99%		
	Propagation rate	$3*10^{5}$	$8.5*10^{5}$	2547	3035	3993	280.1	1546

	[m3/mol.min]							
f_0	Initial initiator efficiency	0.58	0.56	0.001166	0.0013	0.00182	403.2	0.00073
	Solvent transition temperature [K]	142	149.94	0.3906	0.465	0.6123	322.2	0.237

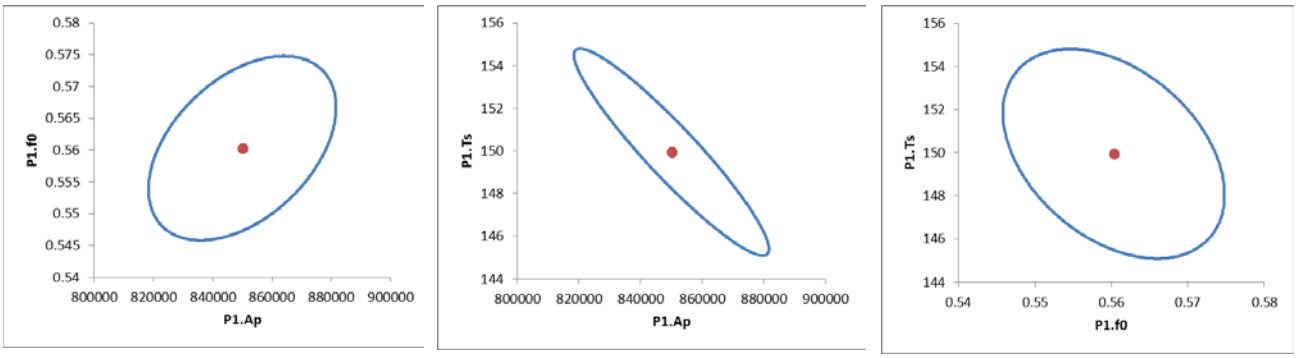

Figure 52: Confidence ellipsoids for final estimated parameters

V.4.2 Off-Line Dynamic Optimization Studies

The objective of the dynamic optimization is to provide optimal set point profiles for the controller to achieve a target polymer. Decision variables in the optimization are selected based on their impact on the product quality and their capability for real time implementation. In the proposed case study, temperature, monomer and initiator flow rates were selected as decision variables. The optimization studies were performed using the gOPT function in gPROMS which applies the control vector parameterization (CVP) technique [28]. On the following the results of the optimization are illustrated for a number of operational scenarios in terms of alternatives trajectories of the M_w.

<u>Case 1:</u> Decreasing Trajectory of M_w

This is the most common trend of M_w in polymerization reactions which naturally occurs in free radical batch reactions. At the beginning of the process when the monomer concentration is high, polymers of high chain length are formed, resulting in high M_w. Gradually, by depletion of monomer in the reactor, the length of the produced polymer reduces, resulting in smaller M_w. By proper formulation of the optimization problem it is possible to obtain a certain decreasing trajectory with a specific final value for M_w. The expression for the objective optimization problem in this case is summarized as follows:

$$J = w_1\left(\frac{X_f}{X_t} - 1\right)^2 + w_2\left(\frac{M_{w,f}}{M_{w,t}} - 1\right)^2 + w_3\sum_{i=1}^{nc}\left(\frac{f_{i,f}}{f_{i,t}} - 1\right)^2 + w_5\left(N_{mf,f}\right)$$

Table 3 provides the values of the different parameters and constraints used in this case. Temperature and flow constraints are used based on the capacity of the pump and jacket while the minimum volume constraint is the minimum volume necessary for proper mixing of the reactor contents. Figure 9 shows the optimal trajectories of the input variables, which are the temperature, monomer

and initiator flows. As it is presented in the flow profiles at the beginning of the reaction the flow rate of monomer to the reactor is high while the initiator feed is rather low. However, in order to decrease the M_w, the optimizer reduces the monomer flow after some time while rising the initiator feed to increase the free radical concentration. This will reduce the instantaneous number average of the polymers and as a result the cumulative weight average molar mass (M_w) also decreases. Results in terms of monomer concentration (which is a more common parameter than conversion in semi batch reactions) and M_w with their corresponding targets are shown in the lower panel of Figure 53. The complete distribution has also been presented at the final time of the simulation. There is a very good agreement between the simulations and the corresponding targets for the three control variables suggesting the advantage of using reagent and monomer flow with temperature to control not only the conversion (monomer concentration) and M_w but also the complete distribution (MMD).

Table 6: Values of the optimization constraints parameters

Variable	Value	Unit
	0.3	mol
	50	mol
	0.005	mol
	5	ml/min
	5	ml/min
	80	°C
	40	°C
	1200	ml
	450	ml

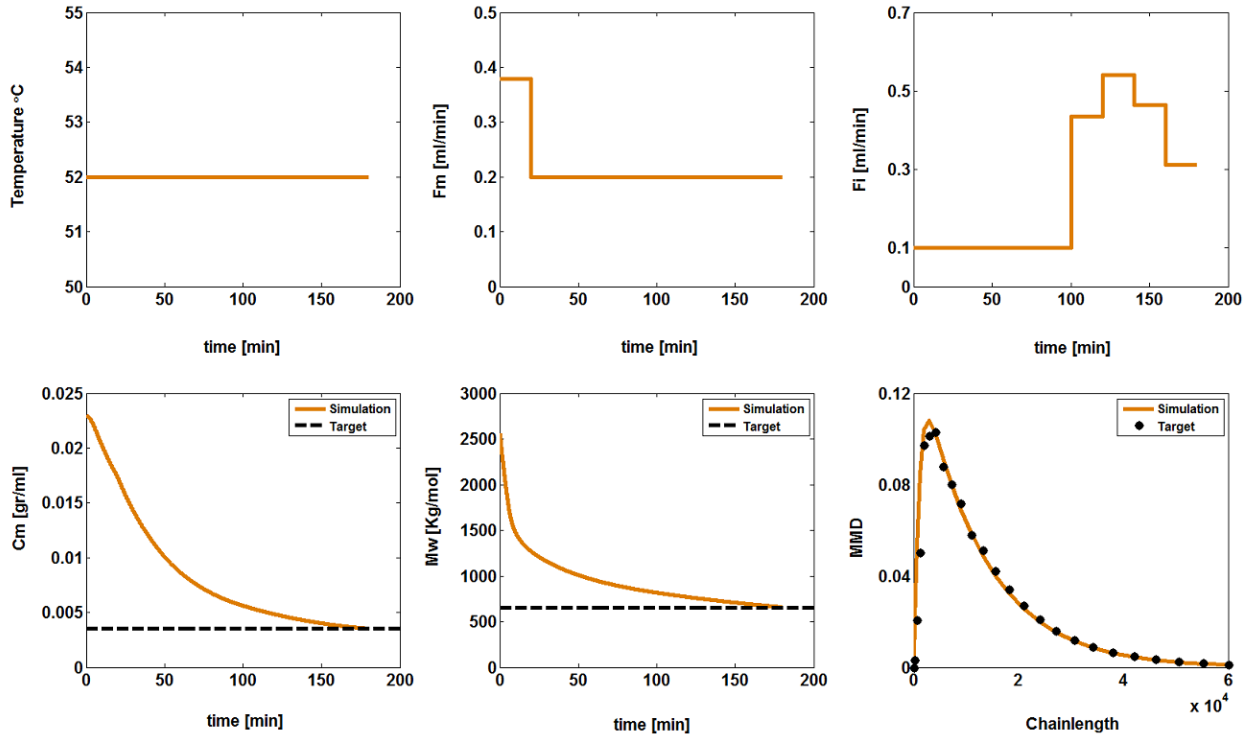

Figure 53: Simulation results applying the optimal trajectories for the decreasing M_w trend

Case 2: Constant M_w

According to Equation 22, by keeping a constant ratio between the monomer and free radical concentration, the instantaneous number average molar mass and as a result M_w will stay constant along the reaction. So an attempt was made to reach a constant trajectory of M_w. The objective function in this case is formulated as follows:

$$J = w_1 \int_0^{t_f} \left| \frac{\partial M_w}{\partial t} \right| dt + w_2 \sum_{i=1}^{nc} \left(\frac{f_{i,f}}{f_{i,t}} - 1 \right)^2 + w_3 \left(N_{mf,f} \right)$$

Monomer conversion was eliminated from the objective function to put more weight on the other terms, as it is more demanding in this case to reach a constant M_w profile. The initial loading of the reactor and the constraints are the same as in the previous case. Simulation results are shown in Figure 54. M_w follows a constant trajectory and there is a good match between the final distribution results and the targets. From the manipulated variable profiles it can be deduced that while the optimizer almost keeps a constant flow rate of monomer it gradually reduces the initiator flow to compensate for monomer consumption and keep the ratio between monomer concentration and free radicals constant.

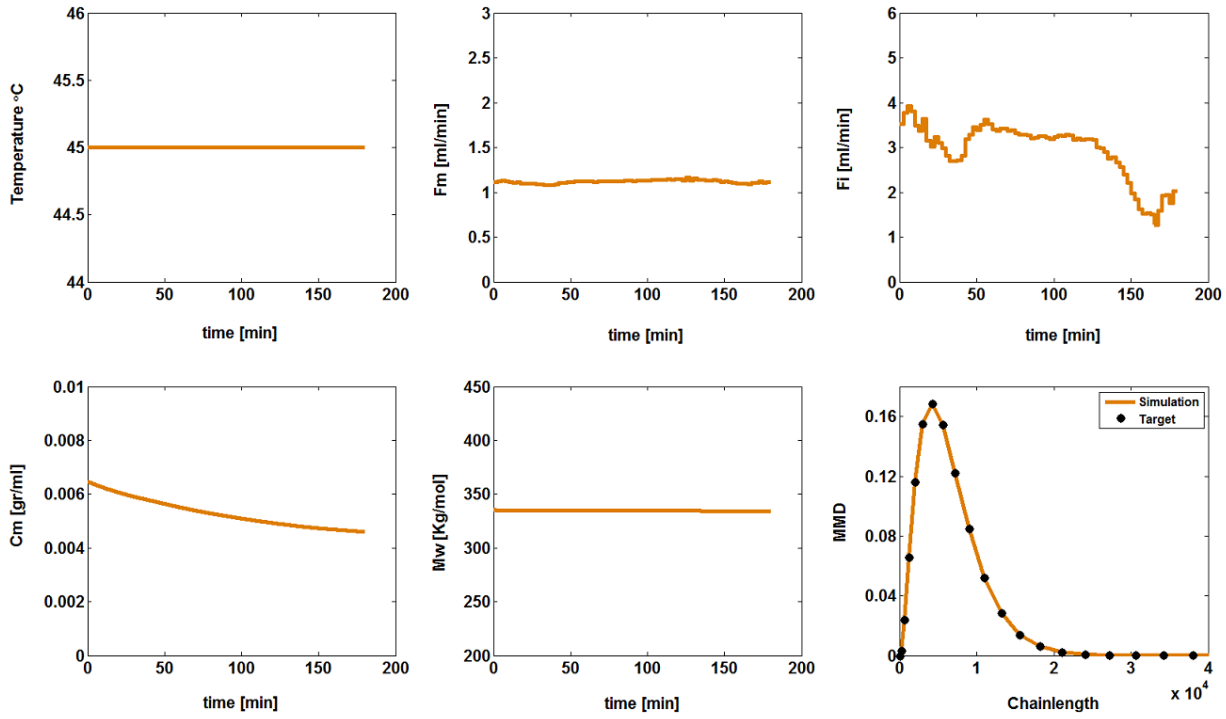

Figure 54: Simulation results using the optimal trajectories for the constant M_w trajectory

Case 3: Increasing M_w

In the previous case studies it was observed how to keep M_w constant by keeping a constant ratio between the monomer and free radical concentrations. It was also shown how to have a decreasing trend of M_w starting from a high value of M_w and reducing the monomer feed while increasing the initiator flow. To complete our analysis, here we focus on an optimization scheme which could lead to an increasing trend of M_w. This requires a higher monomer flow compared with the initiator which was injected to the reactor in case 1 which causes the reactor volume exceeding the maximum value allowed. To meet the optimization constraints, the initiator concentration was reduced and the monomer concentration was increased in their corresponding flows. The objective function in this case is formulated as follows

$$J = w_1\left(\frac{X_f}{X_t} - 1\right)^2 + w_2\left(\frac{M_{w,f}}{M_{w,t}} - 1\right)^2 + w_3\sum_{i=1}^{nc}\left(\frac{f_{i,f}}{f_{i,t}} - 1\right)^2$$

The term N_{mf}, total amount of monomer injected to the reactor, was eliminated to give the extra degree of freedom to add monomer. Results are shown in Figure 3. M_w increases successfully during the simulation and reaches the desired target. There is also a good match in the monomer concentration and MMD results between the targets and simulation profiles. It should be mentioned that although in this case initiator and monomer flow do not change considerably during the process, by changing the feed concentration as explained earlier an increase in C_m and as a result in the instantaneous number average happen. This is also demonstrated in Figure 55 in the monomer concentration profile. More moles of monomer are feeding in than are being polymerized, so the monomer concentration goes up, and thus the M_w.

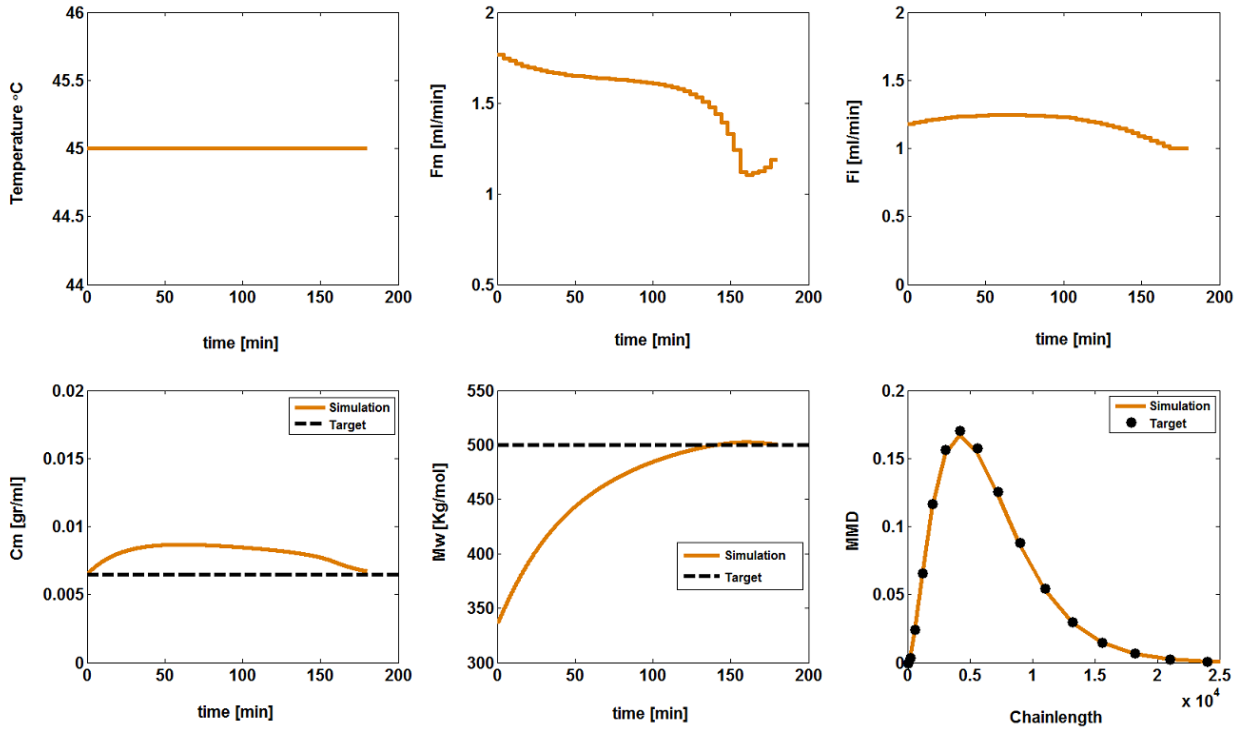

Figure 55: Simulation results using the optimal trajectories for the increasing M_w trajectory

Three optimal trajectories, which correspond to the increasing, constant, and decreasing M_w are formulated and experimentally tested to verify the behavior and flexibility of the model under different operating conditions. As displayed in Figure 56, different trajectories of M_w generate different shapes of MWD which is the ultimate control objective in terms of achieving desired polymer properties. Table 2 provides information of the initial experimental set up as well as the monomer and initiator inlet flows concentration. In the results section, the open-loop optimal trajectories are given and compared with the filtered predictions as well as closed-loop results. All experiments run at the constant temperature of 45 °C.

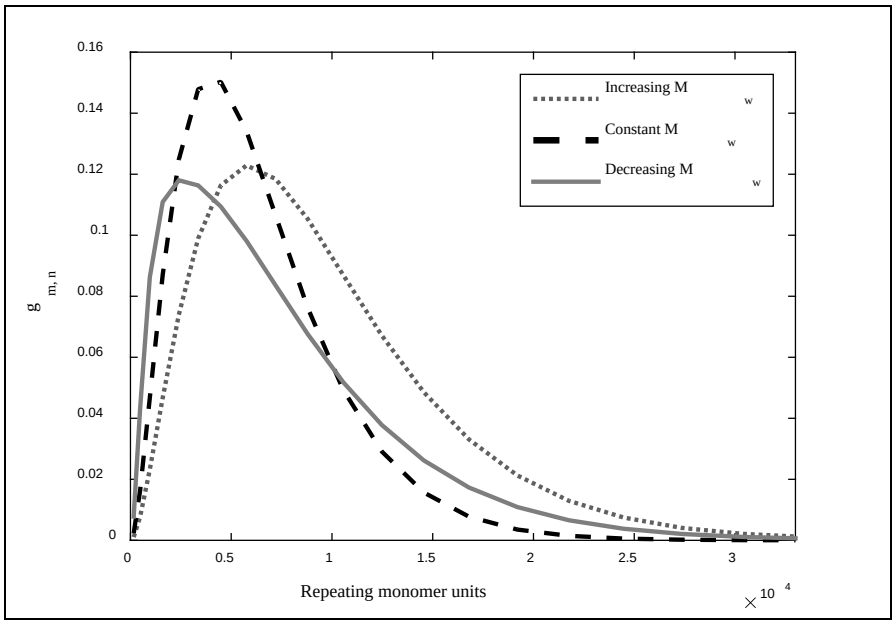

Figure 56. Final MWD of optimal trajectories

V.4.3 Real-time Testing Studies

This section will show the results obtained for all the optimization and control techniques studied in the previous parts. To demonstrate the feasibility of the proposed strategies, different objective functions which were calculated in the optimization section, were validated experimentally using data from ACOMP. Building on these results, three control experiments were implemented in which the controller set-points are the optimal trajectories obtained from the simulation. The feedback control was achieved in all cases using the monomer flow as manipulated variable to control M_w. All other input profiles, namely the temperature and initiator flow rates were set equal to their corresponding optimal trajectories obtained during optimization. Furthermore, for all closed-loop cases the system was initially started using the optimal input trajectories and after 20 minutes the controllers were switched on to provide corrective action. This was to allow enough polymerization to occur for the SLS detector signal to be larger than the baseline noise. Table 7 gives a summary of all the various optimization and control experiments, including the initial loading, feed rate concentrations, and control parameters for each reaction.

Table 7: Summary of all the optimization and control experiments

Exp. #	Exp. description	[mol]	[mol]	[mol]	[mol/m3]	[mol/m3]	[Prop. gain]	[Int. gain]
1	Optimization decreasing M_w	0.3	50	0.005	110.9796	7175.014	N/A	N/A
2	Feedback control decreasing M_w	0.3	50	0.005	110.9796	7175.014	5×10^{-9}	1×10^{11}
3	Optimization const. M_w	0.05	30	0.008	3.699	1406.866	N/A	N/A
4	Feedback control	0.05	30	0.008	3.699	1406.866	2×10^{-8}	1.5×10^{10}

	const. M_w							
5	Optimization increasing M_w	0.05	30	0.008	3.699	1406.866	N/A	N/A
6	Feedback control increasing M_w	0.05	30	0.008	3.699	1406.866	2×10^{-8}	1.5×10^{10}
7	Feedback control C_m	0.3	50	0.005	110.9796	7175.014	N/A	N/A

DEKF Tuning & System Stability

The free parameters of the filter are tuned offline using real data from one OL experiment. The utilized algorithm evaluates a total of 512 points using the proposed cost function. It tests 16 candidate points in each iteration. Figure 57a displays the convergence profile of the cost function during the evaluations. Table 8 shows the tuned free-parameters obtained with *Par*LMSRBF-R. The stability effects of these parameters require verification in order to use them in closed loop experiments. To evaluate the free-parameters, the eigenvalues of the estimation error dynamics per iteration are calculated for all OL experiments. Figure 57b presents the distribution of the eigenvalues in a real-imaginary plane. Clearly, the eigenvalues fall inside the unitary circle. Thus, the propagation of estimation error dynamics exposes stable behavior with the acquired parameters making closed loop experiments promising.

Table 8: *DEKF* Free parameters

Covariance Matrix	Parameter Value
	diag ([6.2868E-03, 1.0E-06, 1.0E-04, 71.7574, 1.7437E-02, 9.8167])
Q	diag ([6.1502E-03, 3.56E-07, 8.21E-05, 8.697, 3.9721E-03, 4.1485E-03])
R	diag ([1.0E-02, 3.3417, 2.9621E-11])

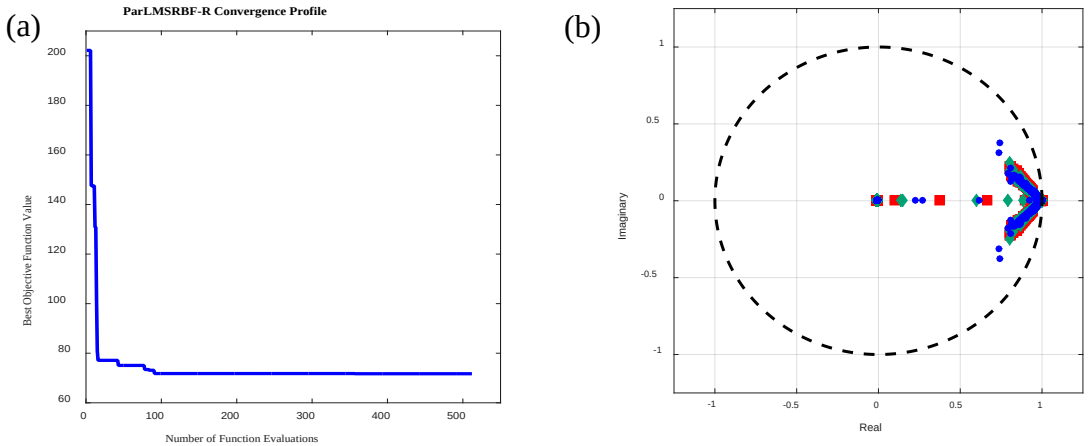

Figure 57: a) Convergence profile when tuning offline the DEKF free parameters using *ParLMSRBF*-R b) Eigenvalues of the estimation error dynamics for the three OL experiments for different M_w, where ■ increasing, ◆ constant and ✤ decreasing trajectory.

V.4.4 Open Loop Testing

Initial tests take place for observing the DEKF performance using real data from ACOMP in OL experiments. These embrace the three optimal trajectories formulated during the offline dynamic optimization stage. Throughout OL experiments, the process behavior follows strictly the dynamic conditions provided by the optimizer without other actions. Thus, F_m and F_i are set equal to the profiles provided by gPROMS, and a constant T is set. Furthermore, while the reaction starts in the pilot plant, the nonlinear model initializes. As the DEKF algorithm explains, prior to filtering action, the nonlinear model is the only one running. After 20 minutes, the module starts estimating state variables and reconciling measurements making the monitoring of free-radical polymerization reactions broader. Unmeasured properties of interest include M_n and MWD.

Figures 58-60 illustrate the DEKF action for all OL scenarios. Each figure presents different combinations of estimated properties, experimental values and optimal trajectories. Figures 58a, 59a & 60a reveal critical information related to the DEKF competency for state estimation and data reconciliation. Reconciled or estimated M_w data points pass through their measurements. It shows how the estimates reduce their noise in contrast to raw measurements, and confirms the ability of the filter to bring the model close to the measurements. On the other hand, the DEKF is able to track the evolution of M_n and MWD, which are unmeasured properties along the reaction. In chemical plants, some properties are simply unmeasurable or take significant time to obtain their experimental values. Thus, the opportunity to expand monitoring is possible when using state estimation techniques combined with the ACOMP online measurements. The estimated M_w and M_n are drawn in parallel with respect to their optimal trajectories presented with dashed lines. This shows physical consistency between estimated and theoretical values. Figures 58b, 59b & 60b and Figures 58c, 59c & 60c depict estimated, measured, and optimal trajectories for C_m and V. Both sets of results present satisfactory response as the estimated values follow the measurements observed by the sensors.

Another important piece of information generated by the filter is the time evolution of the MWD. Figures 58d, 59d & 60d illustrate a comparison between the estimated and measured MWD. The second one is obtained using the standard calibration GPC method. In this regard, the reader should recall that the MWD is not measured online, but a sample is taken only at the end of each experiment. It takes around 15 to 30 min to obtain the experimental result. Thus, in the event that the measurement does not comply with the standard, the entire product is underspecified. Expanding the monitoring to observe the time-evolution of MWD helps to speed up the response during operation in order to achieve satisfactory polymeric products. Moreover, Figures 58e, 59e & 60e present the estimated MWD evolution along the reaction, which evidences the online monitoring capability proposed by the framework. This represents a remarkable tool due to the balanced combination of the power of online data and a mechanistic model.

In summary, all evaluated trajectories show excellent performance in state estimation and data reconciliation by the DEKF. Once the filter switches on, estimated properties move towards the actual measured values and provide a smoother projection of the property while reducing noise significantly. Regarding the online prediction of the MWD, it can be appreciated that results are good, which opens the possibility of enhancing the monitoring of this property. The capability of noise reduction is important towards optimal control, which is the scope of the next section.

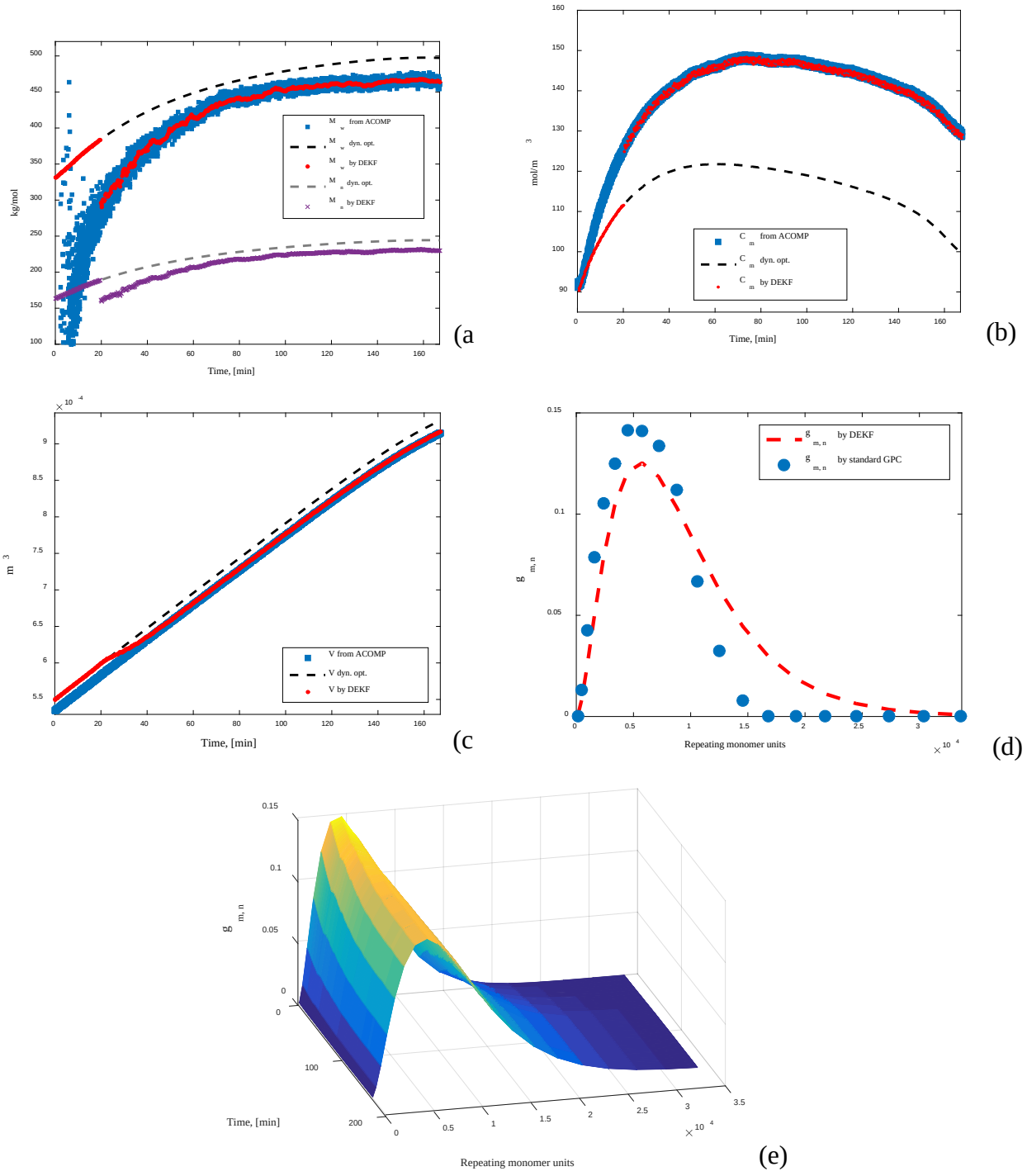

Figure 58: Results for increasing M_w trajectory OL. a) M_w and M_n time evolution, b) Monomer concentration time evolution, c) Reactor volume time evolution, d) Chain length distribution estimated by DEKF and experimental results, e) Chain length distribution estimated by DEKF evolution along the reaction.

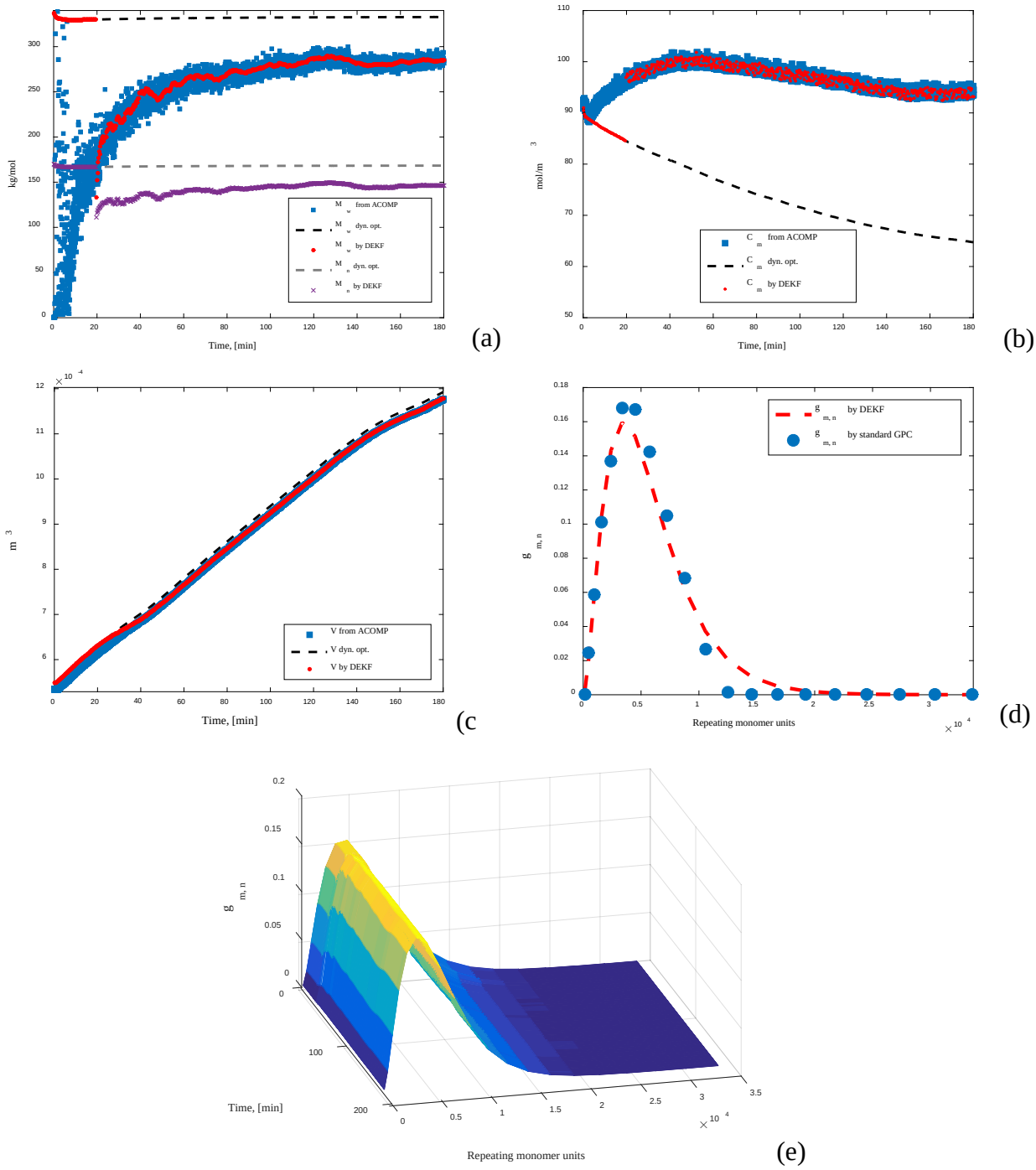

Figure 59: Results for constant M_w trajectory OL. a) M_w and M_n time evolution, b) Monomer concentration time evolution, c) Reactor volume time evolution, d) Chain length distribution estimated by DEKF and experimental results, e) Chain length distribution estimated by DEKF evolution along the reaction.

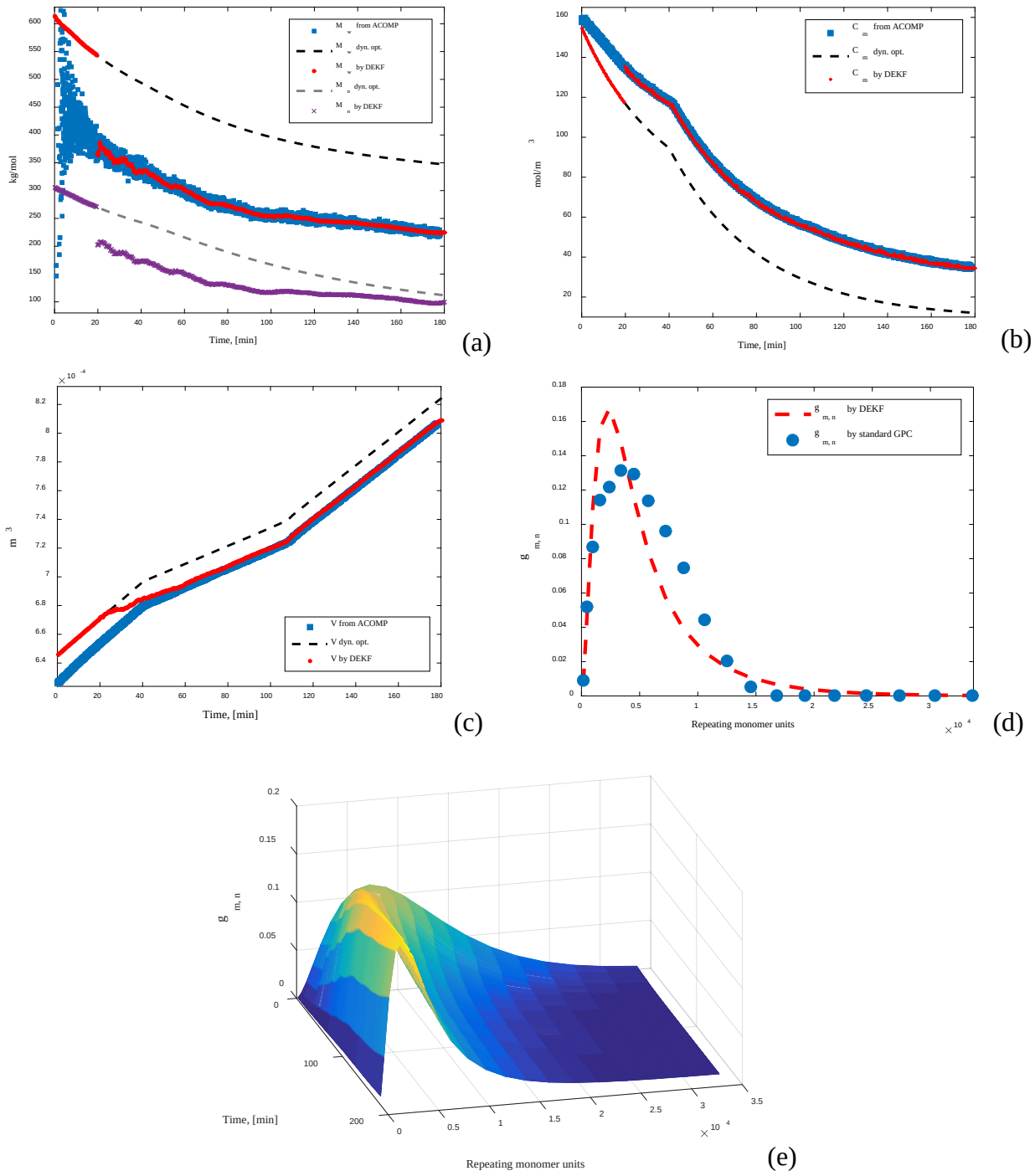

Figure 60: Results for decreasing M_w trajectory OL. a) M_w and M_n time evolution, b) Monomer concentration time evolution, c) Reactor volume time evolution, d) Chain length distribution estimated by DEKF and experimental results, e) Chain length distribution estimated by DEKF evolution along the reaction.

V.4.5 Closed Loop Testing

After validating the DEKF in OL experiments, closed loop behavior is studied. Two kinds of closed loop experiments are designed: PID and PID integrated with DEKF. The control objective is to follow different M_w as set point trajectories by manipulating F_m. Hence, F_i is set equal to its optimal profile, and a constant T is fixed. The idea is to show that small variations of F_m along the optimal input trajectories should only be necessary to achieve target trajectories. In the first set of experiments (PID), the controller collects raw measurements of M_w in an array considering a collecting time of 30 sec. The resultant average from this array is the input value for the controller. The mentioned procedure aims to reduce the noise from data using a simple average method. The second set of experiments (PID+DEKF) proceed as explained in the framework section. In this case, estimated M_w are inputs to the controller. The noise of these estimates is reduced due to the filtering action. The time intervals for control, filtering action as well as the controller parameters, are presented in Table 6. Again, the controller and DEKF activate after 20 min the reaction started.

Figures 61-63 contrast the performance of OL, PID, and PID+DEKF experiments under equal operating conditions. In general, three operating philosophies towards standardized polymers are compared. These set ups include the experiment following an optimal recipe, with simple control, and integrating control and state estimation. Figures 61a, 62a & 63a reveal OL, PID and PID+DEKF experimental values from ACOMP. They also present the estimated M_w and M_n provided by the filter. Clearly, in terms of achieving M_w set points, the coupling of the DEKF to the linear controller improves the quality in the closed loop response. The noise reduction of the DEKF not only improves the controller input but also guides the dynamics of the process as the mathematical model intervenes. In this way, PID results show more oscillatory behaviors even though their inputs are mean values of raw measurements. Likewise, estimated M_w and M_n follow parallel paths of their similar ones acquired during dynamic optimization as observed in OL experiments. Figures 61b, 62b & 63b show the measured values of experimental profiles of F_m. By observation in terms of the manipulated variable, trajectories from PID+DEKF show less deviations from the formulated profiles used in OL experiments. These results imply that the F_m injection behaves more efficiently in the proposed framework while reasonably achieving the desired set point.

Furthermore, the DEKF also provides relevant information of the MWD time evolution. Figures 61c, 62c & 63c contrast the resultant or final MWD between the formulated distributions during dynamic optimization, estimated by the filter, and measured with standard calibration GPC. In all scenarios, the DEKF illustrates its good prediction ability, especially for the constant M_w trajectory. Figures 61d, 62d & 63d present the estimated MWD evolution in different times along the reaction for each trajectory, showing the monitoring ability of the framework. For the increasing M_w trajectory (Figure 61d), MWD evolves from fewer to more repeating units of the polymer chain length distribution. For the constant M_w trajectory (Figure 62d), MWD keeps a constant value in the evolution of the repeating units distribution. Thus, the constant characteristic hints that this trajectory holds a constant evolution of the MWD as well. Finally, for the decreasing M_w trajectory (Figure 63d), MWD evolves from more to fewer repeating units.

Overall, the closed loop experimental results for PID+DEKF demonstrate the best performance in achieving a desired M_w trajectory when compared with PID and OL experiments. In addition, results show an efficient F_m management, as the manipulated variable achieves the control objective with less variation. Noise minimization from data reconciliation represents a remarkable advantage in frameworks governed by a nonlinear model and data from measurements in combination with

feedback control. Finally, the DEKF confirms applicability for online monitoring of unmeasured properties.

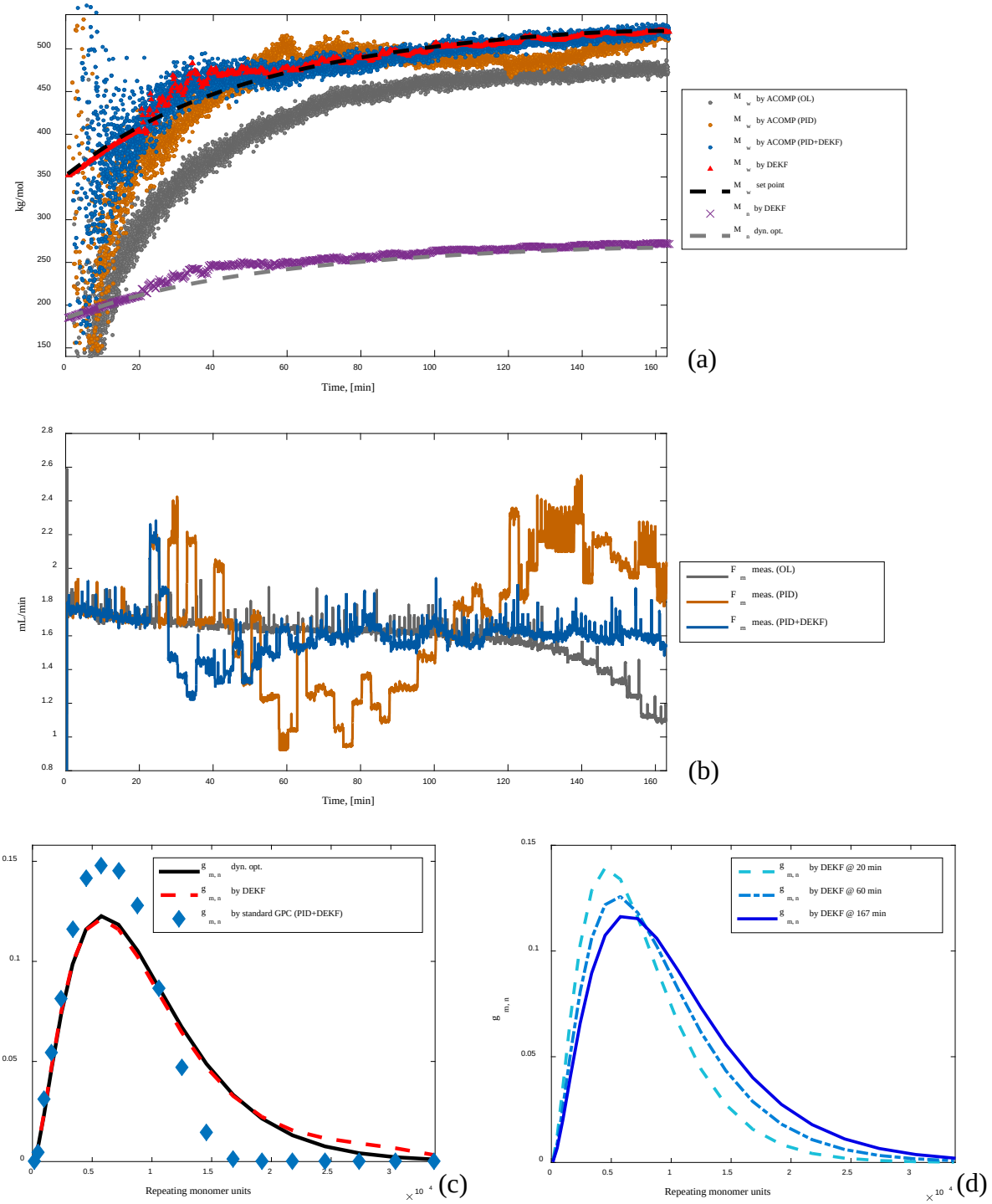

Figure 61: Results for increasing M_w trajectory closed-loop. a) M_w and M_n different trajectories, b) Measured flow rate of monomer different scenarios, c) Final chain length distribution from: dynamic optimization, estimated by DEKF and standard GPC, d) Time evolution of estimated chain length distribution.

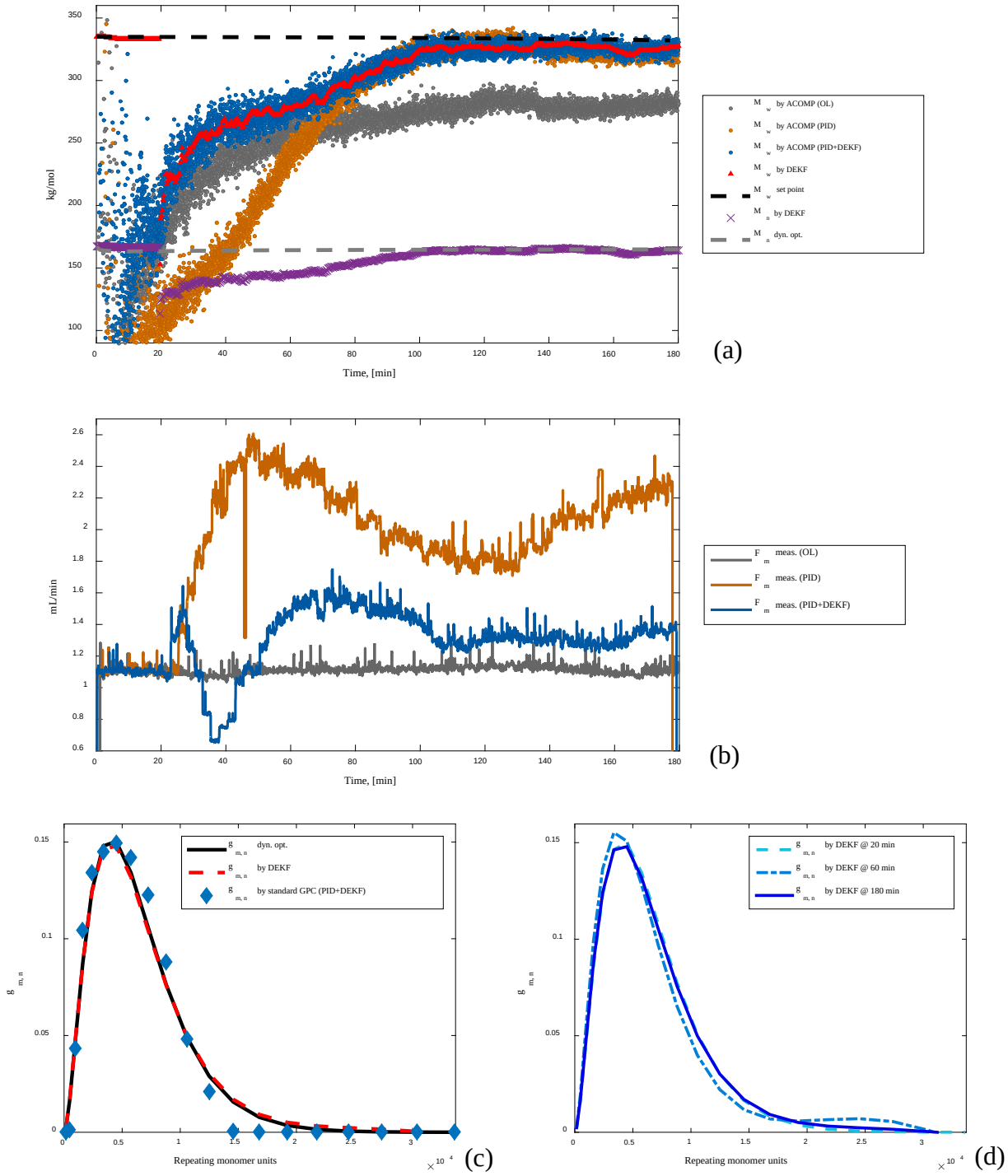

Figure 62: Results for constant M_w trajectory closed-loop. a) M_w and M_n different trajectories, b) Measured flow rate of monomer different scenarios, c) Final chain length distribution from: dynamic optimization, estimated by DEKF and standard GPC, d) Time evolution of estimated chain length distribution.

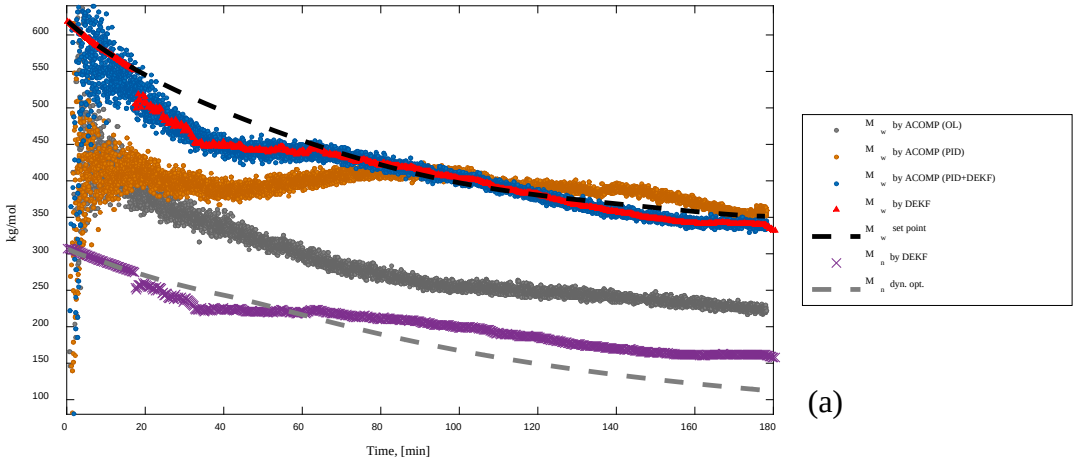
kg/mol
Time, [min]
M w by ACOMP (OL)
M w by ACOMP (PID)
M w by ACOMP (PID+DEKF)
M w by DEKF
M w set point
M n by DEKF
M n dyn. opt.

(a)

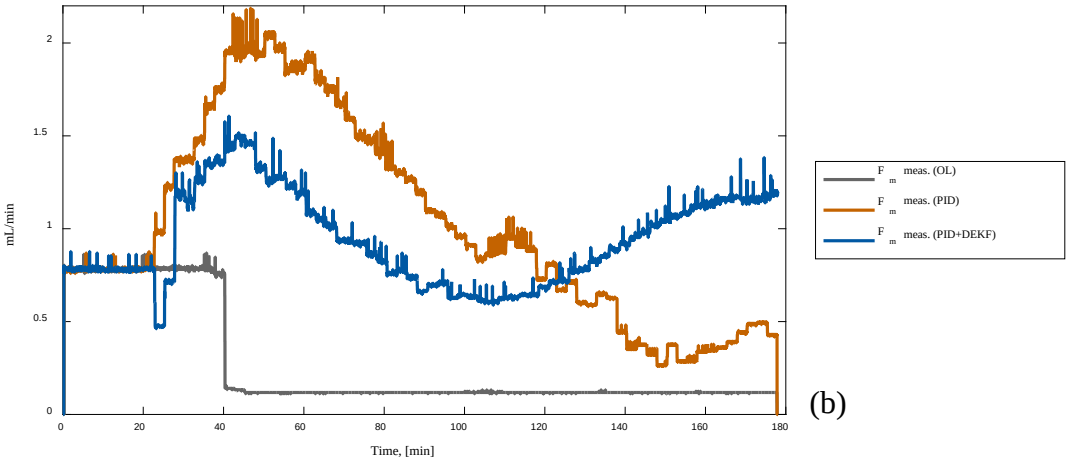
mL/min
Time, [min]
F m meas. (OL)
F m meas. (PID)
F m meas. (PID+DEKF)

(b)

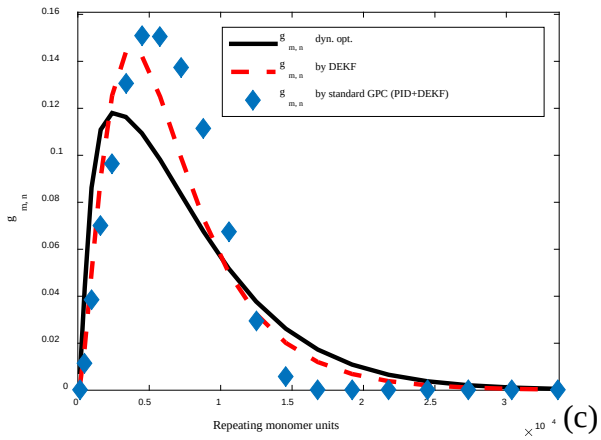
g m, n
Repeating monomer units
g m, n dyn. opt.
g m, n by DEKF
g m, n by standard GPC (PID+DEKF)

(c)

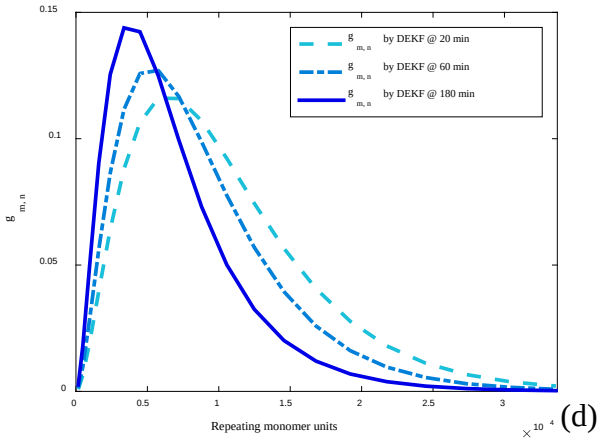
g m, n
Repeating monomer units
g m, n by DEKF @ 20 min
g m, n by DEKF @ 60 min
g m, n by DEKF @ 180 min

(d)

Figure 63: Results for decreasing M_w trajectory closed-loop. a) M_w and M_n different trajectories, b) Measured flow rate of monomer different scenarios, c) Final chain length distribution from: dynamic optimization, estimated by DEKF and standard GPC, d) Time evolution of estimated chain length distribution.

Model-Based Linearizing control of Total Amount of Monomer

Although the focus in this work was to control the weighted average molecular weight M_w, additional experiments were performed to test the functionalities of the nonlinear controller to control total amount of monomer using the monomer flow as manipulated variable. As in the previous case of controlling M_w, all other input trajectories were set equal to their corresponding optimal trajectories obtained during optimization. Furthermore, the target monomer concentration was also obtained from the optimization results. The operating scenario selected for this test was with decreasing M_w.

Figure 64 illustrates the closed loop results in terms of the monomer concentration, manipulated variable (F_m) trajectory, initiator flow trajectory (F_I) and M_w trajectory. Clearly the performance of the controller is excellent forcing the monomer concentration to follow closely the optimal trajectory along the batch by performing small adjustments. The monomer flow trajectory follows the same trend than the optimal trajectory, however small changes are produced due to model uncertainties. However, even perfect control is achieved for monomer concentration, Figure 20c shows that M_w target cannot be achieved with this type of strategy.

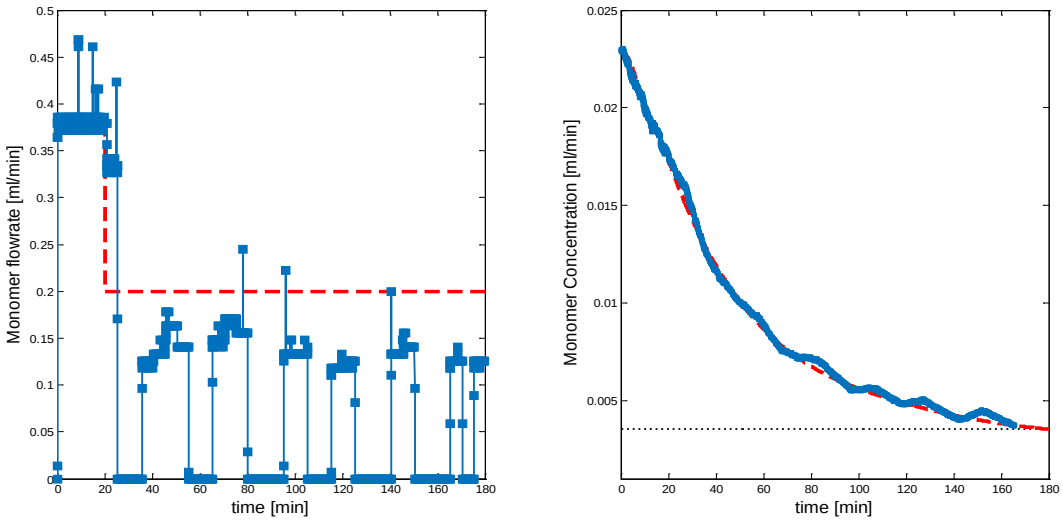

(a) (b)

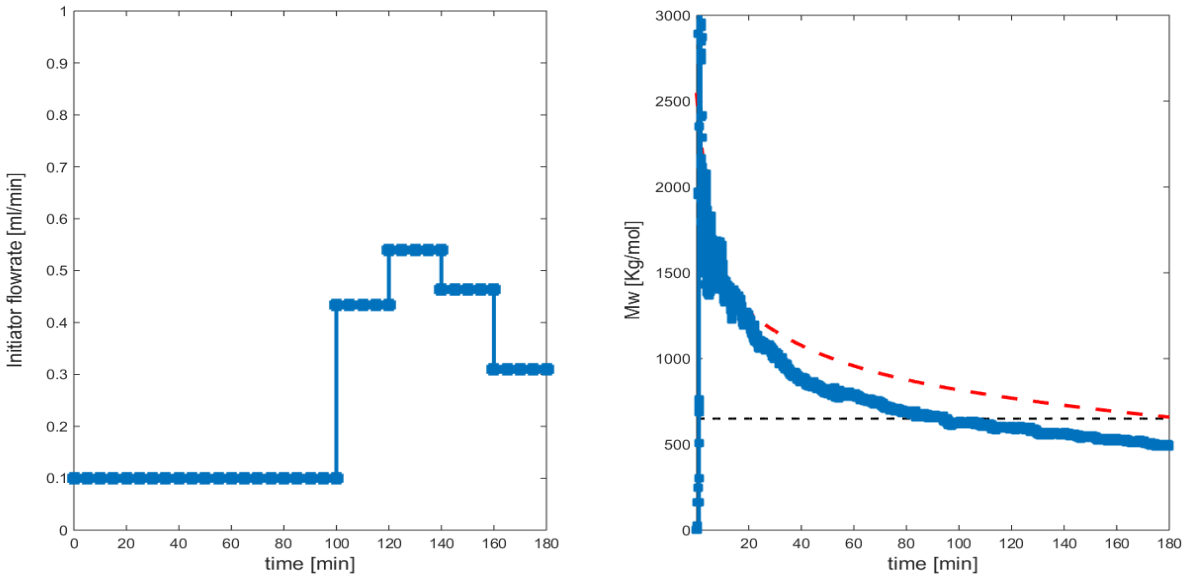

(c) (d)

Figure 64: Experimental results for nonlinear controller (controlling C_m using F_m): a) Monomer concentration, b) Monomer flow; c) Weighted average molecular weight. Red-Target (simulation); blue-Closed-loop.

References for section V from LSU

1. Srinivasan, N.; Kasthurikrishnan, N.; Cooks, R.G.; Krishnan, M.S.; Tsao, G.T. Online monitoring with feedback-control of bioreactors using a high ethanol tolerance yeast by membrane introduction mass-spectrometry. *Anal Chim Acta* **1995**, *316*, 269-276.
2. Eaton, J.W.; Rawlings, J.B. Feedback-control of chemical processes using online optimization techniques. *Comput Chem Eng* **1990**, *14*, 469-479.
3. Ray, W.H. Polymerization reactor control. *Ieee Transactions on Control Systems Technology* **1986**, *6*.
4. Nguyen, T.Q.a.K., H.H. Molecular weight distribution and mechanical properties. **1999**, *3*, 143-150.
5. Isayev.A.I , P.S. *Encyclopedia of polymer blends, volume 2: Processing*. 2011.
6. Cho, H.S.; Chung, J.S.; Lee, W.Y. Control of molecular weight distribution for polyethylene catalyzed over ziegler-natta/metallocene hybrid and mixed catalysts. *J Mol Catal a-Chem* **2000**, *159*, 203-213.
7. Heidemeyer, P.; Pfeiffer, J. Special requirements on compounding technology for bimodal polyolefines and their industrial application. *Macromol Symp* **2002**, *181*, 167-176.
8. Malekmotiei, L.; Samadi-Dooki, A.; Voyiadjis, G.Z. Nanoindentation study of yielding and plasticity of poly(methyl methacrylate). *Macromolecules* **2015**, *48*, 5348-5357.
9. W.McKeen, L. *The effect of temperature and other factors on plastics and elastomers*. William Andrew Inc: 2008.

10. Yoon, W.J.; Kim, Y.S.; Kim, I.S.; Choi, K.Y. Recent advances in polymer reaction engineering: Modeling and control of polymer properties. *Korean J Chem Eng* **2004**, *21*, 147-167.
11. Kreft, T.; Reed, W.F. Predictive control and verification of conversion kinetics and polymer molecular weight in semi-batch free radical homopolymer reactions. *Eur Polym J* **2009**, *45*, 2288-2303.
12. Crowley, T.J.; Choi, K.Y. Experimental studies on optimal molecular weight distribution control in a batch-free radical polymerization process. *Chem Eng Sci* **1998**, *53*, 2769-2790.
13. Crowley, T.J.; Choi, K.Y. Optimal control of molecular weight distribution in a batch free radical polymerization process. *Ind Eng Chem Res* **1997**, *36*, 3676-3684.
14. Crowley, T.J.; Choi, K.Y. Calculation of molecular weight distribution from molecular weight moments in free radical polymerization. *Ind Eng Chem Res* **1997**, *36*, 1419-1423.
15. Chang, J.S.; Liao, P.H. Molecular weight control of a batch polymerization reactor: Experimental study. *Ind Eng Chem Res* **1999**, *38*, 144-153.
16. Kiparissides, C.; Seferlis, P.; Mourikas, G.; Morris, A.J. Online optimizing control of molecular weight properties in batch free-radical polymerization reactors. *Ind Eng Chem Res* **2002**, *41*, 6120-6131.
17. Alhamad, B.; Romagnoli, J.A.; Gomes, V.G. On-line multi-variable predictive control of molar mass and particle size distributions in free-radical emulsion copolymerization. *Chem Eng Sci* **2005**, *60*, 6596-6606.
18. Park, M.J.; Rhee, H.K. Control of copolymer properties in a semibatch methyl methacrylate/methyl acrylate copolymerization reactor by using a learning-based nonlinear model predictive controller. *Ind Eng Chem Res* **2004**, *43*, 2736-2746.
19. Wang, J.F.; Huang, H.Q.; Huang, X.Y. Molecular weight and the mark-houwink relation for ultra-high molecular weight charged polyacrylamide determined using automatic batch mode multi-angle light scattering. *J Appl Polym Sci* **2016**, *133*.
20. Lee, J.H.; Ricker, N.L. Extended kalman filter based nonlinear model-predictive control. *Ind Eng Chem Res* **1994**, *33*, 1530-1541.
21. Henson, M.A. Nonlinear model predictive control: Current status and future directions. *Comput Chem Eng* **1998**, *23*, 187-202.
22. Bindlish, R. Nonlinear model predictive control of an industrial polymerization process. *Comput Chem Eng* **2015**, *73*, 43-48.
23. Maner, B.R.; Doyle, F.J.; Ogunnaike, B.A.; Pearson, R.K. Nonlinear model predictive control of a simulated multivariable polymerization reactor using second-order volterra models. *Automatica* **1996**, *32*, 1285-1301.
24. Florenzano, F.H.; Strelitzki, R.; Reed, W.F. Absolute, on-line monitoring of molar mass during polymerization reactions. *Macromolecules* **1998**, *31*, 7226-7238.
25. Wayne F. Reed, A.M.A. Monitoring polymerization reactions: From fundamentals to applications. **2013**.
26. Giz, A.; Catalgil-Giz, H.; Alb, A.; Brousseau, J.L.; Reed, W.F. Kinetics and mechanisms of acrylamide polymerization from absolute, online monitoring of polymerization reaction. *Macromolecules* **2001**, *34*, 1180-1191.
27. McAfee, T.; Leonardi, N.; Montgomery, R.; Siqueira, J.; Zekoski, T.; Drenski, M.F.; Reed, W.F. Automatic control of polymer molecular weight during synthesis. *Macromolecules* **2016**, *49*, 7170-7183.

28. Ghadipasha, N.; Geraili, A.; Romagnoli, J.A.; Castor, C.A.; Drenski, M.F.; Reed, W.F. Combining on-line characterization tools with modern software environments for optimal operation of polymerization processes. *Processes* **2016**, *4*.
29. Chiu, W.Y.; Carratt, G.M.; Soong, D.S. A computer-model for the gel effect in free-radical polymerization. *Macromolecules* **1983**, *16*, 348-357.
30. Brandrup, J.I., E.H.; Grulke, E.A. *Polymer handbook*. Wiley: 2003; Vol. 2, p 2336.
31. Reed, W. Automated continuous online monitoring of polymerization reactions (acomp) and related techniques. In *Encyclopedia of Analytical Chemistry*, Meyers, R.A., Ed. 2013.

32 Kozub DJ, MacGregor JF. State estimation for semi-batch polymerization reactors. *Chem Eng Sci.* **1992**, 47 (5), 1047-1062.
33 Schuler H, Schmidt CU. Calorimetric-state estimators for chemical reactor diagnosis and control: review of methods and applications. *Chem Eng Sci.* **1992**, 47 (4), 899-913.
34 Srinivasan N, Kasthurikrishnan N, Cooks RG, Krishnan MS, Tsao GT. Online monitoring with feedback-control of bioreactors using a high ethanol tolerance yeast by membrane introduction mass-spectrometry. *Anal Chim Acta.* **1995**, *316*, 269-276.
35 Weiss GH, Romagnoli JA, Islam KA. Data reconciliation - an industrial case study. *Comput Chem Eng.* **1996**, 20 (12), 1441-1449.
36 Romagnoli JA, Sanchez MC. *Data Processing and Reconciliation for Chemical Process Operations*. Academic Press, Vol. 2, **1999**.
37 Nicholson B, López-Negrete R, Biegler LT. On-line state estimation of nonlinear dynamic systems with gross errors. *Comput Chem Eng.* **2014**, 70, 149-159.
38 Hedengren JD, Eaton AN. Overview of estimation methods for industrial dynamic systems. *Optim Eng.* **2015**, 1-24.
39 Eaton JW, Rawlings JB. Feedback-control of chemical processes using online optimization techniques. *Comput Chem Eng.* **1990**, *14*, 469-479.
40 Norquay SJ, Palazoglu A, Romagnoli JA. Model predictive control based on Wiener models. *Chem Eng Sci.* **1998**, *53*(1), 75-84.
41 Cho HS, Chung JS, Lee WY. Control of molecular weight distribution for polyethylene catalyzed over ziegler-natta/metallocene hybrid and mixed catalysts. *J Mol Catal a-Chem.* **2000**, *159*, 203-213.
42 Romagnoli JA, Palazoglu A. *Introduction to Process Control*. CRC Press, **2005**.
43 Ghadipasha N, Romagnoli JA, Tronci S, Baratti R. On-line control of crystal properties in nonisothermal antisolvent crystallization. *AIChE J.* **2015**, *61*(7), 2188-2201.
44 Heidemeyer P, Pfeiffer J. Special requirements on compounding technology for bimodal polyolefines and their industrial application. *Macromol Symp.* **2002**, *181*, 167-176.
45 Isayev AI. *Encyclopedia of Polymer Blends, Volume 2: Processing*. Wiley, **2011**.
46 Gentekos DT, Dupuis LN, Fors BP. Beyond dispersity: deterministic control of polymer molecular weight distribution. *J Am Chem Soc.* **2016**, 138(6), 1848-1851.
47 McKeen LW. *The Effect of Temperature and Other Factors on Plastics and Elastomers*. William Andrew, **2014**.
48 Florenzano FH, Strelitzki R, Reed WF. Absolute, on-line monitoring of molar mass during polymerization reactions. *Macromolecules.* **1998**, *31*, 7226-7238.
49 Reed WF, Alb AM. *Monitoring Polymerization Reactions: from Fundamentals to Applications*. Wiley, **2013**.

50 McAfee T, Leonardi N, Montgomery R, Siqueira J, Zekoski T, Drenski MF, Reed WF. Automatic Control of Polymer Molecular Weight during Synthesis. *Macromolecules.* **2016**, *49* (19), 7170-7183.\Giz A, Catalgil-Giz H, Alb AM, Brousseau JL, Reed WF. Kinetics and mechanisms of acrylamide polymerization from absolute, online monitoring of polymerization reaction. *Macromolecules.* **2001**, *34*, 1180-1191.

51 Kreft T, Reed WF. Predictive control and verification of conversion kinetics and polymer molecular weight in semi-batch free radical homopolymer reactions. *Eur Polym J.* **2009**, 45(8), 2288-2303.

52 Kreft T, Reed WF. Predictive control of average composition and molecular weight distributions in semi-batch free radical copolymerization reactions. *Macromolecules.* **2009**, 42, 5558−5565.

53 Kalman RE. A new approach to linear filtering and prediction problems. *J Basic Eng-T ASME.* **1960**, *82* (1), 35-45.

54 Kalman RE, Bucy RS. New results in linear filtering and prediction theory. *J Basic Eng-T ASME.* **1961**, *83* (3), 95-108.

55 Qin SJ. Process data analytics in the era of big data. *AIChE J* **2014**, 60(9), 3092-3100.

56 Simon D. *Optimal State Estimation: Kalman, H Infinity, and Nonlinear Approaches*. Wiley, **2006**.

57 Hashemi R, Kohlmann D, Engell S. Optimizing control and state estimation of a continuous polymerization process in a tubular reactor with multiple side-streams. *Macromol React Eng.* **2016**, 10, 415−434.

58 Tatiraju S, Soroush M. Nonlinear state estimation in a polymerization reactor. *Ind Eng Chem Res.* **1997**, 36 (7), 2679-2690.

59 Gentric C, Pla F, Corriou JP. Experimental study of the nonlinear geometric control of a batch emulsion polymerization reactor. *Comput Chem Eng*. **1997**, 21, S1043-S1048.

60 Gentric C, Pla F, Latifi MA, Corriou JP. Optimization and non-linear control of a batch emulsion polymerization reactor. *Chem Eng J*. **1999**, 75(1), 31-46.

61 Li R, Corripio AB, Henson MA, Kurtz MJ. On-line state and parameter estimation of EPDM polymerization reactors using a hierarchical extended Kalman filter. *J Process Contr.* **2004**, 14 (8), 837-852.

62 Galdeano R, Asteasuain M, Sánchez MC. Unscented transformation-based filters: performance comparison analysis for the state estimation in polymerization processes with delayed measurements. *Macromol React Eng.* **2011**, 5 (7-8), 278-293.

63 Gopalakrishnan A, Kaisare NS, Narasimhan S. Incorporating delayed and infrequent measurements in extended Kalman filter based nonlinear state estimation. *J Process Contr.* **2011**, *21* (1), 119-129.

64 Beyer MA, Grote W, Reinig G. Adaptive exact linearization control of batch polymerization reactors using a Sigma-Point Kalman Filter. *J Process Contr.* **2008**, 18 (7), 663-675.

65 Ghadipasha N, Geraili A, Romagnoli JA, Castor CA, Drenski MF, Reed WF. Combining on-line characterization tools with modern software environments for optimal operation of polymerization processes. *Processes.* **2016**, *4* (1), 5.

66 Ghadipasha N, Zhu W, Romagnoli JA, McAfee T, Zekoski T, Reed WF. Online optimal feedback control of polymerization reactors: application to polymerization of acrylamide-water-potassium persulfate (KPS) system. *Ind Eng Chem Res.* **2017**, 56, 7322-7335.

67 Crowley TJ, Choi KY. Calculation of molecular weight distribution from molecular weight moments in free radical polymerization. *Ind Eng Chem Res.* **1997**, *36*, 1419-1423.
68 Crowley TJ, Choi KY. Discrete optimal control of molecular weight distribution in a batch free radical polymerization process. *Ind Eng Chem Res.* **1997**, *36*, 3676-3684.
69 Schlegel M, Stockmann K, Binder T, Marquardt W. Dynamic optimization using adaptive control vector parameterization. *Comput Chem Eng.* **2005**, *29*, 1731-1751.
70 Haseltine EL, Rawlings JB. Critical evaluation of extended Kalman filtering and moving-horizon estimation. *Ind Eng Chem Res.* **2005**, *44* (8), 2451-2460.
71 Regis RG, Shoemaker CA. A stochastic radial basis function method for the global optimization of expensive functions. *Informs J Comput.* **2007**, 19 (4), 497-509.
72 Regis RG, Shoemaker CA. Parallel stochastic global optimization using radial basis functions. *Informs J Comput.* **2009**, 21 (3), 411-426.

Benefits Assessment

This project has opened the door for prototype commercial implementation for certain specialty polymers. This is a very important first step since never before has it been possible to control M_w, composition and other polymer and reaction characteristics based on continuous, realtime data and analysis streams. In fact, Fluence Analytics has contracted with a first client to deliver a prototype M_w controller software product based on the basic principles controller developed by Fluence/Tulane during this project. The client, who has very tight specifications for their product, hopes to optimize their manufacturing process and consistently improve product quality (M_w in this instance) with the controller.

It is expected that a growing number of industrial clients in the specialty polymer space will request M_w and copolymer composition controllers as reference case studies are built up, such as the one mentioned above, and as publications, marketing materials and presentations from this project and Fluence Analytics reach the relevant audience.

While these accumulating implementations will have a positive impact on making more efficient use of energy and reducing emission, the big energy picture lies with polyolefin manufacturing and certain other commodity polymers, since those are the most energy intensive, GHG emissive, and largest sectors in the polymer industry.

Table 1 shows the results of studies of energy consumption and potential savings per year in the polyolefin sector.§ It shows that polyolefin production leads to an estimated savings of 60 TBtu per year and 8 million tons/year decrease in GHG emissions if this manufacturing sector adapts ACOMP/CI. This latter figure aligns well with DoE analyses of chemical bandwidth studies (emails and conversation with DoE personnel).

The table shows annual savings per year due to 50% reduction in off-specification product from online polymer monitoring, where off spec production is assumed at 5% of total production. The focus is on a portion of the U.S. Plastic Industry; polyethylene, polypropylene, polystyrene and PVC. This table does *not* include other major products, such as PET, nylon, polycarbonates, synthetic rubbers, and engineering thermoplastics. *Savings numbers will be much higher taking these into account, and these are other areas of opportunity for application of the technology.*

§ Assumes 5% total 'off-specification' or other inefficiencies in production

Annual production data : Plastics Industry Producers' Statistics Group, as compiled by Vault Consulting, LLC; ACC © April 2016 American Chemistry Council, Inc.

Energy data from Franklin Associates: Cradle-to-gate life cycle inventory of nine plastic resins and four polyurethane precursors, 2011

Pollution data from life cycle assessment literature review

Monetary data: spot price Nexant, Bloomberg

Table 9. Estimates of energy consumption and potential savings, and GHG emissions and potential reductions.

	Current Levels/yr	W/Mass Adoption/yr	Savings/yr
Annual Production (million tons/year)	38.38	38.38	Not applicable
Energy Consumption (million GJ/year)	2,612	2,547	65
Energy Consumption (million BOE/year)	428	417	11
Energy Consumption (MBTUs)	2.375×10^9	2.316×10^9	6.1×10^7
GHG Emissions (million tons/year)	301	293	8
SO2 Emissions (million tons/year)	59	57.5	1.5
Production Costs (million $/year, **zero profit environment i.e. price=cost**)	$50,600	$49,335	$1,265

Table 1. Estimates of energy consumption and GHG emissions in the polyolefin manufacturing sector, along with estimates of yearly energy and GHG savings if ACOMP/CI is extended to the polyolefin industry.

Commercialization

With a first Fluence Analytics client requesting a commercial prototype control interface software package for an ACOMP system which has been ordered, the door is now open to further developing and disseminating the basic principles controllers from this project in the industrial sector. Fluence will seek opportunities to integrate the control interface with ACOMP orders as they arise.

Fluence placed its first industrial scale ACOMP (without a control interface) on a 50,000 liter industrial reactor in Fall 2014 at a Louisiana manufacturing site producing specialty polymers in a batch process, and this has run with 97% availability. That installation, which was a Joint Development Project with a Fortune 500 chemical manufacturer led to their purchase of a second ACOMP system in 2016 at the Louisiana site. That company is currently evaluating the possible widespread adoption of ACOMP at its other U.S. and global operations. Along the way, they are acting as a partner in exploring new features of ACOMP, possibly including a control interface in future plans.

In the meantime, as mentioned, a different client has ordered an ACOMP system and requested a prototype control interface. Fluence is currently negotiating with several important polymer manufacturers for ACOMP installation, and the possibility of extending to ACOMP/CI is always a very real possibility as future software ‘add-ons’ to an installed base of ACOMP systems. Until recently, being in start-up mode, Fluence has been focused on working with a limited number of clients to more fully develop the technology before beginning the marketing phase. Now, Fluence has just begun its first active sales and marketing campaign for ACOMP.

Again, it is the polyolefin sector that will yield the greatest energy savings and GHG emissions reduction through implementation of ACOMP/CI. Development of ACOMP/CI for

polyolefins is beyond the financial reach of Fluence, which is still a start-up company with limited resources that need to be focused on more immediate opportunities. *The ACOMP/CI team is seeking further federal funding to develop ACOMP/CI for polyolefins.* This is a formidable challenge, but there are already well developed plans for immediately launching the project once funds are obtained. The team sees DoE as the most likely source of funding.

It is noted that, while it may be possible to obtain private industry sponsorship for developing polyolefin ACOMP/CI, such sponsorship would inevitably come with a heavy price tag in terms of IP, confidentiality, and exclusivity restrictions limiting long-term adoption to the entire sector. Any arrangement that would hinder the quickest and widest possible adoption of ACOMP throughout the polyolefin manufacturing is antithetical to the mission of DoE.

Accomplishments

a. Publications: Refereed Journal Articles acknowledging the DoE project

1. "Automatic control of polymer molecular weight during synthesis", T. McAfee, N. Leonardi, R. D. Montgomery, J. Siqueira, T. Zekoski, M. F. Drenski, W. F. Reed, *Macromolecules*, 49 (19), 7170-7183, **2016**, DOI: 10.1021/acs.macromol.6b01522

2. "Automatic synthesis of multimodal polymers", Natalie Leonardi, Rick D. Montgomery, Julia Siqueira, Terry McAfee, Michael F. Drenski, Wayne F. Reed, *J. Macromolecular Engineering*, **2017**, http://dx.doi.org/10.1002/mren.201600072

3. "Combining on-line characterization tools with modern software environments for optimal operation of polymerization processes", N. Ghadipasha, A. Geraili, J. A. Romagnoli, C. A. Castor, M. F. Drenski, W. F. Reed, *Processes*, 4, (1), 1-23, **2016**

4. "First Steps towards Online Optimal Control of Molecular Weight in Batch and Semi-batch Free Radical Polymerization Reactors", N. Ghadipasha, N. Soleimani, C.A. Castor, W.F. Reed, M. F. Drenski, J.A. Romagnoli, *Computer Aided Chemical Engineering*, 38, 1129-1134, **2016**

5. "A Model-based Robust Control approach for On-line Optimal feedback Control of Polymerization Reactors: Application to Polymerization of Acrylamide-water-Persulfate (KPS) Systems". N. Ghadipasha, A. Geraili, H. Hernandez, J.A. Romagnoli, *Chemical Engineering Transactions*, 57, 110501110, **2017**

6. "Online Optimal Feedback Control of Polymerization Reactors: Application to polymerization of acrylamide-water-potassium persulfate (KPS) system", N. Ghadipasha, W. Zhu, J.A. Romagnoli, T. McAfee, T. Zekoski, W. F. Reed, *Industrial & Engineering Chemistry Research, 7322-7335,* **2017** DOI: 10.1021/acs.iecr.7b01074

7. "Integrated Online Nonlinear State Estimation and Feedback Control Applied to Polymerization Reactors", Salas, S. D.; Ghadipasha, N.; Zhu, W.; Mcafee, T.; Zekoski, T.; Reed, W. F.; Romagnoli, J. A. *AIChE Journal*, **2017**, submitted

8. Terry McAfee, Rick D. Montgomery, Thomas Zekoski, Aide Wu, Wayne F. Reed, "Automatic, simultaneous control of polymer composition and molecular weight during free radical copolymer synthesis" *Macromolecules* , **2017,** submitted

b. Conference presentations

"Recent advances in online monitoring of polymerization reactions", M.F. Drenski, W. F. Reed, Sci-X Conference, Providence, RI, Sept. 27-30, 2015

"Automatic Control of Free Radical Polymerization Reactions", T. McAfee, N. Leonardi, R. Montgomery, J. Siqueira, C. Jarand, T. Zekoski, M.F. Drenski, W.F. Reed, , International Symposium on Polymer Analysis and Characterization, Linz, Austria, June 12-15, 2017

1) "Recent advances in Automatic Continuous Online Monitoring of Polymerization reactions"
2) "Novel use of ACOMP at Pilot and Industrial Scale"
M.F. Drenski, N.C. Leonardi, R.D. Montgomery, P.N. Pham, W.F. Reed
Polymer Reaction Engineering IX, Hamburg, Germany, May 17-19, 2016

"First Steps towards Online Optimal Control of Molecular Weight in Batch and Semibatch Free Radical Polymerization Reactors", N. Ghadipasha, N. Soleimani, C.A. Castor, W.F. Reed, M. F. Drenski, J.A. Romagnoli, , *Proceedings of the 26th European Symposium on Computer Aided Process Engineering*, Slovenia, June (2016)

"Modelling and optimization of free radical polymerization processes in batch and semi-batch mode", N.Ghadipasha, N.Soleimani, C.A.Castor, M.F.Drenski, Prof. Wayne Reed, Prof. Jose Romagnoli, AIChE Meeting, (2016)

"A Model-based Robust Control approach for On-line Optimal feedback Control of Polymerization Reactors: Application to Polymerization of Acrylamide-wate-Persulfate (KPS) Systems". Ghadipasha N., Geraili A., Hernandez H., Romagnoli J.A., *IChEAP'17*, Milan Italy (2017)

"Online DEKF for State Estimation in Semi-Batch Free-Radical Polymerization Reactors" , S.D. Salas, N. Ghadipasha, W. Zhu, J.A. Romagnoli, T. Mcafee, W.F. Reed, *Proceedings of the 27th European Symposium on Computer Aided Process Engineering – ESCAPE 27*, Barcelona, Spain (2017)

"Real Time Optimal Control and State Estimation in Semi-Batch Free-Radical Polymerization Reactors", Salas, S. D.; Zhu, W.; Ghadipasha, N.; McAfee, T.; Reed, W. F.; Romagnoli, J. A., *AIChE Spring Meeting Conference Proceedings*, San Antonio, TX, USA, March 28, 2017.

c. Awards

Awarded the *2016 PSE Model-Based Innovation Prize* for the paper, "Combining on-line characterization tools with modern software environments for optimal operation of polymerization processes"

d. Networks or collaborations fostered

Have established ongoing collaborations in automatic control of polymerization reactions between Tulane University, Louisiana State University, and Fluence Analytics

e. Technologies/Techniques;

Complete working prototypes of the ACOMP/CI (automatic continuous online monitoring of polymerization reactions with control interface). Two systems designed and built by Fluence Analytics; First unit is at Tulane University, with a 2 liter pilot reactor, where the control experiments were carried out and 2) The second unit was contributed as cost share by Fluence and is at Fluence and works with a 64 liter pilot reactor.

Fully automatic control software for the ACOMP/CI without kinetic models by Tulane University and Fluence

Fully automatic non-linear control software for the ACOMP/CI with detailed kinetic models, state estimators, and Kalman filters by the LSU group

f. Inventions/Patent Applications

"Systems and methods for the active control of polymer reactions and processing using automatic continuous online monitoring of polymerization reactions." iEdison serial number 8424601-14-0003, US 15/515,119. W.F. Reed and M.F. Drenski

"Device and methods for determination of molecular weight distributions of polymers," iEdison serial number, 8424601-16-0005. PCT/US 17/28919. W.F. Reed, M.F. Drenski, R.D. Montgomery, A. Wu

g. Other products

A unique modular, generic and flexible model centric framework for advanced operation of polymerization processes has been formulated, implemented and fully tested within an experimental facility. The proposed framework has a number of unique features: a) A single model can be used in a number of activities during process operation including simulation, parameter estimation and steady-state and dynamic optimization; b) By changing the model the same framework can be used in different applications thus expanding the capabilities to study new reaction system where parameters and conditions are not fully known; c) The proposed framework have the capabilities of being used off-line as well as on-line during plant operation.

An in-house made state estimation/controller module was formulated, implemented and tested using open source platform (*python 2.7)* environment. This platform allows full functionality and connectivity to the ACOMP server to update/modify the process behavior. In addition, a user-friendly graphic user interface (GUI) allows visualization and modification of control parameters while the reaction progresses.

Conclusions

Ground-breaking advances in polymer science and engineering have been made in the course of this project. The project achieved first time automatic control of polymerization reactions based on the continuous realtime stream of ACOMP data on the most important polymer and reaction characteristics. The final characteristics controlled of most value to manufacturing are the MWD, intrinsic viscosity, and copolymer composition distribution. As regards this latter, production of copolymers is no longer subordinated to comonomer reactivity ratios, and any desired composition distribution can now be achieved in free radical copolymerization. The latter methods are also directly applicable to the increasingly important family of living type reactions, such as RAFT, ATRP, NMP, and ROMP.

While the initial proposal was for three years of funding, only two were obtained, which reduced the scope of the project somewhat. In a third year there would have been emphasis on moving the technology to more industrial type reactions, especially those in heterogeneous systems, such as emulsions and dispersions, in which there are very large specialty chemical markets. Approaching polyolefin monitoring, however, would not have been within the third year scope, as it requires entirely different reactors than those in the current Fluence ACOMP/CI, and extensive basic R&D in high temperature, high pressure sampling, and high temperature measurements needs to be developed. The R&D needed for this is the subject of ongoing proposal preparation for DoE's CESMII.

The fact that a Fluence Analytics ACOMP manufacturing client has requested a beta version of the Tulane/Fluence basic principles controller demonstrates that there is industrial interest in the ACOMP/CI platform, which must be grown through business development efforts. Fluence recently hired a VP for global business developments who has begun this process and there are a number of active initiatives for marketing and outreach. At the industrial ACOMP level itself (i.e. ACOMP without CI) there are current orders at Fluence and many discussions and proposals with industries are ongoing.

An important lesson learned during this project is that there is considerable inertia and attachment to status quo at the plant and production level; i.e. the main concerns of the plant are to manufacture products at a profit while maintaining sameness of operation and employment status, but resisting change and innovation. In contrast, the Executives of the manufacturing companies, together with manufacturing technology teams and the R&D scientists and engineers, understand that there are large efficiency gains to be had and in some sense are engaged in a struggle with plant operators to usher in innovative technologies.

The promise of ACOMP/CI is that wide scale industrial implementation of the technology will lead to very large efficiency gains in the use of energy, non-renewable feedstocks, and plant and energy time, while decreasing GHG emissions per kilo of product, increasing worker safety (by eliminating manual sampling of dangerous reactors), and enabling the production of new 21st century polymeric materials which are currently still in the R&D phase.

As Fluence Analytics continues to drive ACOMP/CI implementation in both the industrial and R&D spaces this goal will inevitably be met. With continued collaboration and support of DoE the basic advances in using ACOMP/CI in conjunction with Artificial Intelligence and other sophisticated cyber platforms, and in bringing ACOMP/CI to the polyolefin industry, as well as other industries, will be accelerated. An estimated annual 60 TBtu

energy savings and 3 million ton decrease in GHG emissions have been estimated for adaptation of ACOMP/CI to the polyolefin industry alone.

Individual companies will not fund such advances unless they can obtain exclusivity in the use of the innovations. This is antithetical to the mission of DoE, which is to propagate new energy saving technologies as broadly as possible for maximum impact.

Recommendations

It is recommended that funding for adaptation of ACOMP/CI to polyolefins and Smart Manufacturing be provided by DoE in order to bring the technology to the most energy intensive and GHG emissive sector of the polymer manufacturing industry. The project PI will be happy to discuss this with DoE personnel for appropriate mechanisms and RFPs.

It is also recommended that project personnel pursue other DoE opportunities that further the goal of developing and implementing ACOMP/CI as widely as possible, such as in integrative and advanced Artificial Intelligence approaches.

References for pages 1-71**

[1] Lee, H.K.H.; Li, Z.; Constantinou, I. ; So, F. ; Tsang, S.W.; So, S.K, Batch-to-Batch Variation of Polymeric Photovoltaic Materials: its Origin and Impacts on Charge Carrier Transport and Device Performances *Adv. Energy Mater.*, **2014**, *4*, 1400768. DOI: 10.1002/aenm.201400768

[2] Mittal, G.; Sahana, D.K.; Bhardwaj, V.; Ravi Kumar, M.N.V. Estradiol loaded PLGA nanoparticles for oral administration: Effect of polymer molecular weight and copolymer composition on release behavior in vitro and in vivo. *J. Contr. Release*, **2007**, *119*, 77-85 doi:10.1016/j.jconrel.2007.01.016

[3] Kilz, P.; Held, D. *Monitoring Polymerization Reactions: From Fundamentals to Applications.* Eds. W.F. Reed, A.M. Alb, Wiley Interscience: 2014, ch 9.

[4] Schimpf, M.E.; Caldwell, K.; Giddings, J. C. *Field Flow Fractionation Handbook*, John Wiley & Sons, 2000

[5] Cortez, M.A.; Grayson, S.M. Application of Time-Dependent MALDI-TOF Mass Spectral Analysis To Elucidate Chain Transfer Mechanism during Cationic Polymerization of Oxazoline Monomers Containing Thioethers. *Macromolecules*, **2010**, *43*, 10152-10156.

[6] McKenna, T.F.; Othman, S.;, Févotte, G.; Santos, A.M.; Hannouri, H. An Integrated Approach to Polymer Reaction Engineering: A Review of Calorimetry and State Estimation. *Polym. React. Eng.*, **2000**, *8*, 1-38, DOI: 10.1080/10543414.2000.10744537

[7] Leiza, J. R.; Pinto, J. C. Polymer Reaction Engineering. *Polym React Engin* **2007**, 315-361.

[8] Houben, C.; Lapkin, A. A. Automatic discovery and optimization of chemical processes. *Cur Opinion Chem Eng* **2015**, *9*, 1-7.

[9] Salehpour, S.; Dube, M. A. Reaction Monitoring of Glycerol Step-Growth Polymerization Using ATR-FTIR Spectroscopy. Macromolecular Reaction Engineering **2012**, *6*, 85-92.

[10] Hua, H. ; Dubé, M. A. Terpolymerization monitoring with ATR-FTIR spectroscopy. *J. Polym Sci A: Polym Chem* **2001**, 39, 1860-1876.

[11] G. E. Fonseca, M. A. Dubé, A. Penlidis, A Critical Overview of Sensors for Monitoring Polymerizations. *Macromol React Eng* **2009**, 3, 327-373.

[12] Chmela, S.; Pavlinec, J.; Fiedlerova, A.; Catel, Y.; Moszner, N. Determination of Homopolymerization Kinetics of 10-(N-Methylacrylamido)-decylphosphonic acid, Its Diethyl ester, and 10-(Methacryloyloxy)-decylphosphonic acid, and Their Copolymerization with Methyl methacrylate. *Macromol Chem Phys* **2015**, *216*, 2386-2397.

[13] McCaffery, T. R.; Durant, Y. G. Application of low-resolution Raman spectroscopy to online monitoring of miniemulsion polymerization. *Journal of Applied Polymer Science*, **2002**, *86*, 1507-1515.

[14] Skilton, R. A.; Parrott, A. J.; George, M. W.; Poliakoff, M.; Bourne, R. A. Real-time feedback control using online attenuated total reflection Fourier transform infrared (ATR FT-IR) spectroscopy for continuous flow optimization and process knowledge. *Applied Spectroscopy*, **2013**, *67*, 1127-1131.

** References for section V are included at the end of section V

[15] Nogueira, E. S.; Borges, C. P.; Pinto, J. C. In-Line Monitoring and Control of Conversion and Weight-Average Molecular Weight of Polyurethanes in Solution Step-Growth Polymerization Based on Near Infrared Spectroscopy and Torquemetry. *Macromole Mat & Eng*, **2005**, *290*, 272-282.

[16] Mozharov, S.; Nordon, A.; Littlejohn, D.; Wiles, C.; Watts, P.; Dallin, P.; Girkin, J. M. Improved method for kinetic studies in microreactors using flow manipulation and noninvasive Raman spectrometry. *JACS*, **2011**, *133*, 3601-3608.

[17] Sans, V.; Porwol, L.; Dragone, V.; Cronin, L. A self optimizing synthetic organic reactor system using real-time in-line NMR spectroscopy. *Chemical Science* **2015**, *6*, 1258-1264.

[18] XI, Y.-G.; LI, D.-W.; LIN, S. Model Predictive Control — Status and Challenges. *Acta Automatica Sinica* **2013**, *39*, 222-236.

[19] Aller, F.; Blázquez, L. F.; Miguel, L. J. Online monitoring of an industrial semi-batch vinyl acetate polymerization reaction by programmable logic controllers. *IFAC Proceedings Volumes* **2014**, *47*, 1290–1295.

[20] Ohshima, M.; Tanigaki, M. Quality control of polymer production processes. *J Proc Cont* **2000**, 10, 135-148.

[21] Hergeth, W. D.; Jaeckle, C.; Krell, M. Industrial Process Monitoring of Polymerization and Spray Drying Processes. *J. Polym React Eng* **2003**, *11*, 663-714

[22] Rincon, F. D.; Esposito, M.; Hermes de Araujo, P. H.; Lima, F. V.; Le Roux, G. A. C. Robust Calorimetric Estimation of Semi-Continuous and Batch Emulsion Polymerization Systems with Covariance Estimation. *J. Macromol React Eng* **2014**, *8*, 456-466.

[23] BenAmor, S.; Colombie, D.; McKenna, T. Online Reaction Calorimetry. Applications to the Monitoring of Emulsion Polymerization without Samples or Models of the Heat-Transfer Coefficient. *Ind. & Eng Chem Res* **2002**, *41*, 4233-4241.

[24] Urretabizkaia, A.; Sudol, E.D.; El Aasser, M.S.; Asua, J.M. Calorimetric monitoring of emulsion copolymerization reactions. *J. Polym Sci, A, Polym Chem*, **1993**, 31, 2907-2913.

[25] Vega, M.P.; Bellumat, E.; Lima, E.L.; Pinto, J.C. Single-Point Intrinsic Viscosity and Density Measurements for In-Line MIMO Control Purposes of a Lumped-Distributed Polymeric System. *Macromole. React. Eng.* , **2012,** *6*, 482-494.

[26] Ingham, R. J.; Battilocchio, C.; Fitzpatrick, D. E.; Sliwinski, E.; Hawkins, J. M.; Ley, S. V. A Systems Approach towards an Intelligent and Self-Controlling Platform for Integrated Continuous Reaction Sequences. *Angewandte Chemie-International Edition* **2015**, *54*, 144-148.

[27] Florenzano, F.H.; Strelitzki, R.; Reed, W.F. Absolute, On-Line Monitoring of Molar Mass during Polymerization Reactions. *Macromolecules* **1998,** *31*, 7226-7238.

[28] Reed, W.F. Automatic Continuous Online Monitoring of Polymerization Reactions (ACOMP). *Encyc. Analyt. Chem*., Elsevier, 2013. DOI: 10.1002/9780470027318.a9288

[29] Kreft, T.; Reed, W.F. Predictive control and verification of conversion kinetics and polymer molecular weight in semi-batch free radical homopolymer reactions. *Euro Polym J.*, **2009,** *45*, 2288-2303.

[30] Kreft, T.; Reed, W.F. Predictive control of average composition and molecular weight distributions in semi-batch free radical copolymerization reactions. *Macromolecules*, **2009,** *42*, 5558-5565, DOI: 10.1021/ma900745n

[31] Houben, C.; Peremezhney, N.; Zubov, A.; Lapkin, A.A. Closed-Loop Multitarget Optimization for Discovery of New Emulsion Polymerization Recipes. *Org Proc Res Dev.*, **2015**, *19*, 1049-1053.
[32] Geraili, A.; Salas, S.; Romagnoli, J.A., A Decision Support Tool for Optimal Design of Integrated Biorefineries under Strategic and Operational Level Uncertainties. *Ind. & Eng Chem. Res*, **2016,** *55*, 1667-1676.
[33] Dotson, N.A.; Galvan, R.; Laurence, R.L.; Tirrel, M. *Polymerization Process Modelling;* VCH Pub.: New York, 1996.
[34] Zimm, B. H. The Scattering of Light and the Radial Distribution Function of High Polymer Solutions. *J. Chem. Phys.* **1948**, *16***,** 1093-1099.
[35] Zimm, B. H. Apparatus and Methods for Measurement and Interpretation of the Angular Variation of Light Scattering; Preliminary Results on Polystyrene Solutions. *J. Chem. Phys.* **1948**, *16***,** 1099-1115.
[36] Alb, A.M.; Farinato, R.; Calbeck, J.; Reed, W.F. Online Monitoring of Polymerization Reactions in Inverse Emulsions. *Langmuir*, **2006** 22, 831-840.
[37] Mignard, E.; Guerret, O.; Bertin, D.; Reed, W.F. Automatic Continuous Online Monitoring of Polymerization Reactions (ACOMP) of High Viscosity Reactions, *Polym. Mat.: Sci & Eng*, **2003** *88*, 314-316.
[38] Alb, A.M.; Enohnyaket, P.; Shunmugam, R.; Tew, G.N.; Reed, W.F. Quantitative contrasts in the copolymerization of acrylate and methacrylate monomers, *Macromolecules*, **2006**, *39*, 8283-8292.
[39] Alb, A.M.; Drenski, M.F.; Reed, W.F. Simultaneous continuous, non-chromatographic monitoring and discrete chromatographic monitoring of polymerization reactions, *J. Appl. Polym. Sci.*, **2009**, *13*, 190-198.
[40] Alb, A.M.; Reed, W.F. Simultaneous monitoring of polymer and particle characteristics during emulsion polymerization, *Macromolecules*, **2008**, *41*, 2406-2414.
[41] Alb, A.M.; Reed, W.F. Online monitoring of molecular weight and other characteristics during semi-batch emulsion polymerization under monomer starved and flooded conditions, *Macromolecules*, **2009**, *42*, 8093-8101.
[42] Giz, A.; Oncul Koc, A.; Giz, H.; Alb, A.M.; Reed, W.F. Online monitoring of reactivity ratios, composition, sequence length, and molecular weight distributions during free radical copolymerization, *Macromolecules*, 2002, *35*, 6557-6571.
[43] Alb, A.M.; Enohnyaket, P.; Drenski, M.F.; Head, A.; Reed, A.W.; Reed, W.F. Online monitoring of copolymerization using comonomers of similar spectral characteristics, *Macromolecules*, **2006,** *39*, 5705-5713.
[44] Alb, A.M.; Paril, A.; Çatalgil-Giz, H.; Giz, A.; Reed, W.F. Evolution of composition, molar mass, and conductivity during the free radical copolymerization of polyelectrolyte, *J. Phys. Chem. B*, **2007**, *111*, 8560-8566.
[45] Enohnyaket, P.; Kreft, T.; Alb, A.M.; Drenski, M.F.; Reed, W.F. Determination of molecular mass during online monitoring of copolymerization reactions, *Macromolecules*, **2007**, *40*, 8040-8049.
[46] Gonzalez Garcia, G.; Kreft, T.; Alb, A.M.; de la Cal, J.C.; Asúa, J.M.; Reed, W.F. Monitoring the synthesis and properties of copolymeric polycations, *J. Phys. Chem. B*, 2008, *112*, 14597-14608.

[47] Kreft, T.; Reed, W.F. Experimental observation of cross-over from non-condensed to counterion condensed regimes during free radical polyelectrolyte copolymerization under high composition drift conditions, *J. Phys. Chem. B.*, **2009**, *113*, 8303-8309.
[48] McFaul, C.A.; Drenski, M.F.; Alb, A.M.; Reed, W.F. Simultaneous Multiple Sample Light Scattering Detection Of LCST During Copolymer Synthesis, *Polymer*, **2011**, 4825-4833.
[49] Farinato, R.S.; Calbick, J.; Sorci, G.A.; Florenzano, F.H.; Reed, W.F. Online monitoring of the final divergent growth phase in the stepgrowth polymerization of polyamines, *Macromolecules*, 2005, *38*, 1148-1158.
[50] Matyaszewski, K. pp1-17, ACS Symp. Ser. 1197, *Controlled Radical Polymerization*, 2015
[51] Ballard, N.; Mecerreyes, D.; Asua, J.M. Redox Active Compounds in Controlled Radical Polymerization and Dye-Sensitized Solar Cells: Mutual Solutions to Disparate Problems. *Chem. Eur. J.*, **2015**, *21*, 18516-18527.
[52] Erlita, M.; Xiaohui, L.; Zhu, S. Modeling and theoretical development in controlled radical polymerization. *Prog. Polym. Sci*., **2015**, *45*, 71-101.
[53] Flores, J.D.; Abel, B.A.; Smith, D.D.; McCormick, C.L. *Monitoring Polymerization Reactions*, Eds. Reed, W.F.; Alb, A.M. 2014, Wiley Interscience, p 45-58.
[54] Chan, N.; Cunningham, M.F.; Hutchinson, R.A. Copper-mediated controlled radical polymerization in continuous flow processes: Synergy between polymer reaction engineering and innovative chemistry. *J. Polym. Sci, A; Polym Chem*, **2013**, *51*, 3018-3096.
[55] Barner-Kowollik, C.; Delaittre, G.; Gruendling, T.; Pauloehrl, T. Elucidation of Reaction Mechanisms and Polymer Structure: Living/Controlled Radical Polymerization. *Mass Spect. Polym. Chem*., **2012**, *373-403.*
[56] Hemp, S.T.; Long, T.E. DNA-Inspired Hierarchical Polymer Design: Electrostatics and Hydrogen Bonding in Concert. *Macromole. Biosci*., **2012,** *12*,29-29.
[57] Cheng, S.; Zhang, M.; Dixit, N. ; Moore R.B.; Long, T.E. Nucleobase Self-Assembly in Supramolecular Adhesives. *Macromolecules*, **2012**, *45*, 805-812.
[58] Roy, R.K., Laure, C. ; Verchin, C.; Lutz, J.F. Design and synthesis of digitally encoded polymers that can be decoded and erased. *Nature Comm.*, **2015**, doi:10.1038/ncomms8237
[59] Lutz, J.F.; Ouchi, M.; Liu, D.R. ; Sawamoto, M. Sequence-controlled polymers.. *Science*, **2013,** *341, 1238149*
[60] McKenna, T.F. ; Soares, J.B.P. ; Simon, L.C. Polyolefin Reaction Engineering – An Overview of Recent Developments. *Macromole. Mat. & Eng.*, **2005**, *290*, 507-510.
[61] McKenna, T.F.; Kiparissides, C.; Weickert, G.; Storti, G Results of the CATAPOL Project: Advances in studies on single catalyst/polymer particles for polyolefins. *DECHEMA Monographien*, 2001, *137*, 345-352.
[62] Hamielec, A.E.; Soares, J.B.P. Polymerization reaction engineering metallocene catalysts. *Prog. Polym. Sci.*, **1996**,*21*m 651-706.
[63] Tuchbreiter, A.; Marquardt, J. ; Kappler, B. ; Honerkamp, J.; Kristen, M.O.; Mulhaupt, R. High-Output Polymer Screening: Exploiting Combinatorial Chemistry and Data Mining Tools in Catalyst and Polymer Development. *Macromole Rapid Comm*, **2003**, *24*, 47-62.
[64] Isayev, A. I. *Encyclopedia of Polymer Blends Vol. 2: Processing* **2011**
[65] Cho, H. S., Chung, J. S., Lee, W. Y. *Journal of Molecular Catalysis A: Chemical* **2000**, *159*(2), 203-213
[66] Heidemeyer, P., Pfeiffer, J. *Macromol. Symp.* **2002**, *181*(1), 167-176

[67] Deslauriers, P. J., Mcdaniel, M. P., Rohlfing, D. C., Krishnaswamy, R. K., Secora, S. J., Benham, E. A., Beaulieu, B. B. *Polym. Eng. Sci.* **2005**, *45*(9), 1203-1213
[68] Lenzi, M. K., Cunningham, M. F., Lima, E. L., Pinto, J. C. *Ind. Eng. Chem. Res.* **2005**, *44*(8), 2568-2578
[69] Jovanović, R., Ouzineb, K., Mckenna, T. F., & Dubé, M. A. *Macromolecular Symposia* **2004**, *206*(1), 43-56
[70] Zhang, M., Ray, W. H. *J. Appl. Polym. Sci.* **2002**, *86*(5), 1047-1056
[71] Yoo, J., Kim, M., & Chang, Y. (1998). *U.S. Patent No. 5852147*. Washington, DC: U.S. Patent and Trademark Office.
[72] Kasuya, T., Suematsu, H., Tomiyama, K., Yusa, H., Kobori, T., & Katada, M. (1998).*U.S. Patent No. 5736288*. Washington, DC: U.S. Patent and Trademark Office
[73] Reed, W.F. "Automatic Continuous Online Monitoring of Polymerization Reactions (ACOMP)", Encyclopedia of Analytical Chemistry, Elsevier, **2013**. DOI: 10.1002/9780470027318.a9288
[74] T. McAfee, N. Leonardi, R.D. Montgomery, J. Siqueira, T. Zekoski, M.F. Drenski, W.F. Reed, *Macromolecules*, 2016, 49 (19), 7170-7183. DOI: 10.1021/acs.macromol.6b01522
[75] Grassl, B., Reed, W.F. *Macromole. Chem. and Phys.*, **2001,** 203, 586-597.
[76] D. W. Wang, W. M. Thomas, in: Encyclopedia of Polymer Science and Engineering, Wiley Interscience, New York, **1991**, 73, 2359-2368.
[77] Fevola, M.J.; Hester, R.D.; McCormick C.L., J. Polym. Sci.: Part A: Polym Chem, **2003,** 41, 560-568.
[78] Vega, M.P.; Bellumat, E.; Lima, E.L.; Pinto, J.C. *Macromole. React. Eng.* , **2012,** *6*, 482-494.
[79] D.P. Norwood, W.F. Reed, *Int. J. Polym. Ana. and Char.* **1997**, 4, 99-132.
[80] Li, X.; Liang, S.; Wang, W.-J.; Li, B.-G.; Luo, Y.; Zhu, S. Model-Based Production of Polymer Chains Having Precisely Designed End-to-End Gradient Copolymer Composition and Chain Topology Distributions in Controlled Radical Polymerization, A Review. *Macromolecular Reaction Engineering* **2015,** 9 (5), 409-417 DOI: 10.1002/mren.201500012.
likelihood method. *Aiche Journal* **2004,** 50 (6), 1260-1272 DOI: 10.1002/aic.10109

[81] Wang, R.; Luo, Y. W.; Li, B. G.; Sun, X. Y.; Zhu, S. P. Design and control of copolymer composition distribution in living radical polymerization using semi-batch feeding policies: A model simulation. *Macromolecular Theory and Simulations* **2006,** 15 (4), 356-368 DOI: 10.1002/mats.200600007.
[82] Ballard, N.; Mecerreyes, D.; Asua, J. M. Redox Active Compounds in Controlled Radical Polymerization and Dye-Sensitized Solar Cells: Mutual Solutions to Disparate Problems. *Chemistry-a European Journal* **2015,** 21 (51), 18516-18527 DOI: 10.1002/chem.201503098.
[83] Mastan, E.; Li, X. H.; Zhu, S. P. Modeling and theoretical development in controlled radical polymerization. *Progress in Polymer Science* **2015,** 45, 71-101 DOI: 10.1016/j.progpolymsci.2014.12.003.
[84] Matyjaszewski, K., Controlled Radical Polymerization: State-of-the-Art in 2014. In *Controlled Radical Polymerization: Mechanisms*, American Chemical Society: 2015; Vol. 1187, pp 1-17.
[85] Reed, W. F. ; Alb, A. M., *Monitoring polymerization reactions : from fundamentals to applications*. Hoboken, New Jersey : Wiley: Hoboken, New Jersey, 2014.

[86] Chan, N.; Cunningham, M. F.; Hutchinson, R. A. Copper-mediated controlled radical polymerization in continuous flow processes: Synergy between polymer reaction engineering and innovative chemistry. *Journal of Polymer Science Part a-Polymer Chemistry* **2013,** 51 (15), 3081-3096 DOI: 10.1002/pola.26711.

[87] *Elucidation of Reaction Mechanisms and Polymer Structure: Living/ Controlled Radical Polymerization*. Weinheim, Germany: Wiley-VCH Verlag GmbH & Co. KGaA: Weinheim, Germany, 2012; p 373-403.

[88] Hemp, S. T.; Long, T. E. DNA- Inspired Hierarchical Polymer Design: Electrostatics and Hydrogen Bonding in Concert. *Macromolecular Bioscience* **2012,** 12 (1), 29-39 DOI: 10.1002/mabi.201100355.

[89] Cheng, S. J.; Zhang, M.; Dixit, N.; Moore, R.; Long, T. Nucleobase Self- Assembly in Supramolecular Adhesives. *Macromolecules* **2012,** 45 (2), 805-812 DOI: 10.1021/ma202122r.

[90] Raj Kumar, R.; Anna, M.; Chloé, L.; Laurence, C.; Claire, V.; Jean-François, L. Design and synthesis of digitally encoded polymers that can be decoded and erased. *Nature Communications* **2015,** 6, DOI: 10.1038/ncomms8237.

[91] Badi, N.; Lutz, J.-F. Sequence control in polymer synthesis. *Chemical Society Reviews* **2009,** 38 (12), 3383-3390 DOI: 10.1039/b806413j.

[92] Denbigh, K.G. Continuous reactions. Part II. The kinetics of steady state polymerisation. *Trans. Faraday Soc*. **1947**, 43, 648-660.

[93] Gee, G.; Melville, H.W. The kinetics of polymerisation reactions. *Trans. Faraday Soc.* **1944**, *40*, 240-251.

[94] Schulz, G. V. On the relationship between the rate of reaction and composition of the reaction products in macro polymerisation processes. *Z. Phys. Chem*. **1935**, B30, 379.

[95] Flory, P.J. The Mechanism of Vinyl Polymerizations. *J Am. Chem. Soc.* **1937**, 59, 241-253

[96] Stockmayer, W.H. Distribution of chain lengths and compositions in copolymers. *J. Chem Phys*, **1945**, 13, 195-207.

[97] Soares, J.B.P. The Use of Instantaneous Distributions in Polymerization Reaction Engineering. *Macromole. React. Eng*. **2014,** *8*, 235-259.